INCORPORATION OF ELEMENTAL BORON DURING SILICON AND SILICON GERMANIUM MOLECULAR BEAM EPITAXY

CARL PATRICK PARRY

THESIS SUBMITTED IN PARTIAL FULFILMENT OF THE REQUIREMENTS FOR THE DEGREE OF DOCTOR OF PHILOSOPHY.

UNIVERSITY OF WARWICK, DEPARTMENT OF PHYSICS

SEPTEMBER 1991

abstract

Most of the improvements in silicon devices over recent years have been brought about by reductions in the lateral geometry of devices, owing to developments in processing technology. Structures featuring reduced *vertical* dimensions are of considerable interest because they will show novel electronic properties, compared with their conventional Si equivalents, though these impart stringent demands on profile control. Using low temperature processes, such as Molecular Beam Epitaxy, it may be possible to fabricate such devices, though improvements in our present understanding of dopant incorporation will be necessary before the technique can realise its full potential for the production of doping profiles featuring atomically abrupt doping interfaces.

A key area addressed in the present study is the incorporation behaviour of boron in Si and $Si_{1-x}Ge_x$ using co-evaporation of the element. It is shown here that although elemental boron is a relatively well behaved dopant during MBE, it *can* show severe profile smearing in Si, depending on the growth temperature, by forming a *surface-accumulated* phase of boron. This collects at the growing surface at coverages of up to 0.25 ML, with any attempt to exceed this amount leading to the rapid formation of inactive boron precipitates. The surface phase is shown to modify dopant incorporation behaviour, leading to badly smeared doping profiles. The incorporation properties of the surface phase have been used to determine equilibrium solid solubilities of boron that show good agreement with previously published *bulk* data. The present study has been extended to 450°C. The low temperature incorporation of boron in Si is quite different as the processes causing profile smearing become increasingly kinetically limited. This is observed as a strong reduction in profile smearing and an associated rise in boron solubility limits.

For the case of boron incorporation during $Si_{1-x}Ge_x$ MBE, it is found that boron shows a complex dependency on temperature, growth rate, and Ge fraction. A mechanism for this behaviour is elucidated, involving the influence of both the change in matrix, and the availability of favourable incorporation sites, during co-evaporation of Ge.

Previously observed dopant incorporation behaviour has been discussed in terms of segregation of dopant from underlying layers, though the work presented in this thesis is qualitatively consistent with models for dopant incorporation considering only processes occurring at the *immediate* surface.

CONTENTS

TABLES AND FIGURES

ACKNOWLEDGEMENTS

I would like to acknowledge the help of the following people during this programme and the preparation of this thesis.

My sincerest thanks go to both my supervisor Evan Parker, and to Richard Kubiak, for their encouragement and support during the course of this programme.

I would especially like to thank Mark Dowsett, Harvey Fox, and Bob Barlow for SIMS discussions that have made an invaluable contribution to this work.

To all my other colleagues in the ASR group, past and present, including Engin Basaran, Robin Biswas, Jim Brighten, John Emeleus, Richard Houghton, Nevil Mattey, Richard Morris, Tim Naylor, Simon Newstead, Pete Phillips, Govind Pindoria, and Dave Smith; a big thanks to you all for your excellent companionship and your help and advice over the years.

Finally I would like to express my heartfelt gratitude to my family, for their moral and practical support throughout my academic career.

DECLARATION

This thesis is submitted to the University of Warwick in support of my application for the degree of Doctor of Philosophy. It is presented according to the Department of Physics guide-lines, Phys/PG3. The work in this thesis is the result of my own research except where specifically acknowledged in the text.

Much of this study has been published. This includes

Parry C P, Newstead S M, Barlow R D, Augustus P, Kubiak R A, Dowsett M G, Whall T E and Parker E H C P, "Elemental boron doping behaviour in silicon molecular beam epitaxy", Appl. Phys. Lett. **58** (5), 481 (1991). Incorporated into Chapter 3.

Parry C P, Kubiak R A, Newstead S M, Whall T E and Parker E H C P, "Temperature dependence of surface processes occurring during elemental boron doping in silicon molecular beam epitaxy", J. Appl. Phys. **71**(1), 118 (1992). Incorporated into Chapter 4.

Parry C P, Kubiak R A, Newstead S M, Whall T E, Parker E H C, "Boron accumulation behaviour during Si MBE", 1991 *MRS Proc* **220** 121.Incorporated into Chapter 4.

Parry C P, Kubiak R A, Newstead S M, Whall T E, Parker E H C, "An investigation of boron incorporation in SiGe MBE", 1991 *MRS Proc* **220** 103. Incorporated into Chapter 5.

CHAPTER 1
INTRODUCTION

1.1 WHAT IS Si MOLECULAR BEAM EPITAXY ?

Si molecular beam epitaxy (MBE) involves the deposition of epitaxial Si on a heated clean substrate using an atomic flux of elemental Si. Dopants are simultaneously incorporated during growth, usually supplied by coevaporation from thermal sources, and are controlled by using mechanical shutters. Unlike chemical vapour deposition (CVD) and related techniques [Tsang 1987], Si MBE growth occurs by surface adsorption and direct incorporation of Si and dopant atoms, and does not involve any surface chemistry or vapour phase. Thus MBE growth relies on spontaneous incorporation of atoms. This occurs at steps, and layer growth involves these propagating across the surface. The steps act as perfect 'sinks' so that their growth is limited by diffusion of adatoms. Diffusion coefficients are higher at the immediate surface than in the bulk, so that adatoms have enough mobility to find an incorporation site over a wide temperature range. Another important aspect of Si MBE is that growth takes place under UHV conditions (typically $\approx 10^{-9}$ mbar) thereby reducing unwanted impurity adsorption from the residual gas, which would otherwise have to be prevented by elevating the growth temperature.

Because MBE involves direct incorporation from atomic beams under UHV conditions, growth occurs at temperatures well below those for which significant solid state diffusion of dopant is expected (< 750°C). This means that Si MBE is capable of producing arbitrary doping profiles that are almost atomically abrupt.

1.2 Si MBE - AN HISTORICAL PERSPECTIVE

The earliest attempt at Si MBE was carried out by Unvala in the early 60's who grew *p-n* diodes on 2cm substrates [Unvala 1962]. Unvala used a bell jar system consisting of a resistively heated substrate and a crude Si electron impact evaporation source. The layers showed poor morphology, with high levels of defects causing large leakage currents under reverse bias. These defects were shown later to be due to incorporation of carbon from the residual gas. Carbon and oxygen contamination were discovered to be detrimental to epitaxial growth as early as 1968, when they were shown to impede the motion of Si steps across the growing layer and thus prevent 2D growth [Abbinks *et al* 1968, Joyce *et al* 1969]. The use of oil-based diffusion pumps, which dominated the vacuum technology until the 1970's, was the main source of hydrocarbons [Maurice *et al* 1979]. Incorporation of hydrocarbons was prevented by raising the growth temperature to $\approx 1000°C$, but this hindered the potential of Si MBE to produce abrupt doping profiles. It appeared that growth temperatures could be reduced to a level sufficient to achieve abrupt doping profiles by improving the vacuum. The main developments in UHV technology arrived in the 70's [see Kubiak *et al* 1988] especially with the advent of oil-free 'clean' pumping techniques and the use of dedicated stainless steel MBE systems, with all components able to withstand 'baking' at 200°C (see Chapter 2). These improvements enabled a vacuum quality of better than 10^{-10} mbar after a bakeout.

Other developments in the hardware [Hill 1976] and proposals for devices featuring hyperabrupt doping profiles [reviewed in Luryi and Sze 1988] stimulated a fresh investigation into Si MBE as a viable technique for the production of devices with reduced *vertical* dimensions. Many research groups were established by industrial companies, notably IBM, AT&T, NEC, Hitachi, Texas Instruments, and AEG Telefunken. For a review of progress made in the field made in the late 70's, readers are referred to the extensive review article by Ota [Ota 1983]. At this time the temperature for epitaxial growth was reduced to, typically, 700°C with

defects in undoped films reported to be less than in the substrate (< 500 cm^{-2}). This was achieved principally by improvements in substrate pre-cleaning procedures and the availability of high quality substrates.

Proposals for novel optical and electronic devices grown by strained layer epitaxy, involving the ordered growth of $Si_{1-x}Ge_x$ ($0 < x < 1.0$) layers on Si substrates [Bean 1985], maintained the world-wide interest in Si MBE. These devices exploit the electrical and structural properties of $Si/Si_{1-x}Ge_x$ heterointerfaces, though the commensurate growth of strained $Si_{1-x}Ge_x$ layers presents a formidable challenge to the technique for reasons that will be discussed in a following section.

Progress in the understanding of growth kinetics during Si MBE developed rapidly during the late 80's and into the 90's, and much of this acquired knowledge is discussed in this Chapter.

The work presented in this thesis was aimed at producing an improved understanding of dopant incorporation during Si and $Si_{1-x}Ge_x$ MBE. The optimum conditions for controlled boron doping have been characterised using an elemental effusion source. At the onset of this work elemental boron was thought to be a relatively well-behaved dopant during Si MBE capable of producing arbitrary doping profiles. However in this thesis it has been established that boron *does* show significant profile smearing dependent on the growth temperature [Parry *et al* 1991 A]. The effect is observed only using high resolution SIMS depth profiles, though is sufficient to adversely affect the production of devices requiring sharp doping profiles. It is also shown that boron doping at high levels can produce more severe profile smearing, owing to the formation of a surface–accumulated phase of boron [Parry *et al* 1991 B].

Boron solubility limits during Si MBE have been determined using the incorporation properties of the boron phase, important for the growth of thin layers (≈ 2 nm) with sheet concentrations of 10^{14} cm^{-2} [Parry *et al* 1991 C]. The first

results of boron incorporation in $Si_{1-x}Ge_x$ ($0 < x < 25\%$) suggest that boron is a useful dopant in this new materials system [Parry *et al* 1991 D].

1.3 Si EPITAXIAL GROWTH

The surface processes during Si homoepitaxy are examined here. The following is a brief review of the subject, including the classical model for epitaxial growth and some of the modifications appropriate for epitaxial growth on 'real' Si surfaces.

1.3.1 CLASSICAL MODEL FOR EPITAXIAL GROWTH

The work of Burton Cabrera and Frank (BCF) has been tremendously influential in the developments of study of epitaxial growth since its publication in 1951 [Burton *et al* 1951]. Indeed, to this day publications and developments of our understanding of Si epitaxy use this work as a starting point (see section 1.3.2).

In the BCF model an ideal planar surface is examined with no consideration of bonding arrangements or surface reconstruction. Epitaxial growth is modelled according to processes occurring at the immediate surface, including surface diffusion (migration) and capture of adatoms at steps (incorporation) shown in Fig. 1.1. It is demonstrated that Si clusters containing steps can be nucleated spontaneously on planar surfaces (see Fig. 1.1), though the formation of 2D clusters becomes rate limited at lower temperatures. Once the clusters are formed they continue to grow limited by adatom migration to the steps. During the time before incorporation there exists a finite probability of the adatom desorbing back into the 'vapour'. The desorption probability is temperature dependent, increasing with increasing temperature. Otherwise the steps act as perfect sinks so that all atoms reaching the steps are incorporated there. The steps advance across the

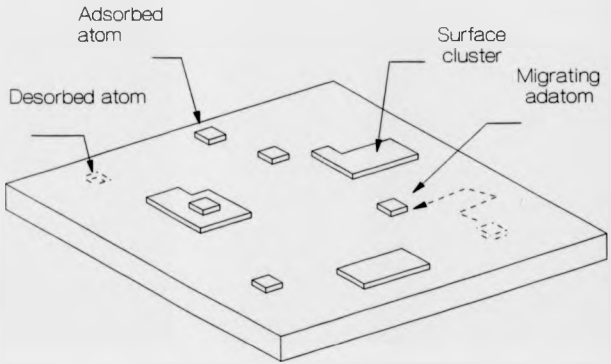

Fig. 1.1 Schematic representation of 2D growth and processes according to the classical BCF theory.

surface until growth of a monolayer is completed. If the next monolayer is nucleated by this stage, layer by layer growth is observed.

In the BCF theory 2D growth is modelled by considering the equilibrium exchange of molecules between an adsorbed layer and the vapour, as well as diffusion and capture at steps which propagate across the growing surface.

1.3.2 EPITAXIAL GROWTH ON Si SUBSTRATES

In practice MBE occurs on non-ideal surfaces, often at low temperatures and therefore under non-equilibrium conditions. Real Si surfaces will feature some reconstruction of surface atoms, which have fewer bonds than in the bulk. Growth occurs typically at low temperatures under non-equilibrium conditions. These lead to deviations from the classical theory during Si epitaxy and are discussed here.

Abbink *et al* (1968) confirmed 2D growth on Si(111) substrates using a surface replication electron microscopy technique. Joyce *et al* (1969) independently verified monolayer growth on Si(111) surfaces using LEED measurements. Both authors observed directly the nucleation and propagation of monolayer steps, confirming layer by layer growth, providing the temperature was high enough to reduce any impurity incorporation. Incorporation of carbon precipitates was shown to 'pin' the motion of the steps leading to 3D growth.

At present Si(100) substrates are preferred for Si MBE rather than Si(111) substrates, since the minimum temperature for epitaxial growth has been shown to be lowest on Si(100) surfaces [Kasper 1982]. Vicinal substrates are often used for MBE growth. These are deliberately misorientated, typically by 0.3°, towards the [110] direction. Tilted substrates can be considered as being terminated by terraces of equal length, separated by steps whose height is equivalent to an atomic spacing. A misorientation of 0.3° means that there will be on average some 10^5 steps/cm. Voigtlander *et al* (1986) showed that substrate misorientation reduces the importance of step nucleation by artificially inducing a number of competitive steps. Also the average diffusion distance for adatoms from terraces to

incorporation sites is reduced, essential for crystalline growth at very low temperatures for which Si adatoms have a low surface mobility.

Jorke *et al* (1989) demonstrated that epitaxial growth could occur at temperatures as low as 200°C, depending on the growth rate and vacuum quality. Under poor vacuum conditions, impurity incorporation (mostly H_2O) forces a transition from crystalline to disordered growth at temperatures below 400°C. Above this temperature, impurities are re-evaporated before incorporation. Under good vacuum conditions ($< 10^{-10}$ mbar), Jorke *et al* observe a critical temperature for Si epitaxy that decreases with decreasing growth rate. This is an important consideration in any study of dopant incorporation at low temperature. If growth continues below the critical temperature, a proportion of the Si adatoms will have insufficient energy to reach a crystalline incorporation site before the start of the next monolayer. Hence disordered growth will occur eventually leading to polycrystalline or even amorphous material. Because the effects of disordered growth are cumulative, there exists a finite thickness that can be grown, at a given temperature, before the onset of damage becomes so severe that disordered growth occurs. A model of this crystalline-disorder transition was developed by considering the incorporation of Si atoms on Si(100) surfaces [Jorke *et al* 1989]. Initially atoms are weakly bound in a precursor (PC) state, and will incorporated in a covalently bonded (CB) state provided they have enough energy to surmount an energy barrier. This process is thermally activated so that the probability of an atom reaching a CB state after some time t can be represented as

$$P^* = \exp\left\{-\nu\, t \exp\left(\frac{-\theta}{kT}\right)\right\} \qquad (1.1)$$

where

Θ is an energy barrier (eV)

ν represents a frequency factor (s^{-1})

T is the temperature (K)

The probability of an atom incorporating in a PC state is represented as

$$P = 1 - P^* \tag{1.2}$$

An atom is 'frozen-in' after the time for the deposition of a monolayer, so that $t=t_m$ in equation (1.1). To determine a critical thickness the probability of finding an atom in a CB state needs to be determined during the growth of successive layers. Once an atom in a layer is incorporated into a PC state defect, successive layers will contain PC states. Hence the probability of finding a CB atom in the $(n+1)^{th}$ layer is the product of the probabilities of finding a CB atom in each previous layer yielding

$$P^*_{n+1} = P^*_n \left\{1 - P(t_m)\right\} \tag{1.3}$$

where $P^*_0 = 1$ (substrate) and each n corresponds to a monolayer thickness. The critical thickness for the onset of disordered growth is chosen, somewhat arbitrarily, so that $P^*_n = 0.5$. This and equations (1.1), (1.2), and (1.3) gives

$$\Delta = \frac{a_0}{4} \ln 2 \exp\left\{\nu t_m \exp\left(\frac{-\theta}{kT}\right)\right\} \tag{1.4}$$

The authors grew epitaxial layers at temperatures as low as 200°C, and at growth rates between 0.2 and 0.05 nms^{-1}, determining the critical thicknesses from observations of XTEM micrographs. These were in good agreement with equation (1.4) except at higher temperatures for which damage annealing becomes significant. Θ was determined to be $\approx +0.25$ eV and $\nu \approx 1500$ Hz. A family of curves exhibiting this behaviour is shown in Fig. 1.2. For the temperatures and growth rates employed in this thesis the epitaxial thickness for Si homoepitaxy is effectively infinite (see Fig. 1.2). For the case of growth during coevaporation of dopant, however, Δ_E is probably reduced and conservative thicknesses were used

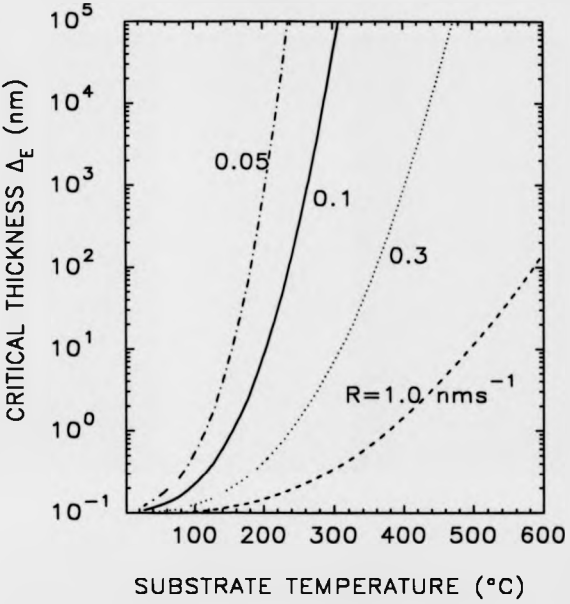

Fig. 1.2 Graph showing maximum thickness for Si epitaxial growth versus temperature, for different growth rates, using equation (1.3) (after Jorke *et al* 1989.)

for layers grown in studies of dopant incorporation in Si (see Chapters 3 and 4). Maximum thicknesses in $Si_{1-x}Ge_x$ (see Chapter 5) are limited to values $< \Delta_E$ at temperatures above 400°C, for reasons other than the breakdown in 2D growth (see section 1.4.2).

Another deviation from the classical BCF theory was the observation of steps on vicinal Si(100) surfaces that were *two* atomic layers in height. These were reported by authors using LEED and STM experiments [Kaplan 1980, Aizaki and Tatsumi 1986, Doi and Ichikawa 1988]. Biatomic steps on Si(100) surfaces were shown to be associated with surface reconstruction [Chadi 1987]. For the case of Si(100) substrates surface atoms have two 'unoccupied' bonds. These 'pair' to form weak dimers, which are orientated parallel and perpendicular to the step edges on consecutive terraces [Barnett and Rockett 1988]. A schematic of a dimerised surface is shown in Fig. 1.3. Barnett and Rockett used Monte-Carlo simulations to analyse growth on reconstructed Si(100) substrates. These suggest that epitaxial growth occurs as though atoms on a Si(100) surface re-order into bulk-like positions. This is probably an oversimplification of the growth process since surface anisotropy would be expected to yield a difference in adatom surface diffusion across the two types of terraces and this was not accounted for.

No apparatus for *in-situ* analysis was available in this present work, so that it is unclear which growth mode (single or double step) was occurring. Both monatomic step and biatomic steps have been observed under apparently identical growth conditions [Kaplan 1980, Aizaki and Tatsumi 1986, Doi and Ichikawa 1988, Sakamoto *et al* 1989]. Sakamoto *et al* presented an extensive set of experiments to show that *both* biatomic and monatomic growth could be induced on slightly misorientated substrates depending on the growth temperature and angle of misorientation. It was also noted that biatomic steps were unstable, since on interrupting growth these would often revert to surfaces composed of monatomic steps [Sakamoto *et al* 1989]. For growth rates and substrate misorientations similar

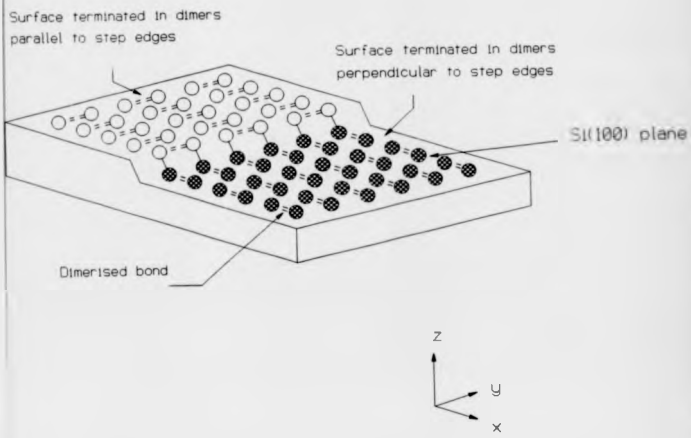

Fig. 1.3 Schematic of a Si(100) surface terminated by (2x1) and (1x2) reconstructions. The surface dimers are caused by the 'pairing' of unoccupied bonds on Si(100) surfaces. The step height is equivalent to a monolayer of atoms.

to those used in the present work, it is likely that monolayer growth occurs at temperatures above 700°C, and biatomic steps will be observed at temperatures below 550°C. These will revert to monatomic steps when the growth is terminated. There is likely to be a transition from biatomic to monatomic step growth occurring between 550 and 700°C.

Hence epitaxial growth under MBE conditions is governed by adatom diffusion on reconstructed surfaces under conditions of high supersaturation. 2D growth is established by adatom incorporation at surface step sites. Steps are artificially induced by misorientating the substrate so that the growth of the steps is diffusion limited, except at temperatures below 600°C for which there exists a finite thickness before the onset of disordered growth.

1.4 DEVELOPMENT OF $Si_{1-x}Ge_x$ MBE

The current interest in $Si_{1-x}Ge_x$ based heterosystems and their useful electrical properties represents a response by the Si community to developments made in the growth of III-V structures which allow improved transport and optical properties over their 'conventional' Si counterparts [Herman and Sitter 1989]. Indeed the success of $Si_{1-x}Ge_x$ MBE may well prove vital in maintaining Si as the dominant semiconductor material for the advanced electronics industry. The subject area is reviewed briefly, discussing how the electrical properties of $Si/Si_{1-x}Ge_x$ interfaces can be used for high speed device applications and how the growth of ordered $Si_{1-x}Ge_x$ layers sets a formidable challenge to the MBE technique. Emphasis is placed on factors related to dopant incorporation.

1.4.1 NOVEL DEVICES BY $Si_{1-x}Ge_x$ MBE

Following the demonstration in 1984 that coherently strained $Si/Si_{1-x}Ge_x$ layers could be grown by Si MBE [Bean *et al* 1984], there has been there has been much interest in the production of $Si_{1-x}Ge_x$ devices which can exploit bandgap

engineering. The bandgaps of Si and Ge are 1.2eV and 0.65eV respectively [Sze 1981]. Early theoretical work established that the bandgap difference at strained $Si/Si_{1-x}Ge_x$ heterojunctions can be controlled, in principle, by varying the Ge fraction (x) [People and Bean 1986]. To date most of the work on band edge alignment at heterointerfaces is theoretical [Jain and Hayes 1991], although the electrical characteristics of structures grown by MBE have been used to solve important questions on the properties of these interfaces [Jorke and Herzog 1985]. For the case of $Si/Si_{1-x}Ge_x/Si$ structures most of the band edge misalignment will be in the valence band, so that the $Si_{1-x}Ge_x$ layer can act as an energy well for holes [People and Bean 1986]. Carriers can be produced in the well by introducing a *p*-type region near the heterointerface, typically at a distance of 10 nm. Modelling of the properties of such modulation doped $Si/Si_{1-x}Ge_x$ interfaces suggests that at room temperature holes will become confined in the well if a bandgap difference of 0.1eV is achieved (see Fig. 1.4), equivalent to a $Si/Si_{1-x}Ge_x$ heterojunction with a Ge fraction of 20% [People and Bean 1986]. The significance of this structure is that the confined holes are spatially separated from their parent ions, resulting in hole transport parallel to the interface with enhanced mobilities compared with bulk doped layers. This mobility enhancement is particularly strong at low temperatures for which ionised impurity scattering dominates in bulk-doped material.

Devices that can exploit such bandgap engineering include the $Si_{1-x}Ge_x$ *p*-channel field-effect transistor (FET) [Pearsall *et al* 1985]. This utilises a modulation doping layer placed some 10nm from the $Si_{1-x}Ge_x$ channel. For such a device, carriers can move more quickly in the channel than in an equivalent conventional Si FET, allowing faster switching speeds.

Other structures utilising the properties of heterojunctions include the $Si_{1-x}Ge_x$ base heterojunction bipolar transistor (HJBT) [Iyer *et al* 1989], first fabricated by the IBM group in 1988 [Patton *et al* 1988]. The HJBT uses high doping levels ($>10^{19}cm^{-3}$) in the $Si_{1-x}Ge_x$ base allowing a reduction in base resistance, for faster switching speeds, without the loss in current gain associated

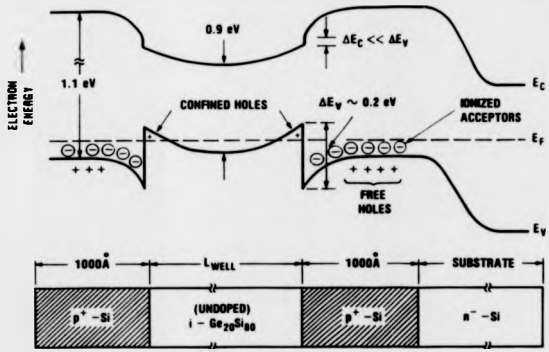

Fig. 1.4 Energy band diagram of a modulation doped $Si/Si_{1-x}Ge_x/Si$ structure (after People and Bean 1986).

with conventional bipolar transistors [Iyer *et al* 1990]. Theoretical investigations have suggested that operating frequencies of 75 GHz may be possible for a 100 nm thick base, and further improvements are expected using thinner bases [Won and Morcoç 1989]. *P*-type doping is the ideal choice for the base of an HJBT, because nearly all the energy difference at the heterointerface is in the valence band edges. The first $Si_{1-x}Ge_x$ HJBT's were grown with Ga doped bases [Patton *et al* 1988]. The first results of boron incorporation in $Si_{1-x}Ge_x$, presented in Chapter 5, suggest that boron doped $Si_{1-x}Ge_x$ bases can be made much thinner than their Ga doped counterparts resulting in higher performance devices. The stringent demands on profile control for the growth of the modulation doped $Si_{1-x}Ge_x$ layers will be discussed in a following section.

1.4.2 GROWTH OF $Si_{1-x}Ge_x$ LAYERS BY MBE

The growth of strained $Si_{1-x}Ge_x$ layers with good structural properties sets a significant challenge for the MBE community. Ge has a lattice parameter $\approx 4\%$ larger than that of Si so that commensurate $Si_{1-x}Ge_x$ layers will contain a large amount of strain [see Bean 1985]. This strain can be accommodated by tetragonal distortion of the lattice or can be partially released by the formation of defects at the heterointerface. The strain compensation mechanism involves a balance between the energy reduction, by maintaining a defect free interface, and the strain energy per atom produced by deformation. For a given Ge fraction, the energy reduction at the interface is fixed. As the layer thickness (and hence the number of strained atoms) is increased, the energy reduction at the interface will eventually be overcome. This results in a transition to misfit accommodated growth after some finite 'critical' thickness is achieved. The relaxation process involves the shearing of atomic bonds along the heterointerface, which will be kinetically limited at low temperatures. This means that metastable $Si_{1-x}Ge_x$ layers, with thicknesses greater than the equilibrium critical value, can be grown by MBE [People and Bean 1985]. Measurements of critical thicknesses of $Si_{1-x}Ge_x$ layers ($0<x<0.5$) appear to

confirm this [Bean *et al* 1985, Kohama *et al* 1987]. A plot of critical thickness versus Ge fraction is presented in Fig. 1.5. This upper limit to thickness of $Si_{1-x}Ge_x$ layers was an important consideration in Chapter 5, which discusses boron incorporation in strained $Si_{1-x}Ge_x$ layers for $0 < x < 0.25$.

Practical limits to epitaxial growth *temperatures* also exist, owing to a tendency towards Ge islanding at higher temperatures. The behaviour is brought about by the large interfacial energies induced by incorporation of Ge, and therefore increases with increasing Ge fraction [Bean *et al* 1984]. This maximum growth temperature at a given Ge fraction is plotted in Fig. 1.6. Island growth during $Si_{1-x}Ge_x$ MBE was avoided in the work of Chapter 5, which discusses the influence of substrate temperature on the incorporation properties of boron in $Si_{1-x}Ge_x$ in the temperature range 650° to 450°C.

Although the study of $Si_{1-x}Ge_x$ has advanced significantly in recent years, both in the structural and electrical properties of heterointerfaces [see the extensive review article by Jain and Hayes 1991], little work has been carried out in the incorporation of dopants during $Si_{1-x}Ge_x$ epitaxy. The need to establish the conditions for the growth of very abrupt boron depth profiles is discussed in section 1.5.1.

1.5 ASPECTS OF DOPING DURING Si AND $Si_{1-x}Ge_x$ MBE

1.5.1 THE NEED FOR ABRUPT PROFILES IN Si AND $Si_{1-x}Ge_x$ MBE

The electrical properties of most devices, whether involving Si or $Si_{1-x}Ge_x$ epitaxy, depend in some way or another on the quality of doping interfaces in the active part of the device [Luryi and Sze 1988]. Sharp dopant profiles in Si are required for the modulation doped $Si_{1-x}Ge_x$ channel FET because it features a doping spike near the $Si/Si_{1-x}Ge_x$ interface. Any redistribution of dopant from the

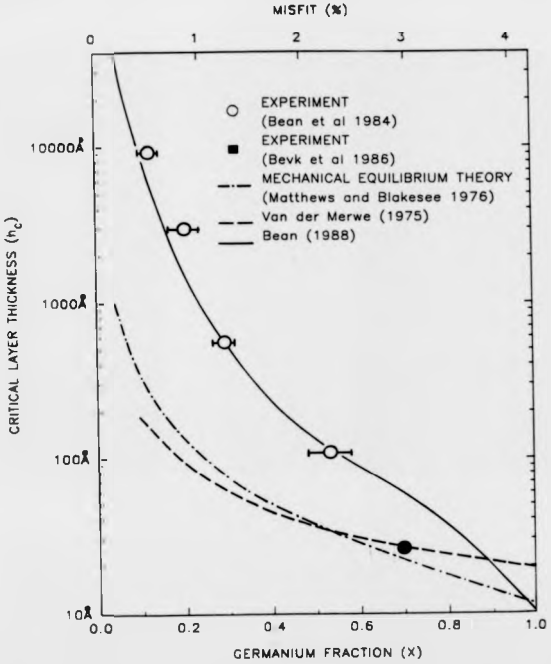

Fig. 1.5 Graph of critical thickness versus Ge fraction for strained $Si_{1-x}Ge_x$ layers grown by MBE. (see Iyer *et al* 1989 and references therein).

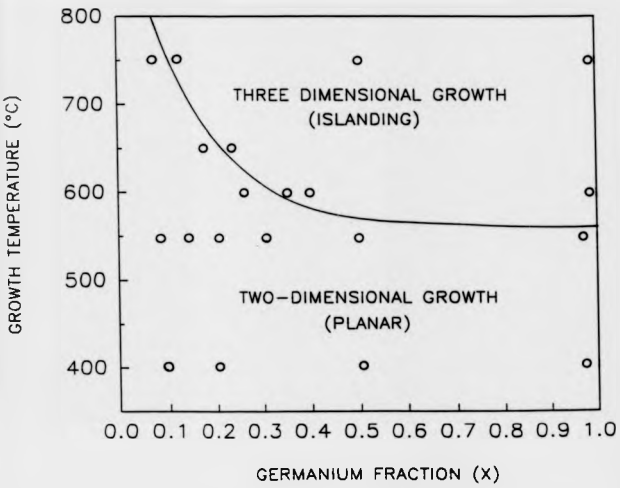

Fig. 1.6 Graph of $Si_{1-x}Ge_x$ layer morphology vs. growth temperature and Ge fraction for layers grown by MBE (after Bean *et al* 1984).

Si into the $Si_{1-x}Ge_x$ channel can introduce ionised impurities into the well, which can adversely affect low temperature mobilities [Mishima *et al* 1990].

For the case of doping in $Si_{1-x}Ge_x$, sharp profiles are also required for the *p*-type $Si_{1-x}Ge_x$ base HJBT. The base should be ideally as narrow as possible (< 50 nm), because of the small critical thickness of $Si_{1-x}Ge_x$ at the Ge fractions often used, and to increase the speed of the device [Iyer *et al* 1990]. Modelling of dopant redistribution from the $Si_{1-x}Ge_x$ base into the collector and emitter regions has shown that very small diffusion distances ($\sqrt{Dt}$ = 2.5 nm for a 100 nm base) can cause a serious degradation in device performance [Prinz *et al* 1991, Slotboom *et al* 1991].

P-type doping is preferred for growth of $Si_{1-x}Ge_x$ FET's and $Si_{1-x}Ge_x$ base HJBT's, owing to the nature of the bandgap alignment in $Si_{1-x}Ge_x$ on Si substrates [People and Bean 1986]. Results presented for boron incorporation during Si and $Si_{1-x}Ge_x$ MBE in Chapters 4 and 5 demonstrate boron can produce either severely smeared or atomically abrupt doping profiles depending on the growth conditions. The ideal growth conditions for boron incorporation in Si and $Si_{1-x}Ge_x$ are established and these results suggest that coevaporated elemental boron is likely to be the prime choice for doping in Si and $Si_{1-x}Ge_x$ MBE.

1.5.2 CHOICE OF DOPANTS AND DOPANT SOURCES

The simplest method of doping is by coevaporation of dopant from a thermal effusion source (see Chapter 2), relying on spontaneous surface incorporation. Low energy ion implantation of dopant has been used by other groups with some success [Ni *et al* 1989] but is technologically demanding, and hence costly, and was not available in the present work. The choice of the groups III and V elements, for *n*- and *p*-type doping in Si MBE, is a compromise between their physical, chemical, and electrical properties [Kubiak and Parry 1991]. Coevaporation of the element is preferred to reduce impurity incorporation; ideally at temperatures such that the element does not react with the containment vessel.

The vapour pressure of the dopant should be high enough to allow high doping levels to be achieved without using excessively elevated crucible temperatures, yet low enough to prevent unwanted re-evaporation of the dopant from hot parts of the MBE chamber. It is also desirable to use a dopant with shallow activation energies and high solid solubilities at the temperatures used in MBE growth (ie $>10^{19}cm^{-3}$ in the temperature range 200 to 900°C).

Early attempts at doping in Si MBE include the use of Ga and Al [Becker and Bean 1977], Sb [Bean 1978], and In [Knall *et al* 1984]. These were found to give depth profiles that differed strongly from the temporal changes in dopant flux, owing to surface enrichment of dopant (see section 1.5.4). This profile smearing took place although growth temperatures were well below those for which solid-state diffusion would be expected. The use of As and P compound sources was found to give high background levels in undoped layers [Kubiak *et al* 1985C and Kubiak *et al* 1986]. This was due to the high vapour pressures of these elements, which re-evaporated from hot parts of the growth chamber. Sb has become the best characterised of the available dopants, after it was observed that the profile smearing observed during *n*-type coevaporation doping could be reduced by the application of a negative potential to the substrate [Kubiak *et al* 1985C]. However most of the devices discussed in section 1.4.1 require abrupt *p*-type doping profiles. Although Ga, In, and Al are relatively easy to coevaporate, their associated problems of profile smearing has led to a decline in their use [Kubiak and Parry 1991].

Boron is the ideal choice of *p*-type dopant, due to its high solid solubility and shallow acceptor level [Sze 1981]. However elemental boron requires crucible temperatures in the range 1500 to 2000°C for adequate doping fluxes, necessitating careful choice of crucible material. Indeed its low vapour pressure has until quite recently dissuaded many authors from its use. The alternative is coevaporation of compound boron species, which have higher vapour pressures. The relative merits of both methods are discussed in the next section.

1.5.3 BORON DOPANT SOURCES

Many authors have tried to circumvent the problems associated with co-evaporation of elemental boron. The successful use of compound boron sources such as HBO_2, B_2O_3, P-BN, and B doped Si has been reported in the literature (see Table I). The relative advantages of each are discussed here.

1.5.3a Compound boron sources

Effusion sources based on compound boron require lower operating temperatures than those involving elemental boron. Evaporation of molecular species takes place, necessitating some dissociation stage at the Si surface. Impurity incorporation from such sources, often deleterious to epitaxial growth, has impeded boron incorporation studies at low temperature.

Table I Boron sources commonly used during Si Molecular beam epitaxy

Source	Operating Temperature/°C	Comments
HBO_2 [a,b]	700 - 1000	O_2 incorporation severe at low growth temps (< 700°C)
B_2O_3 [b,c]	1000 - 1300	O_2 incorporation quite severe at temps below 600°C
P-BN [d]	900 - 1400	Unstable dopant source
B doped [e] silicon	e-beam evaporator	A useful source though relatively unproven
Elemental B [f]	1500-2000	The use of a graphite crucible introduces C impurities at high boron levels

(a) Aizaki and Tatsumi 1985.

(b) Tatsumi 1990 B.

(c) Lin *et al* 1990.

(d) Kubiak *et al* 1985B.

(e) Eberl *et al* 1991.

(f) Newstead *et al* 1991 (see Chapter 4).

Thermodynamic studies of oxygen incorporation with compound boron sources have been discussed for B_2O_3 [de Frésart *et al* 1986, Tuppen *et al* 1988] and for HBO_2 sources [Lin *et al* 1990]. Interactions of B_2O_3 and HBO_2 with Si surfaces were modelled, applying equilibrium thermodynamics to previously published data. The two types of compound sources show different chemical reactions between the impinging molecular species and the Si surface. Both involve many stages with the final product, gaseous SiO from solid SiO_x, being the rate limiting step to preventing oxygen incorporation. The reactions are thermally activated processes, the reaction rate increasing with increasing growth temperature. If the process does not proceed quickly enough, at a given growth rate and temperature, oxygen is incorporated more quickly than it is desorbed. This will disturb epitaxial growth, and potentially induce stacking faults during any subsequent annealing stage [Ravi 1981]. Aizaki and Tatsumi (1985) reported oxygen levels using an HBO_2 source were greater than 10^{19} cm^{-3} in layers grown at 750°C. These induced defect levels $>10^7$ cm^{-2}. The critical temperature T_c for the onset of oxygen incorporation at a given boron concentration [B] and growth rate G was determined by Tuppen *et al* (1988) and is shown in Fig. 1.7. However the decomposition of the boron compound is likely to be kinetically limited at low substrate temperatures, leading to higher oxygen incorporation than that predicted by equilibrium theory.

A consequence of this oxygen incorporation is that studies of boron doping at different growth temperatures are only useful above 600°C [Jackman *et al* 1988, Tatsumi *et al* 1988B]. An attempt by de Frésart *et al* (1988) to investigate incorporation parameters at low temperatures, using a compound source, yielded incorporation parameters which were closely correlated to epitaxial material quality at temperatures below 750°C [de Frésart *et al* 1988].

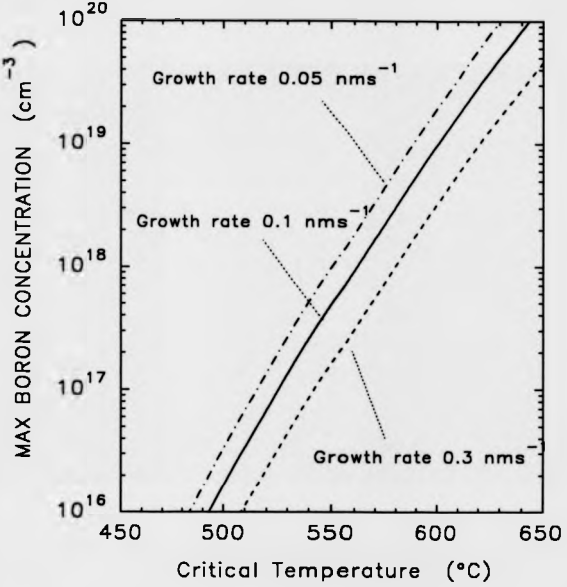

Fig. 1.7 Maximum boron level versus critical temperature for the onset of severe oxygen incorporation (after Tuppen *et al* 1988).

Despite this compound sources have been used in the growth of device structures. HBO_2 sources have been used to fabricate 90 GHz IMPATT diodes with good electrical characteristics compared with their CVD equivalents [Tatsumi *et al* 1988 A]. However the same group acknowledged difficulties in using an HBO_2 source. HBO_2 was used to dope the *p*-type $Si_{0.8}Ge_{0.2}$ base of HJBT's [Tatsumi 1990 B]. The boron doped base was grown at a temperature of 700°C to avoid oxygen incorporation; too high a temperature for the growth of strained $Si_{1-x}Ge_x$ and the devices showed inordinately high leakage currents at the $Si/Si_{1-x}Ge_x$ interface. It seems likely that these problems will mean a decline in the use of compound sources.

1.5.3b Elemental sources

Initial attempts to dope using elemental boron were carried out by Kubiak *et al* using a resistively heated boat manufactured from refractory metals [see for example Kubiak *et al* 1985A, Kubiak *et al* 1985B]. These were found to give good dopant profile control over the 10^{15} to 10^{18} cm^{-3} range and epilayers with bulk-like mobilities, for growth temperatures between 700 to 900°C [Kubiak *et al* 1987]. However the cells were found to have a limited lifetime, owing to etching of the crucible material by molten boron. The cell design was modified, employing a resistively heated graphite crucible (see Chapter 2). This method provides the high temperatures necessary to provide adequate boron fluxes ($\approx$2000°C) and the low vapour pressure of carbon at these temperatures ensures little contamination of epilayers [Honig 1962]. However to determine the extent of the contamination associated with this source, a SIMS investigation was undertaken by the present author (see Chapter 4).

For growth at low temperatures, which is of great importance to the growth of $Si/Si_{1-x}Ge_x$ structures, the use of an elemental boron source has been advantageous (see chapters 3,4, and 5). During the course of this project other elemental boron sources were developed by many authors, most designs featuring

electron beam heating of a graphite crucible [Andrieu 1988, Denhoff 1990, Kibbel *et al* 1990]. Indeed such cell designs are now commercially available [Caburn, UK], although no studies of boron incorporation in the low temperature regime have been reported.

Before the work carried out for this project, *it was generally perceived that elemental boron sources do not produce smeared profiles* [Kubiak *et al* 1985A and 1985B, Andrieu 1988, Headrick *et al* 1990]. Boron profile smearing was apparently only seen with compound sources and thought to be associated with oxygen incorporation [de Frésart *et al* 1988]. The work in this thesis shows that although profile smearing during boron doping is much less than that associated with other dopants, significant profile smearing is evident during boron doping under certain conditions (see chapters 4 and 5).

1.5.4 DOPANT INCORPORATION

For most dopants used in Si MBE the degree of profile smearing during growth at relatively low temperature ($< 750°C$) can actually be worse than that due to solid state diffusion. An example of this effect is given in Fig. 1.8 (after Becker and Bean 1977). This shows a capacitance-voltage depth profile of Al doped layers grown by Si MBE, at a temperature of 700°C. This shows a severely smeared depth profile though the solid state diffusion length should not exceed 5 nm at this growth temperature [Becker and Bean 1977]. Surface accumulation and associated profile smearing was also observed for Ga, Sb, and In doping during MBE [Becker and Bean 1977, Bean 1978, Knall *et al* 1984].

This profile smearing is due to a propensity of the dopants to *accumulate at the growing surface*, forming a reservoir that can act as a secondary source of dopant after the dopant flux has been terminated. Mechanisms explaining profile smearing during Si MBE have been suggested including thermal desorption of dopant [Allen *et al* 1982], enhanced diffusion of dopant from below the surface (segregation) [Barnett and Greene 1985, Jorke 1985], and step climbing of dopant

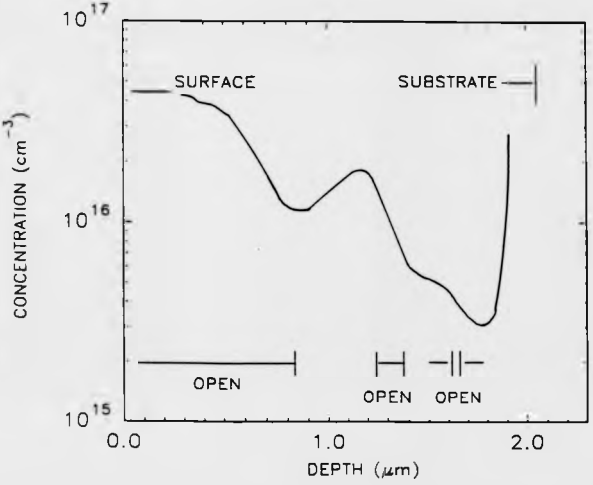

Fig. 1.8 A capacitance-voltage depth profile of an Al doped epilayer grown by Si MBE (after Becker and Bean 1977). The Al doped layers were grown at a temperature of 700°C, by opening and closing a shutter (see figure).

[Andrieu *et al* 1989]. These models are discussed in detail in Chapter 4, and will be discussed only in general terms here.

It seems likely that dopants are partially incorporated at step sites, in the first instance, as is the case with Si atoms. However to do so they must overcome strain-related energy barriers, depending on how different their atomic radii are from that of the matrix species (eg Si) [Pindoria *et al* 1990A]. After the growth of the next monolayer the dopant is fully incorporated. But why do some dopants form surface coverages at concentrations much higher than in the bulk? There exist two possible mechanisms by which dopants can collect at the surface. The first mechanism is one of back-diffusion of dopant from bulk sites, so-called *surface segregation* [Barnett and Greene 1985, Jorke 1985]. The second proposed mechanism is one of *surface accumulation* of dopant for which dopant atoms collect at the surface by omitting the incorporation stage, by climbing over the advancing steps. This model differs from the segregation one in that surface accumulated dopant has never fully incorporated, and thus collects at the growing surface rather than diffusing there. The segregation models are cited in the literature because impurity segregation is a well-known phenomenon observed in studies of surface enrichment during thermal annealing of binary alloys [Kryistyan 1989, Pindoria *et al* 1990 A]. However it will be shown in this thesis that segregation models, as applied to MBE, cannot account for the observed incorporation behaviour of boron in Si and $Si_{1-x}Ge_x$.

The differences between the segregation and accumulation models are important for a full understanding of dopant incorporation, and are discussed more fully in Chapters 4 and 5. The term segregation is used commonly throughout the literature, even by authors who propose accumulation models. In discussions of dopant incorporation in this thesis the term employed by the authors is given, but expressed in quotation marks, where, in this author's opinion, the proposed model not strictly a segregation one.

1.6 STRUCTURE OF THESIS

In Chapter 1 previous work on aspects of Si and $Si_{1-x}Ge_x$ epitaxy has been discussed, with the emphasis on factors influencing dopant incorporation. It has also been shown that there is a need for abrupt boron doping profiles using an elemental source. Surface enrichment of other dopants, contributing to profile smearing, has also been discussed. Possible mechanisms for dopant accumulation have also been introduced.

In Chapter 2 the reader is familiarised with the growth apparatus used in the present work, as well as the experimental apparatus and techniques used to characterise boron incorporation behaviour in Si and $Si_{1-x}Ge_x$.

In Chapter 3 the existence of a saturated boron surface-accumulated phase is verified, found to occur under dynamic growth conditions at temperatures above 650°C. The incorporation properties of this have been used to determine solid solubilities of boron in Si for temperatures between 900 and 650°C, which show good agreement with previously published data for bulk doped layers. The present study has been extended to 450°C.

In Chapter 4 it is shown that elemental boron, at levels $\approx 10^{18}$ cm^{-3}, *does* show profile smearing in Si, although at a much reduced level compared with other co-evaporated dopants. Boron profile smearing in the presence of a surface phase is shown to be more severe and is suggested as being caused by surface clustering of boron. This has important implications for existing models of dopant incorporation. The existence of a kinetically limited boron incorporation regime is verified, which shows a steep increase in profile sharpness. In this temperature regime boron doped layers with a profile abruptness < 2 nm/decade can be achieved, which is ideal for the growth of narrow highly doped structures.

In Chapter 5 the first results of boron incorporation in $Si_{1-x}Ge_x$ are presented ($0 < x < 25\%$). These show that profile smearing in this materials system shows a dependency on temperature, growth rate and Ge fraction. This complex behaviour is explained by the influence of both the change in lattice parameter

induced by Ge incorporation, and the availability of favourable surface incorporation sites.

CHAPTER 2
EXPERIMENTAL

2.1 INTRODUCTION

In this Chapter, the performance of the experimental apparatus used in this work is outlined and a discussion of the characterisation techniques used in Chapters 3 4 and 5 is given. This is split into two sections; *MBE Growth Apparatus*, and *Characterisation Techniques*. With respect to the apparatus section the use and performance of the MBE equipment supplied is given, rather than the relative merits of different apparatus available. Reviews of the range of apparatus available (ion implantation versus thermal doping sources for example) are given in the text. Also given are modifications to the apparatus carried out specifically for this project.

In the *Characterisation Techniques* section a more critical approach is taken to the range of techniques used. This is important since various methods were available, some more suitable than others. Also some of the well-used techniques in the study of Si, such as SIMS and e-CV, were applied to the study of dopant incorporation in $Si_{1-x}Ge_x$, after careful consideration and justification.

2.2 MBE GROWTH APPARATUS

Summary: Epilayers were grown on Si(100) substrates in modified V80H and V90S research systems under UHV conditions. Substrates were rotated during growth and substrate temperatures were monitored using an optical pyrometer. Si and Ge fluxes were provided using electron beam evaporators, controlled using electron impact emission spectroscopy flux monitors, and managed by a computer. Boron was co-evaporated from a thermal effusion source calibrated by measuring doping levels obtained at constant source heater current.

2.2.1 MBE GROWTH CHAMBER

Epilayers were grown in modified commercial V80H and V90S (VG Semicon, UK) systems. Initially work was carried out in both systems, although the majority of this work was carried out in the V90S system. (The reader is asked to assume layers were grown in the V90S system unless told otherwise.) A schematic diagram of the MBE systems used in this work is presented in Fig. 2.1.

Both the MBE systems and the components used in them were UHV compatible, the importance of which has already been discussed in Chapter 1. All components were capable of sustaining a 200°C bakeout so that base pressures of $\approx 10^{-11}$ mbar could be achieved, rising to 10^{-9} mbar during growth in the V90S. Residual gas analysis, using a quadrupole mass spectrometer, indicated that most of the increase in pressure during growth was caused by outgassing of H_2, associated with the Si source (see Section 2.2.3). A combination of cryopump, getter-ion pump, titanium sublimation pump, and liquid nitrogen cryopanel pumps was used. For a discussion of these pumps and their modification for MBE use the reader is referred to Roth 1979 and Kubiak *et al* 1988. The use of a separate load lock and preparation chamber (see diagram) enabled vacuum integrity to be maintained during transfer of substrates to and from the system.

2.2.2 SUBSTRATE HEATER ASSEMBLY

Substrates were radiatively heated using Ta strips and a graphite meander for the V80H and the V90S systems respectively. Growth temperature was an important parameter in this study of dopant incorporation. However, it is technically complex to measure temperatures *in-situ*, owing to difficulties in attaching thermocouples to substrates, so temperatures were measured using an infra-red pyrometer via a quartz viewport. The pyrometer could not operate at temperatures below 550°C, since Si becomes opaque in the infra-red region below this temperature. Above this temperature the absolute error in temperature measurement was ±25°C with a

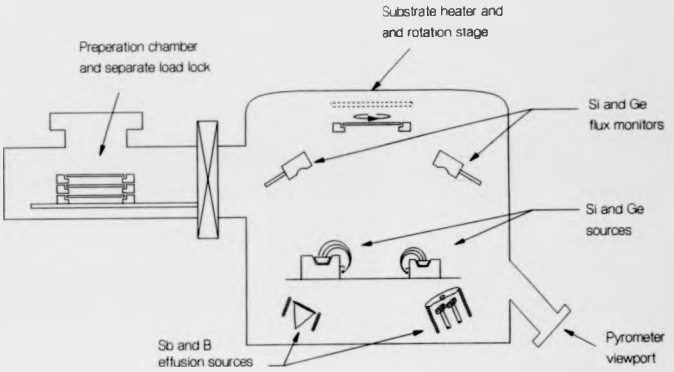

Fig. 2.1 Schematic diagram of an MBE system of the type used in the present work.

reproducibility of $\pm 10°C$. Extrapolation of the heater temperature versus current characteristics was used to determine substrate temperatures below 550°C, with an absolute error of $\pm 40°C$. Substrates were rotated to ensure uniformity of temperature and fluxes across the wafer. Uniformity of temperature and deposit properties across the wafer was an important consideration, and early work established that temperature gradients across the surface may induce slip lines [Ota 1983]. Flux uniformities were found to be better than $\pm 10\%$ across the 3" wafers used in the V80H and $\pm 5\%$ across the 4" wafers used in the V90S, owing to its larger chamber size and improved geometry [Kubiak *et al* 1988], easily adequate for this work. Substrate rotation can produce particle-induced defects during MBE growth, at rotations above 60 rpm, owing to flaking of material from the substrate manipulator and its bearings [Farley *et al* 1988]. To this end substrate rotations of $\leq$ 20 rpm were used. Substrates were pre-cleaned *in-situ* before growth by raising the substrate temperature to 800°C and growing a thin (< 10 nm) Si 'cap' on the wafer at a low rate. This reduces the native oxide present on the Si wafer and the product, gaseous SiO, desorbs into the vacuum leaving a clean Si surface free from oxide. The substrate temperature is lowered to the required value, and growth is continued, avoiding any 'sudden' change in temperature and growth rate.

2.2.3 Si AND Ge SOURCES

The chemically reactive nature of hot Si and Ge and their low vapour pressures [Honig 1962] are thought to preclude the use of a thermal effusion source, of the type used for boron for example (see Section 2.2.5). Although Si thermal sources have been used in III-V MBE as *dopant* sources [Miller and Sullivan 1987], the high flux rates needed to maintain a usable growth rate in Si MBE prevents their use. Ge becomes molten and highly reactive at temperatures necessary to produce an adequate growth flux, readily forming eutectics with the few materials suitable for Si molecular beam epitaxy. Ge effusion sources have been used to produce

$Si/Si_{1-x}Ge_x$ heterojunctions, with some success, although impurity data were not given [Wagner and Janocko 1989].

The use of electron-beam evaporators (e-guns) avoids such problems providing stable pure sources of Si and Ge at moderate expense to UHV environment [Hill 1986, Graber 1987, Kubiak *et al* 1988]. A schematic of the 40 cc Airco Temescal [Edwards, UK] electron beam evaporator is given in Fig. 2.2. A high current carrying tungsten filament produces electrons by thermionic emission. These are extracted using an electrostatic potential, typically 8 kV with respect to the filament. The electron beam is deflected through 270°C, using an electromagnetic coil, so that it impacts with the Si or Ge charge. The charges are high-purity semiconductor grade single-crystal Si and Ge and are shaped to fit in the water-cooled copper hearth. Most of the electron beam will impinge on the charge and heat the surface of it by electron impact. The highly localised nature of the beam heating effect and the good thermal contact of the charge with the copper hearth ensure that the charge forms a solid external crust. Hence the charges act as their own high purity containment vessels. The Si and Ge beams produced by the e-guns are mostly atomic species with some ionised [Hill 1986]. Ionised species have been found to be beneficial to dopant incorporation, especially Sb, since the application of a -ve potential to the substrate is found to reduce profile smearing [Kubiak *et al* 1985C].

For the case of Ge, the use of e-guns is likely to be contentious since they may directly contribute to Cu contamination of epilayers. Unlike Si, the Ge charge is almost entirely molten. Under these conditions Cu may diffuse from the hearth into the charge. Indeed Cu was detected by SIMS, uniformly distributed in $Si/Si_{1-x}Ge_x$ epilayers at levels from 10^{17} to 10^{19} cm^{-3}, showing no correlation with Ge growth rate or level. These levels are high enough to affect the electrical properties of modulation doped structures, though there is no evidence at present to suggest that the Cu contamination can affect incorporation of dopants. This is suggested by the lack of any dependence of boron profile smearing on Cu levels, at

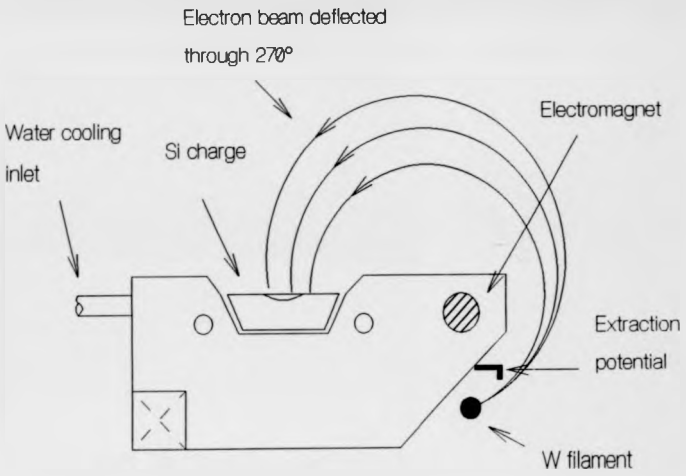

Fig. 2.2 Schematic of the magnetically focussed electron beam evaporator used in the present work.

a given temperature and growth rate. However Cu contamination has been shown to cause strained $Si_{1-x}Ge_x$ to 'relax' (see Chapter 1) after annealing [Higgs *et al* 1990]. However the good crystallinity in individual layers used in a study of dopant incorporation in $Si_{1-x}Ge_x$, as determined by defect etch measurements, precludes serious copper contamination in the samples investigated in the present work.

2.2.4 MATRIX FLUX MEASUREMENT AND CONTROL

Steady Si and Ge fluxes can be established by running an e-gun at constant emission current, since e-guns produce a flux rate proportional to the intensity of the electron beam. However the emission current versus flux characteristic is non-linear, due to the water cooling of the copper hearth [Bhatia 1989], and changes as the charge depletes. Many of the dopant incorporation parameters discussed in Chapters 3 4 and 5 are strongly growth rate dependent. The need to produce stable reproducible growth rates means that *in-situ* flux measurement and feedback control are necessary. Quartz crystal flux monitors have been used to control growth rates, but these suffer the disadvantage of low lifetimes and can introduce Si flakes into the growth chamber [Kubiak *et al* 1988]. Instead growth rates were controlled using a modified Sentinel III [Inficon, NY] electron impact emission spectroscopy (EIES) flux controller [Gogol and Cipro 1985]. These operate using a cross-beam analyzer positioned in line of sight to the e-gun. In the sensor the collision of matrix fluxes with an electron beam produces light in the infra-red regime, the wavelength of which is a characteristic of the element being monitored. This light is collected by a photomultiplier producing a signal current that is directly proportional to the flux rate. This allows very stable growth rates to be achieved over a usable range of 0.001 to 0.3 nms^{-1} with an absolute error of $\pm 10\%$. The Sentinel system is microcomputer compatible and therefore allows growth rate to be controlled precisely and reproducibly. The Si growth rate was calibrated by determining epilayer thicknesses using a surface profilometer, after a given growth time. The determined correction factor is entered into the Sentinel

controller software. Ge growth rates cannot be calibrated using this method, since the thick films necessary for an accurate determination of epilayer thickness would deplete the smaller Ge charge. Ge levels were calibrated using X-ray spectroscopy measurements of $Si/Si_{1-x}Ge_x$ superlattices, to determine Ge composition at given Si and Ge flux rates [Powell *et al* 1991]. The reproducibility of Ge composition was $\pm 10\%$, after calibration of Si and Ge fluxes.

2.2.5 ELEMENTAL BORON SOURCE

Boron doping was achieved by co-evaporation of the element using a high temperature source shown in Fig. 2.3. The crucible material is manufactured from high purity graphite. The graphite is resistively heated, using Ta/Mo contacts, reaching temperatures of $\approx 2000°C$ at a doping level of $\approx 10^{20}$ cm^{-3}. Flux rates are controlled by operating the cell at constant current (100-180 A), calibrated against doping level with a reproducibility of $\pm 25\%$. During the course of this project other elemental boron sources were developed [Andrieu 1988, Denhoff *et al* 1990, Kibbel *et al* 1990], indeed similar cell designs are now commercially available [Caburn 1991]. Data on impurity incorporation during co-evaporation of boron is presented in Chapter 4.

2.3 EPILAYER CHARACTERISATION TECHNIQUES

The following is a description of the experimental techniques used or investigated by the author to characterise boron doped layers in Si and $Si_{1-x}Ge_x$ grown by MBE. The techniques are all *ex-situ* methods yielding atomic composition (SIMS), electrical properties (Hall and e-CV), and structural information (defects) of boron doped layers grown at temperatures between 900 and 450°C.

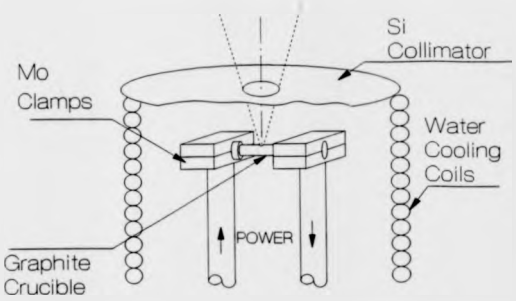

Fig. 2.3 Boron thermal effusion source of the type used in the present work. The cell crucible is maufactured from high purity graphite, and is resistively heated.

2.3.1 ELECTRICAL CHARACTERISATION

The dependence of electrical properties of boron doped epilayers on growth temperature, such as maximum carrier concentration and carrier mobilities, are of considerable importance to the exploitation of MBE in device fabrication. Both bulk techniques and depth profiling methods were used. The techniques available for analysis of electrical properties were Hall effect, four-point probe, spreading resistance, and electrochemical capacitance-voltage profiling. Experience in the characterisation of the electrical properties of boron doped Si obtained by the bulk semiconductor industry [Sze 1981] was helpful in enabling evaluation of boron doped epilayers grown by Si MBE although not directly applicable (see Chapter 3). For the case of the $Si_{1-x}Ge_x$ system, however, little work has been carried out in the electrical characterisation of this relatively new system. For example the Hall mobility versus carrier concentration curves are unknown for boron in $Si_{1-x}Ge_x$.

A brief review of the important aspects of these techniques is given here. For more extensive reviews the reader is referred to the appropriate articles indicated in the text.

2.3.1a FOUR-POINT PROBE

This method was used by the author for routine assessment of carrier concentration of uniformly boron doped Si layers. It offers the advantage of being non-destructive and has a rapid measurement time because the technique readily lends itself to computer control. During the measurement four collinear probes are lowered gently onto the sample surface establishing an electrical contact. A constant current I is applied between the outer contacts and a precision voltmeter is used to measure the resulting voltage V between the inner pair. To ensure that the current flows through the epilayer, and not into the substrate, layers must be grown on substrates of opposite type for *p-n* junction isolation. The resistivity of the epilayer

is calculated, using a correction factor that depends on the probe geometry according to equation (2.1).

$$\text{Resistivity } \rho = \frac{V}{I} t\, C.F. \qquad (2.1)$$

where t is the epilayer thickness (cm)

C.F. is a correction factor depending on the probe geometry.

For thin (< 100 μm) layers the correction factor C.F. can be approximated to (π/ln2) [Sze 1981]. The measured voltage will contain components due to the contact resistance of the probes and offsets as well as the resistivity of the semiconductor layer. The effects of voltage offsets can be reduced by reversing the current and repeating the measurement. This is repeated at different currents, to verify good junction isolation and integrity of contacts, ensuring that resistivity values vary by less than 5%. For thick uniformly doped layers at levels above 10^{19} cm^{-3}, depletion effects can be ignored [Sze 1981]. Carrier concentrations can be deduced from resistivity measurements, for epilayers of known type and thickness, assuming bulk-like mobilities or using previously published data. The error in the measurement is approximately $\pm 25\%$, due to uncertainty in the probe geometry.

2.3.1b HALL EFFECT

This technique was used by the author to obtain carrier concentrations and mobilities of uniformly doped epilayers grown on substrates of the opposite type. The technique is destructive and involves etching a sample cross, and forming electrical contacts with an In-Ga amalgam and gold pads. This was carried out according to ASTMS standards [ASTMS 1976A], using a Greek cross geometry and the Van der Pauw technique for determining resistivities of arbitrary shaped samples [Van der Pauw 1958]. This method accounts for errors due to sample geometry and non-ideal contacts. For highly doped boron samples (> 10^{19} cm^{-3}) a Hall scattering factor was used to determine *carrier* concentrations from Hall

concentrations. The two are different owing to the appreciable effect of Coulombic scattering on carrier mobilities at these levels [Sasaki *et al* 1988]. With some care in the sample preparation, and by ensuring ohmic contacts and junction isolation, carrier concentrations can be determined to within an absolute error of $\pm 10\%$ and mobilities to within $\pm 20\%$. Epilayer quality can be determined qualitatively by comparing mobilities with previously published data at room temperature and 77K [Sze 1981].

2.3.1c SPREADING RESISTANCE PROFILING (SRP)

Spreading resistance measurements were carried out on behalf of the author at Semiconductor Analysis (London). This method is similar to the 4-point probe technique except that a depth profile is obtained by stepping the contact probes across the sample, which is bevelled at a shallow angle (typically $\approx 1°$). The technique has been extensively used for characterisation of layers grown by Si MBE (see for example Pawlik 1985). Carrier concentrations are determined from the resistivity data, assuming bulk mobilities. The raw data is smoothed and processed using an appropriate algorithm, and a certain amount of deconvolution is necessary since the measured resistivity at any point contains contributions from the underlying layers. It has been claimed that the deconvolution process "... presents no great difficulties" [Pawlik 1985]. However the deconvolution process requires some prior knowledge of the sample to achieve a final depth profile. This can lead to erroneous results, as was the case with a modulation doped structure used to determine solubility limits of boron in Si. A depth profile for this structure obtained by SRP is shown in Fig. 2.4. The boron doped layers were grown at levels of 1×10^{20} cm^{-3} at temperatures between 900 and 450°C (see diagram). A SIMS profile of this structure is shown in Fig. 3.2a. The SIMS profile indicates that layers grown at temperatures below 600°C are close to ideal and that at 650°C, and above, redistribution of boron has occurred resulting in the formation of inactive precipitates and shoulders (see Chapter 3). The SRP profile is markedly different,

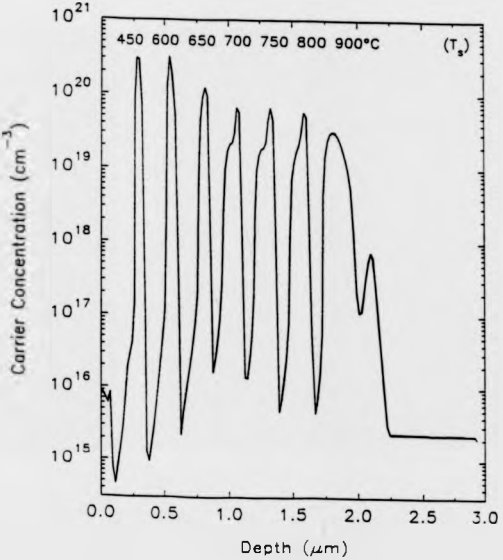

Fig. 2.4 Depth profile of a boron doped 'hi lo' structure obtained by SRP. This should be compared to the carrier concentration profile obtained by e-CV (see Fig. 3.2b), and the chemical concentration profile obtained by SIMS (see Fig. 3.2a).

showing exaggerated levels in the boron peaks, grown at 450 and 650°C, and underestimating the boron background level by an order of magnitude. The distinct 'overshoot' in the boron doped layers is due to the smoothing of the raw data at points of inflexion, where there is an insufficient density of data points. Also the loss in depth resolution in the SRP profile can be attributed to the fact that the measurement yields the free carrier versus depth distribution, which is unlikely to be the same as the dopant versus depth distribution. This is especially the case for abrupt modulation doped structures which feature carriers separated from their parent ions [Casel *et al* 1990]. The overestimate of carrier concentration in the shoulders levels is more serious, since they were an important aspect to the work in Chapter 3.

During SRP profiling of $Si_{1-x}Ge_x$ layers it was discovered that the technique appears to be sensitive to defect levels, which are generally higher in this materials system. These problems and the success in obtaining carrier concentration profiles by e-CV measurements (see next Section) meant that the SRP technique was not used further in this work.

2.3.1d Electrochemical capacitance-voltage (e-cv) profiling

This technique was used by the author to obtain carrier concentration profiles of boron doped layers in Si. The e-CV technique is based on the CV measurement except that the depth profile is obtained by alternately removing some of the epilayer, using an anodic etch, and determining the carrier concentration at known depth [Blood 1985]. This means that the maximum depth that can be profiled is not limited by junction breakdown at high doping levels, as it is with conventional CV measurements. The technique has been used extensively for Si profiling [Leong *et al* 1985], and has been used with some success in determining carrier concentration profiles in boron doped $Si_{1-x}Ge_x$ [Basaran 1991]. The choice of electrolyte is important since it must act both as an etchant and a Schottky contact. Diluted (0.05ML NaF_2\0.1ML H_2SO_4), and (0.1ML NHF_2) electrolytes

were used, though the NHF_2 etch gave more reliable measurements with boron doped at high levels ($> 10^{19}$ cm^{-3}) in Si and $Si_{1-x}Ge_x$. Profiles were obtained using Polaron 4200 and 4300 instruments [Biorad, UK], the Polaron 4300 model being a superior instrument, owing to its ability to obtain profiles using compensation for both parallel and series resistance components during the CV measurement.

Carrier concentrations are determined from expressions for the capacitance of the depletion region X_d near a Schottky barrier under reverse bias [Blood 1985]. Analysis of the properties of the depletion region formed at the electrolyte/semiconductor interface yields the capacitance C, expressed as:

$$C = \frac{\varepsilon A}{X_d} \tag{2.2}$$

where ϵ is the dielectric constant, and A is the effective area of the sample/electrolyte interface and X_d is the depletion width at the interface.

Carrier concentrations at a given depth X are measured by modulating the bias potential V, to obtain C and dC/dV using:

$$N(X) = \frac{-C^3}{e\varepsilon A^2}\left(\frac{dC}{dV}\right)^{-1} \tag{2.3}$$

C is determined using an AC signal treating the sample as part of a voltage divider network [Blood 1985], dC/dV is obtained modulating the AC signal. The output signal contains real and imaginary components, separated into resistive and capacitance components using a pair of phase sensitive detectors. These operate at the carrier and modulation frequencies to determine C and dC/dV. For high carrier concentrations optimum results were achieved using carrier signals of ≈ 0.1 $V_{pk\text{-}pk}$ at a frequency of 1 kHz, and modulation signals of ≈ 0.28 $V_{pk\text{-}pk}$ at a frequency of 30 Hz.

The etched depth X_r is usually obtained from the time integration of the etch current during anodic dissolution expressed using Faraday's law as:

$$X_r = \frac{M}{ZFDA} \int I \, dt \qquad (2.4)$$

where M is the molar weight of Si

Z is the Si valency during the Si anodic etch

F is the Faraday constant

D is the density of Si

A is the area of sample in contact with the electrolyte.

The depth X is defined as the sum of X_d and X_r.

The area measurement is obtained using an optical microscope to determine the diameter of the final crater formed after profiling. It should be noted that for the case of *n*-type dopants an areal correction factor should be used, since for such samples dissolution occurs by illumination of the specimen. It is often the case that the illuminated area, used to determine the etched depth in equation (2.4), is different from the area of sample under the Schottky barrier used in equations (2.2) and (2.3) [Blood 1985].

During the dissolution step H_2 bubbles are generated at the sample surface, which can cause non-uniform etching. The use of agitation via a pump was helpful in eliminating these, but not 100% reliable. Therefore all craters were routinely monitored using an optical microscope. Profiles obtained with non-uniform craters were rejected and the measurement repeated.

The choice of measurement conditions is established using various diagnostic tests before starting the depth profile. The choice of V is the most important, since in practice the depletion approximation is often only valid over a narrow voltage window. V must be chosen to yield a continuous value of dC/dV and to give a low reverse-bias leakage current. If these criteria cannot be met, then the sample must be rejected and the process must be repeated using a fresh sample.

Carrier concentrations are obtained with an absolute error of ±20% (in the range 10^{17} to 10^{20} cm^{-3}), and the use of a surface profilometer to measure the depth of the final crater determines the depth scale to an accuracy of ±10%. However there is often some loss in depth resolution during the measurement for two important reasons. Firstly the carrier profile obtained by the e-CV may not be the same as the dopant profile, because of carrier diffusion [Sze 1981]. Secondly the etch rate is not always uniform, especially during a $Si/Si_{1-x}Ge_x$ profile [Basaran 1991]. Although the e-CV measurement is more reliable than the SRP, both in depth resolution and in accuracy of determined carrier concentration, it should still only be used as a *qualitative* guide at present.

2.3.2 SECONDARY ION MASS SPECTROSCOPY (SIMS)

Most of the analysis in this thesis relies, in some way or other, on the interpretation of high resolution SIMS profiles of boron doped structures in Si and $Si_{1-x}Ge_x$. SIMS is the best technique available for obtaining chemical concentration profiles of abrupt modulation doped samples owing to its high sensitivity and dynamic range and its excellent depth resolution. Although SIMS is a well proven technique in the characterisation of dopant profiles in Si [Dowsett *et al* 1991], it is relatively unproven for the $Si_{1-x}Ge_x$ system. Key problems were identified with the technique as applied to $Si_{1-x}Ge_x$, which were evaluated by the author for a study of boron incorporation. The technique is discussed here, briefly, with a more detailed evaluation presented in Appendix I.

The SIMS technique generates a chemical concentration depth profile by sputtering the sample surface, using a primary ion beam at low energy (typically <4 keV), and monitoring the secondary ions produced. (Oxygen primary ion beams were used for obtaining SIMS profiles of Ge, Mo, Cu and boron, Cs^+ ions for C and O.) Primary ions impacting with the sample undergo a series of random collisions, sputtering atoms from their bulk positions. Of these the positive ions are usually collected, using an extraction potential. These are then mass filtered. A

count rate for the species of interest is then obtained at an ion detector. The primary ion beam is scanned across the surface, ideally forming a square crater with sides of $\simeq 400\mu m$, collecting ions from a well-defined area that is typically 40% smaller than the SIMS crater to avoid effects of enhanced sputtering from the crater walls. This is achieved either using ion optics or by rastering the primary ion beam and using an electronic gate. To a good approximation, the count rate is a function of the chemical concentration of a given species. The count rate is compared with that obtained from a known sample or standard profiled under the same conditions to give a chemical concentration accurate to $\pm 5\%$. The process takes place under high vacuum conditions, to avoid contamination of the sample, and to allow high sensitivities for the elements of interest. The effect of mass interference is avoided by either careful selection of isotope or by high resolution mass filtering. The continual erosion and measuring of the material produces a depth profile.

The final crater depth is measured *ex-situ* using a surface profilometer and the depth is calibrated, assuming uniform etch rate (see Appendix I).

Initially SIMS depth profiles were carried out in two instruments. The instrument and profiling conditions appropriate for the sample under investigation were instigated by the author (see Appendix I). SIMS was carried out by the Advanced Semiconductor Research group at Warwick using EVA 2000, a research instrument, and at Cascade Scientific (Uxbridge), a commercial facility, employing a Cameca IMS 4f machine.

2.3.3 DEFECT ANALYSIS

As with other growth methods, defects are inherent to the MBE technique, although they are at levels such that research into the growth and characterisation of devices with novel electrical properties is possible [Luryi and Sze 1988]. There are a large number of parameters involved in the study of defect formation, including the quality of the growth environment, substrate preparation, the degree of metallic contamination from the hardware (eg e-guns, substrate heater) and the use of

moving components such as the substrate rotating stage and shutters [Pindoria *et al* 1990B]. For an insight into the effect of defects on device performance readers are referred to Ravi (1981). The effect of MBE growth conditions on defect levels and on the nature of the defects are discussed by Pindoria *et al* (1990B).

Of interest in this work is how co-evaporation of boron at a given growth temperature affects material quality, either by adsorption of impurities directly associated with the boron effusion, or by any disturbance to the atomic processes during epitaxial growth.

Furthermore the difference in boron incorporation properties in strained and unstrained $Si_{1-x}Ge_x$ is unknown. Strained $Si_{1-x}Ge_x$ layers were studied, since these are most often used in the fabrication of novel devices by MBE (see Chapter 1). Relaxed $Si_{1-x}Ge_x$ layers show inordinately large defect levels, therefore defect assessment was used by the author for a qualitative determination as to whether or not the layers were strained. Defect levels were monitored by a combination of defect etch-reveal and electron microscopy measurements.

2.3.3a DEFECT ETCH-REVEAL

Most types of defects are invisible to the naked eye though a defect revealing etch can often be used to discern them. The choice of suitable etchant is one that will preferentially etch defects, and not dopant for example, at a controllable rate. For thin epitaxial layers the etch rate should be as slow as possible without compromising the uniformity of etch. The etch procedure should ideally be carried out according to a recognised 'standard', to enable comparison by future authors [ASTMS 1976B]. The dilute Schimmel etch (1.5 H_2O : 1 CrO_3 (0.75 ML) : 2 HF) was used for boron doped Si and $Si_{1-x}Ge_x$ layers. For the thin layers studied in the present work ($\approx 1\mu m$) it was found that defects were revealed best by removing ½ of the total thickness of the layer. Defect levels were assessed using an optical microscope, sampling different parts of the epilayer to account for the lateral inhomogeneity in defect density. Defect levels were quantified by measuring the

number of defects in a fixed sample area, and scaling this value to give a count in defects per cm^2. Defect levels often varied by at least an order of magnitude across the wafer; these statistical variations contributing to the largest source of error in the measurement.

2.3.3b ELECTRON MICROSCOPY

These techniques are advantageous for investigating defects in films that are too thin to be distinguished by a preferential etch. Scanning electron microscopy (SEM) and cross sectional transmission electron microscopy (XTEM) were both used. XTEM micrographs were used to resolve 'buried' features, such as boron precipitates, in highly doped regions grown at different temperatures (see Chapter 3). These measurements were time consuming and expensive, however, and were used sparingly. SEM was carried out in-house and XTEM measurements were carried out at Plessey Research (Caswell), under conditions discussed in Augustus *et al* (1990).

The optimum conditions for sample preparation and analysis of semiconductors are usually different from the procedures used in conventional XTEM measurements and are discussed in Pawlik (1988). For the present work samples were thinned, using an Ar^+ beam, then illuminated using a many beam symmetrical [110] condition to obtain a bright field image. This method is sensitive to changes in lattice parameter caused by strain or microdefects.

Under these conditions, boron precipitates and fully activated boron layers (at levels of $10^{20} cm^{-3}$) were observed in XTEM measurements, though the strain contrast mechanism was not clear [Augustus *et al* 1990].

The XTEM measurement provides a very large magnification ($\approx$ 100K), its field of view is very limited. Therefore the sensitivity of the technique to defects is generally $\approx 10^5\ cm^{-2}$.

CHAPTER 3

BORON SURFACE–ACCUMULATED PHASES FORMED DURING HEAVY DOPING

3.1 INTRODUCTION

A series of arguments will be used to show that boron solubility limits during Si MBE can be determined as the maximum *atomic* concentration under established growth conditions. This is as opposed to more conventional methods, which determine maximum *carrier* concentrations by annealing of boron 'saturated' bulk doped layers. Many of these arguments are developed in parallel, and the reader is introduced to the scope of the present work before they are given.

This Chapter is concerned with surface processes occurring after heavy boron doping using an elemental coevaporation source. At temperatures above 650°C, it is established that a surface accumulated phase of boron is observed. Evidence from SIMS depth profiles suggests that when a surface phase is formed under dynamic growth conditions it is self-limiting at coverages equivalent to 0.25 ML. Any attempt to exceed this surface coverage leads to the rapid formation of inactive boron precipitates that are observed in XTEM measurements. A mechanism for precipitation is proposed, involving enrichment and clustering of boron at the *immediate* surface.

The subsequent incorporation properties of the surface phase will be used to determine the solid solubility of boron in Si. These give good correlation with previously reported *equilibrium* solubility measurements determined in bulk doped layers for temperatures down to 700°C, the current lower limit. The present study has been extended to 450°C using Hall measurements in uniformly doped layers to determine maximum carrier concentrations. The low temperature behaviour is quite different, as the formation of the surface phase becomes kinetically limited, leading to a sharp upturn in solubility limits. In this non-equilibrium temperature regime,

maximum carrier concentrations are dominated by reductions in incorporation efficiencies. No evidence of boron precipitation was observed at temperatures below 600°C.

3.2 PREVIOUS WORK

Reports in the literature, notably by Jackman *et al* (1988 and 1989), suggested that the use of boron compound sources led to strong redistribution of dopant during heavy doping. In their investigation of boron incorporation from B_2O_3 sources and its temperature dependence, highly doped layers were grown at temperatures varying from 800 to 600°C, at doping levels above the solubility limit. This work established that at doping levels greater than $10^{20}cm^{-3}$, severe "segregation" of boron occurred, manifested by a shoulder formed in the growth direction and by narrow spikes in SIMS depths profiles formed by boron precipitation. However, the mechanism by which precipitation occurred was not clear [Jackman *et al* 1989]. The authors reported an areal density in the shoulders equivalent to 0.35 ML (1 ML=$6.78x10^{14}cm^{-2}$ on Si(100) surfaces). No further analysis of the shoulder features was presented. At 600°C, the shoulder formation was inhibited allowing reasonable profile control at this temperature. However this abrupt change in temperature behaviour coincided with a sharp uptake in oxygen, at levels $> 10^{20}cm^{-3}$, responsible for an increase in defect levels and poor crystalline quality. This made the observed results inconclusive since such transitions in incorporation behaviour had been already been associated with a sharp uptake of oxygen from compound sources [de Frésart *et al* 1988].

Headrick *et al* (1990) observed a maximum electrically active coverage equivalent to 0.5 ML by interrupting Si growth and depositing large surface sheet concentrations of boron at temperatures down to 450°C. An HBO_2 source was used. Oxygen incorporation was removed by elevating the growth temperature to 700°C for ten minutes. However, the use of an annealing stage to investigate the temperature dependence of dopant incorporation must be regarded as suspect.

Clearly further work was necessary, first in verifying any existence of a temperature regime ideal for the growth of narrow highly doped layers. These are often necessary for doping in the $Si_{1-x}Ge_x$ system. Secondly, a *mechanism* for precipitation and dopant redistribution was needed. The lack of impurity incorporation associated with the use of elemental boron sources would enable a more thorough investigation of boron incorporation at heavy doping levels to be carried out at temperatures as low as 450°C.

3.3 THE 'REDISTRIBUTION EXPERIMENT'

The 'redistribution experiment' was carried out by the author using an elemental boron source. This avoids direct oxygen incorporation, responsible for the poor layer morphology at low temperatures observed by Tatsumi (1990 A), de Frésart *et al* (1988) and Jackman *et al* (1989). Boron doped layers were grown at doping levels of $1.4x10^{20}$ and $5x10^{18}cm^{-3}$, and at temperatures between 900 and 450°C, thus extending the previous studies to temperatures below 600°C.

3.3.1 BORON PROFILE CONTROL IN LOW DOPED LAYERS

For the first part of this study, the temperature dependence of boron incorporation was investigated, for temperatures between 900 and 450°C, at boron doping levels well below the solid solubility limit [Vick and Whittle 1969]. This was achieved by growing a modulation doped structure (denoted structure A) in the V80H MBE system (see Chapter 2). Structure A features 50 nm thick boron doped Si layers (doped at $5x10^{18}cm^{-3}$) separated by 200 nm of undoped Si. The growth rate was 0.28 nms^{-1}. The SIMS depth profile of this structure is presented in Fig. 3.1a. This appears to show excellent profile control over the entire temperature range, although solid state diffusion effects are evident at temperatures above 800°C. However a closer investigation revealed a profile smearing dependence on temperature, but only on a nanometre scale (see Chapter 4). An e-CV profile of this

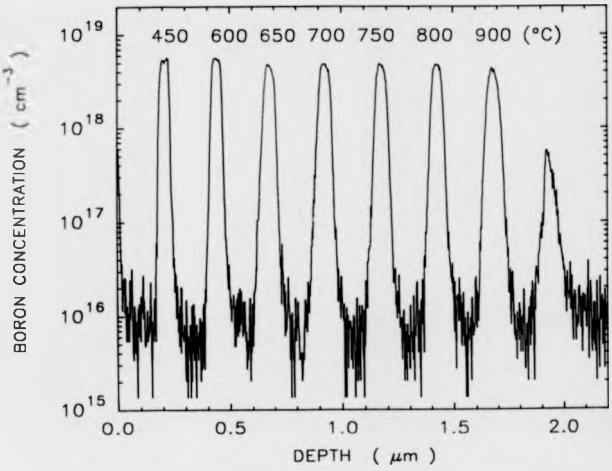

Fig. 3.1a. Boron SIMS depth profile of a modulation doped structure grown at 0.28 nms^{-1} (denoted structure A). Boron doped layers were doped at a peak level of 5×10^{18}cm^{-3} and grown at temperatures varying from 900 to 450°C.

structure, obtained by the author (see Fig. 3.1b), indicates complete activation of dopant of the entire temperature range. A SIMS study indicated carbon incorporation below the detection limit, at this doping level, and oxygen incorporation of $\approx 10^{19}cm^{-3}$, only at the lowest temperature, owing to incorporation from the residual gas (see Chapter 4). Further improvements in oxygen levels at low temperature are expected with an improvement in vacuum quality.

3.3.2 BORON REDISTRIBUTION IN HIGHLY DOPED LAYERS

For the second part of this study a similar structure was grown, also in the V80H system, except that boron layers were doped at a level of $1.4x10^{20}cm^{-3}$ (denoted structure B). These levels are well above previously published bulk solubility limits [Vick and Whittle 1969, Schwettman 1974]. Otherwise the growth conditions were the same as those for structure A. Boron SIMS and carrier concentration depth profiles of structure B are given in Figs. 3.2a and 3.2b respectively. The SIMS depth profile shows severe redistribution of boron occurring for temperatures at and above 700°C and discernible redistribution at temperatures of 650°C. The severe redistribution is observed as narrow 35 nm wide spikes, at higher than intended peak concentrations, and shoulders $\approx$ 100 nm wide extending in the growth direction into the nominally undoped region. The shoulder levels determined from the e-CV measurements and by SIMS are in good agreement, within the experimental error, indicating that the shoulders are completely activated. The narrow spikes do not appear to be active, as they are not observed in the e-CV profile. Evidence from thicker spikes, grown under similar conditions, suggests that these are indeed inactive and not too thin to be resolved by the e-CV technique.

At temperatures of 600°C and below profiles appear almost 'ideal', though some improvement in profile abruptness is observed by reducing the growth temperature from 600 to 450°C (see Chapter 4).

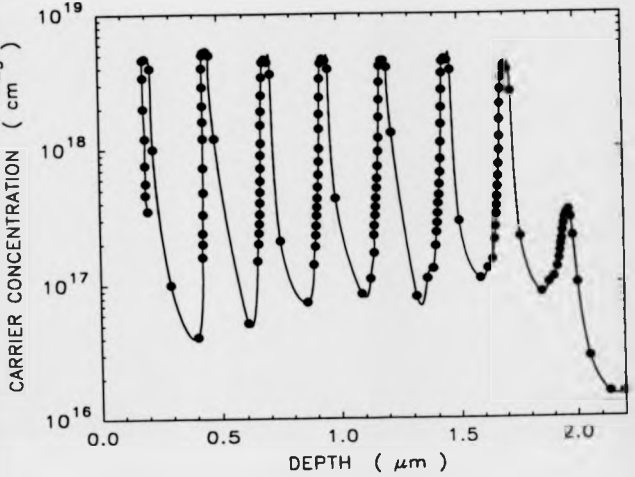

Fig. 3.1b E-CV depth profile of structure A.

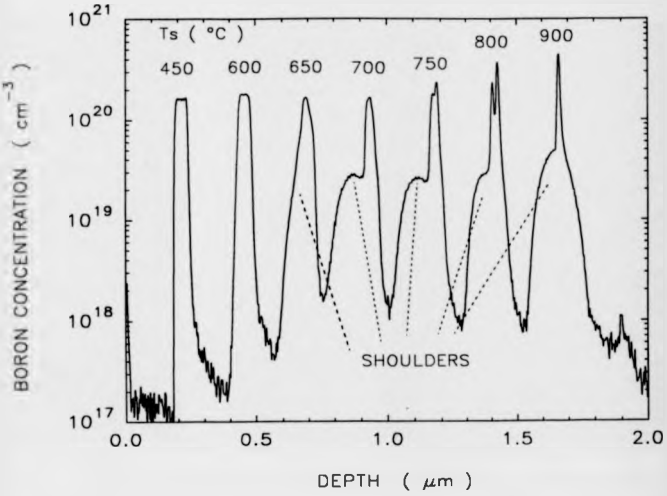

Fig. 3.2a Boron SIMS depth profile of structure B, containing boron doped regions nominally 50 nm thick, separated by 200nm of undoped Si, grown at temperatures indicated on the diagram. The shoulders observed above 650°C are caused by surface accumulation of boron. The narrow spikes by boron precipitates (see text).

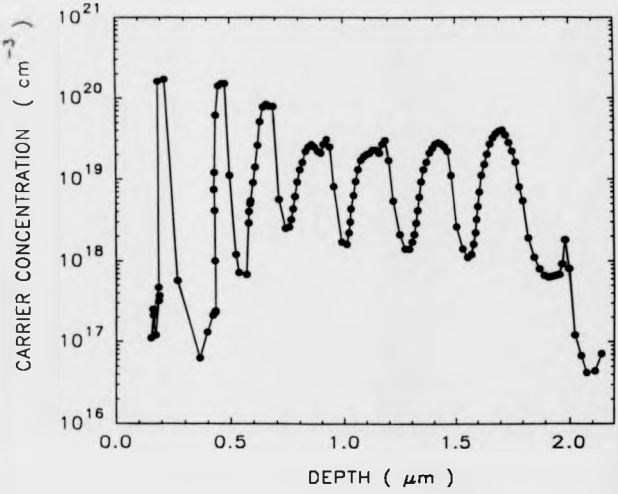

Fig. 3.2b E-CV profile of structure B. The shoulders observed in the SIMS profile above 650°C are also seen in the e-CV profile, and at the same level. The narrow spikes, observed in the SIMS profile, are not seen in the e-CV profile.

The mechanism responsible for the dopant deactivation in the narrow spikes was investigated using XTEM microscopy. Fig. 3.3a shows a bright field image of structure B. The fully activated layers, grown at temperatures of 600 and 450°C, appear as uniform dark bands 50 nm thick, thought to be due to strain contrast at this high incorporation level [Augustus *et al* 1990]. At and above 650°C, the boron doped layers and the shoulders are not readily resolved, and are seen instead as regions containing small ≈30 nm precipitates. The SIMS spikes and XTEM precipitated regions appear at the same depths. An increased magnification (see Fig. 3.3b) reveals the precipitates more clearly, seen as planar in distribution at temperatures above 750°C, with a double layer of precipitates forming at 800°C.

These results indicate that the boron precipitation and associated profile redistribution, observed at heavy doping, is not unique to the use of compound sources. These effects were investigated by the present author, to try to elucidate some mechanism by which these phenomena occur.

3.3.3 TEMPERATURE DEPENDENCE OF SHOULDER FORMATION

The contrasting temperature behaviour of boron incorporation is clearly seen at three temperatures in structure B. Figs. 3.4a, 3.4b and 3.4c show enlargements of structure B grown at 750, 450 and 650°C respectively. Features in these identify three temperature regimes that will be discussed separately before solubility limits are discussed.

3.3.3a) High temperature behaviour (750-900°C)

Each boron doped region in structure B was grown in approximately 10 minutes. However considerable dopant deactivation has occurred during this time (see Fig. 3.4a). Comparison between dopant precipitation during Si epitaxial growth and precipitation in bulk doped layers can be made by annealing a uniformly doped layer grown by Si MBE. This was 300 nm thick, grown at a temperature of

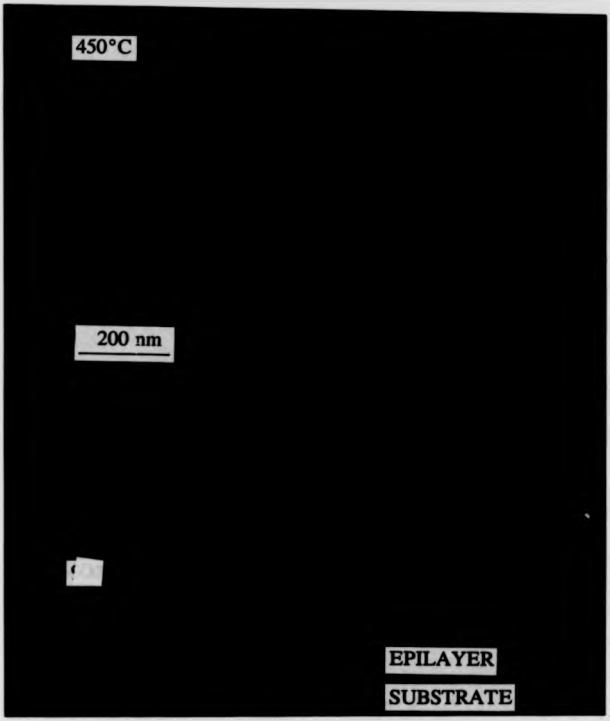

Fig. 3.3a XTEM micrograph of structure B. Boron doped regions grown at low temperatures appear as 50 nm dark bands. The precipitates are seen as narrow lines at depths which coincide with the spikes in the SIMS depth profile.

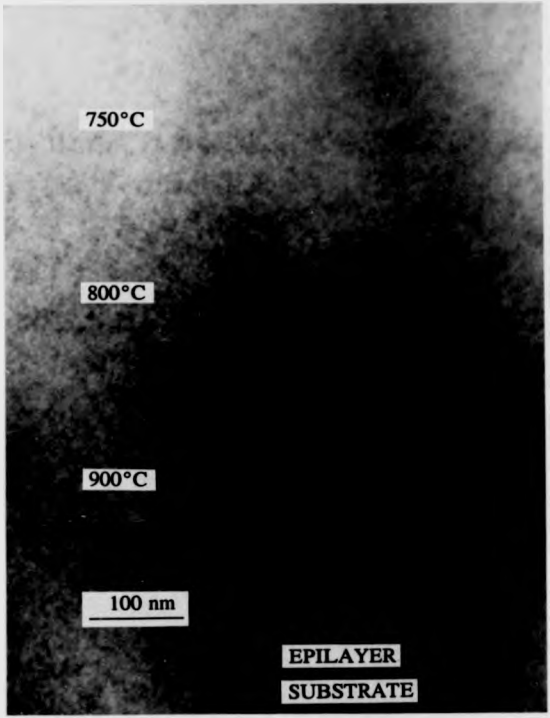

Fig. 3.3b XTEM micrograph of structure B, using an increased magnification, revealing more detail in the layers grown at temperatures above 750°C. Here the precipitates are observed as being planar in distribution, at temperatures above 750°C. A double layer of precipitates is seen at 800°C.

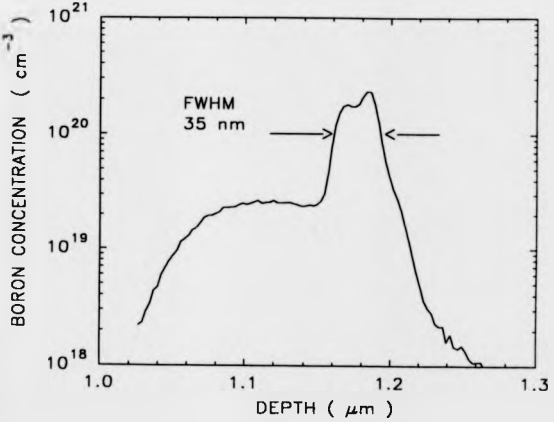

Fig. 3.4a Enlargement of the layer in structure B grown at 750°C.

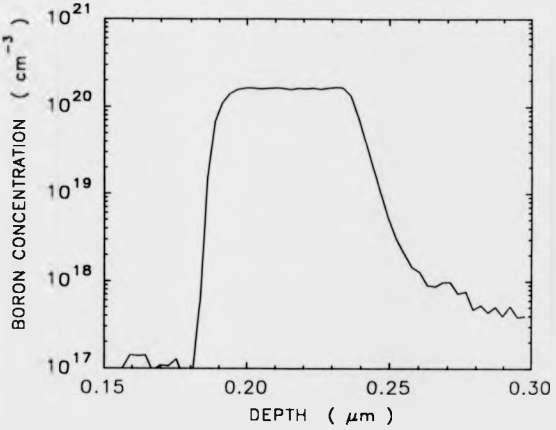

Fig. 3.4b Enlargement of the layer in structure B grown at 450°C.

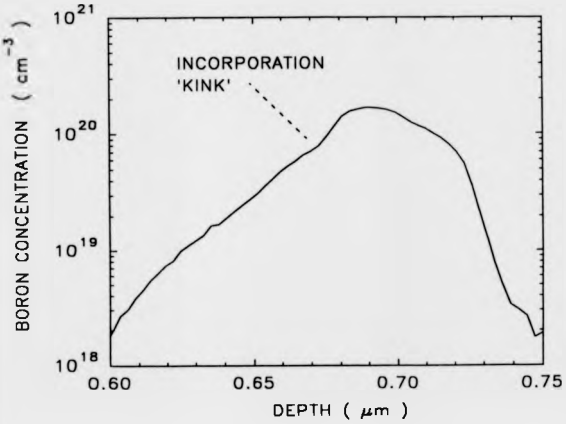

Fig. 3.4c Enlargement of the layer in structure B grown at 650°C.

600°C, and was completely activated with an initial carrier concentration of $1.3x10^{20}cm^{-3}$. This carrier concentration is similar to the level as that intended in structure B. Shown in Fig. 3.5 is a graph of carrier concentration, obtained from Hall measurements, versus anneal time for this sample. Anneal temperatures of 750 and 900°C were used. It can be seen that there is little change in carrier concentration after a 2 hour anneal at 750°C, indicating that fully incorporated dopant is stable to thermal anneals and that precipitation processes occurring in bulk-doped material proceed much more slowly than during Si MBE. The stability of this layer to an *ex-situ* anneal reflects the good material quality obtained by Si MBE [Landi *et al* 1988]. The precipitation rates in bulk material must be contrasted with those in the boron doped regions in structure B grown at temperatures between 900 and 700°C, which show strong precipitation although they were each grown in 10 minutes.

It is possible to identify the mechanisms responsible for the difference in precipitation rates in bulk-doped material and during epitaxial growth at temperatures above 700°C. It will be inferred that the two factors contributing to the rapid precipitation rates observed in Si MBE are a) a strong tendency for boron to surface accumulate, at these doping levels, leading to the build-up of a boron surface adlayer and b) large enhancements in boron diffusion. These factors suggest that precipitation occurs at the immediate surface during Si MBE, and will be discussed in turn.

Evidence for a high degree of surface accumulation at the growing surface comes from the shoulder formation seen in structure B (see Fig. 3.4a). This suggests strong surface enrichment leading to the formation of a boron adlayer. The shoulder in the SIMS profile is formed when the cell shutter is closed and the adlayer accommodates. The boron adlayer formation is not observed in structure A, suggesting that the adlayer formation is associated only with heavy doping. Surface accumulation of boron leading to an increase in precipitation rates can be considered as a 2D analogue to bulk-doped studies, for which a high starting bulk

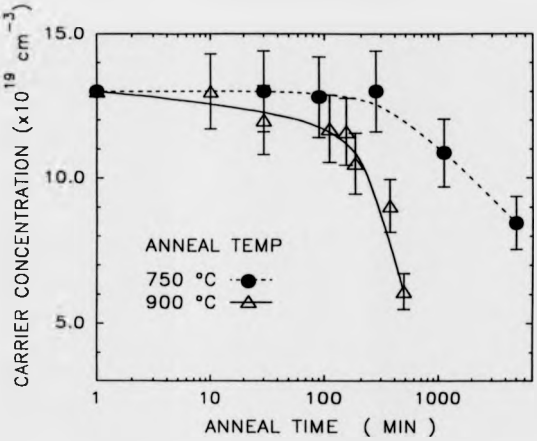

Fig. 3.5 Carrier concentration versus time for *ex-situ* annealing of a uniformly doped boron layer grown by Si MBE, with an initial carrier concentration of $1.3 \times 10^{20} cm^{-3}$. Annealing temperatures of 900 and 750°C were used.

concentration, or 'supersaturation', of dopant reduces the nucleation time necessary for the formation of precipitate sites [Solmi *et al* 1990] and thus increases precipitation rates.

However, the formation of a surface adlayer is not in itself the mechanism responsible for precipitation during epitaxial growth. There must also be some diffusivity of dopant reflected by the observed clustering of dopant. An enhancement in boron diffusivity is evidenced from the distribution of precipitates in an XTEM micrograph of structure B in Fig. 3.3b. This shows that the precipitates are distributed in a quasi-planar manner suggesting that they are formed, at the immediate surface, by a net lateral migration of dopant atoms. If boron adatoms migrate across the surface, in a similar manner to which Si atoms find an incorporation site during 2D epitaxial growth (see Chapter 1), the mean spacing of the precipitates can be used to infer dopant diffusion parameters [Burton *et al* 1951]. For the case of boron an Arrhenius plot of precipitation spacing in structure B yields an approximate value for the activation energy for nearest neighbour surface diffusion. This is found to be $Ea \approx (0.5 \pm 0.2)$eV. The large error is due to the scarcity of data points and the difficulties in resolving the precipitates in Fig. 3.3b. Hence, although further studies are necessary, the rapid precipitation rates and their distribution is qualitatively consistent with a nearest neighbour activation energy of ≈ 1 eV. In bulk-doped studies the activation energies for solid-state diffusion of boron are much higher, at approximately 4eV [see Dominguez and Jaraiz 1985 and references therein]. Large enhancements in dopant diffusivity near the surface have been observed previously in studies of Sb segregation [Barnett *et al* 1985, Greene *et al* 1985, Jorke *et al* 1988]. It is suggested that diffusion coefficients become orders of magnitude higher than in bulk material, since Sb adatoms are only weakly bound near the growing surface, reducing the activation energy for each diffusion step. Hence the planar distribution of the precipitates in structure B is consistent with boron diffusing at the immediate surface rather than in the bulk. However the observations of Sb incorporation

behaviour usually assume back-diffusion of dopant from *below* the surface, and cannot account for the strong lateral diffusivity implied by the planar distribution of the boron precipitates. This will be discussed further in a following section.

3.3.3b) Low temperature behaviour (<600°C)

The surface enrichment and clustering processes causing precipitation become severely kinetically limited at 600°C and below. In this temperature regime complete activation of dopant is achieved in structure B, indicated by the good agreement of carrier concentrations and total concentrations (determined by SIMS). Surface enrichment is almost *completely* inhibited at 450°C in structure B (see Fig 3.4b), indicated by the SIMS leading edge slope that is steeper than the accepted 2 nm/decade resolution limit of the SIMS technique under these profiling conditions [Dowsett *et al* 1991]. E-CV measurements suggest that in this temperature regime boron is fully activated at levels of $1.4 \times 10^{20} cm^{-3}$. This temperature is ideal for the growth of narrow highly doped layers, and higher levels than those achieved here are possible (see section 3.5.2).

3.3.3c) Intermediate temperature behaviour (650-700°C)

In this temperature regime an abrupt transition in shoulder formation and precipitation processes is observed. At intermediate temperatures the processes of surface accumulation and surface clustering, which contribute to precipitation, become inhibited. Fig. 3.4c shows the peak in structure B grown at 650°C. This peak is of interest because it shows a change in boron incorporation behaviour in the slope formed after the source shutter has been closed. This is seen as a discontinuity or 'kink' in the SIMS leading edge (denoted by an arrow). The kink appears to be due to incorporation of a boron phase still on the surface after the boron shutter had closed, in the same way that the shoulders were formed at higher

temperatures, although it is not defined as clearly. E-CV measurements indicate that dopant up to the level of the kink is fully activated at a level of $8x10^{19}cm^{-3}$. So although surface accumulation of boron is still evident at 650°C, causing dopant 'supersaturation' at the growing surface, the lateral diffusion necessary for the growth of the precipitates becomes retarded, causing a sharp rise in carrier concentrations during Si MBE at low temperatures.

Such an abrupt change in incorporation behaviour (in this case surface enrichment and surface clustering) is characteristic of a transition from equilibrium-limited to kinetically-limited incorporation processes [Barnett and Greene 1985, Jorke 1985], suggesting that in the high temperature regime, equilibrium may be achieved. This will be discussed further in section 3.5.1.

3.4 VERIFICATION OF A BORON SURFACE PHASE

An interesting property of the shoulders in structure B is that they have an areal density of $(1.68\pm0.08)x10^{14}cm^{-2}$, equivalent to a boron coverage of 0.25ML. The only exception to this result was observed in the layer grown at 800°C that contains an areal density equivalent to 0.4 ML of boron. This layer is also unique in that a double spike is formed (see Figs. 3.2(a) and 3.3(b)). Jackman *et al* (1989) observed a sheet density of 0.35 ML in the shoulders of a similar structure, though the boron doped regions in this work were grown too close to each other to define the shoulders properly. Headrick *et al* (1990) observed a self-limiting coverage of 0.5 ML though this was achieved, under static conditions, by interrupting growth and 'building up' a boron layer.

The apparent agreement in shoulder sheet densities in structure B was investigated by growing further modulation doped structures. These contained highly doped boron regions grown at temperatures of 700°C, but at different growth rates and boron sheet densities. These were grown at rates of 0.15 and 0.10 nms^{-1}. SIMS profiles of these structures (denoted C and D respectively) are shown in Figs. 3.6a and 3.7a. In structure C, solid-state diffusion effects are

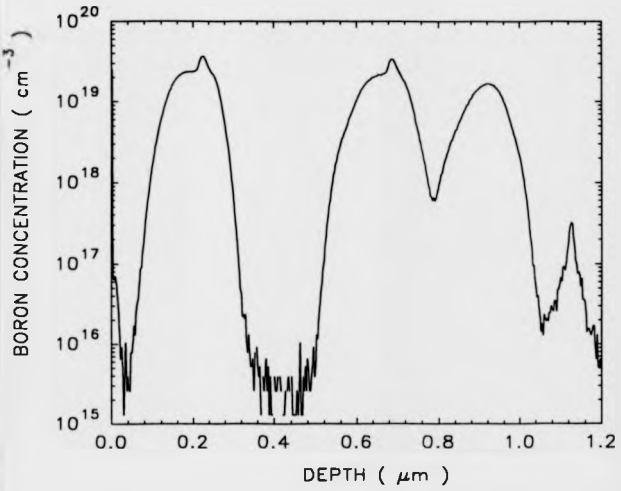

Fig. 3.6a Boron SIMS depth profile of a modulation doped structure grown at 700°C and at a rate of 0.15 nms^{-1} (structure C).

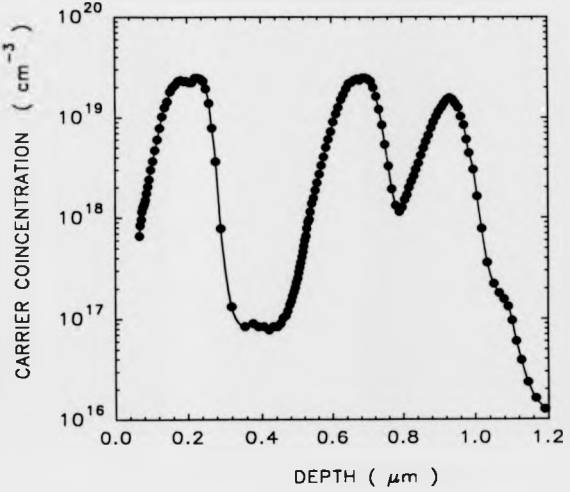

Fig. 3.6b E-CV depth profile of structure C. The spikes in the SIMS are not seen in the carrier concentration profile.

evident, since the precipitates in the peak nearest the substrate have completely redissolved. The two peaks nearer the surface in structure C feature a shoulder at a level that is significantly lower than the comparable shoulder in structure B which was grown at a rate of 0.28 nms^{-1}. Fig 3.7a shows that at a lower growth rate still (0.1 nms^{-1}) the shoulder appears at a level of $1.3x10^{19}cm^{-3}$. E-CV measurements of these structures confirm the electrically inactive nature of the 'spikes' (see Figs. 3.6b and 3.7b respectively). Dopant in the shoulders is completely activated, consistent with the behaviour in structure B.

As in structure B the shoulders contain a sheet density of boron equivalent to 0.25 ML. Hence despite the fact that the boron doped layers were all grown at different temperatures, growth rates, and sheet concentrations, with the one exception, there appears to be some common upper limit to the boron surface adlayer at high doping levels. A mechanism for precipitation in structures B C and D can be inferred from this observation. During heavy doping, surface enrichment of boron occurs until a surface phase with a coverage of 0.25 ML is formed. Because the phase is 'limited' at this value, any attempt to continue doping at this level leads to the formation of precipitates. The *lateral* distribution of the precipitates depends on the growth temperature and on boron diffusion rates, but the position of the precipitates in the *depth* profile relates to rate of development of the surface phase. Hence the planar distribution of the precipitates is explained.

3.5 DETERMINATION OF SOLID SOLUBILITY LIMITS FOR BORON IN Si

3.5.1 CRITERIA FOR DEFINING SOLUBILITY LIMITS

The boron surface phase surface accumulates, until the cell shutter is closed, after which it becomes unstable and incorporates. Because the surface phase exists at such a high coverage it seems likely that, until it depletes, it releases boron at a

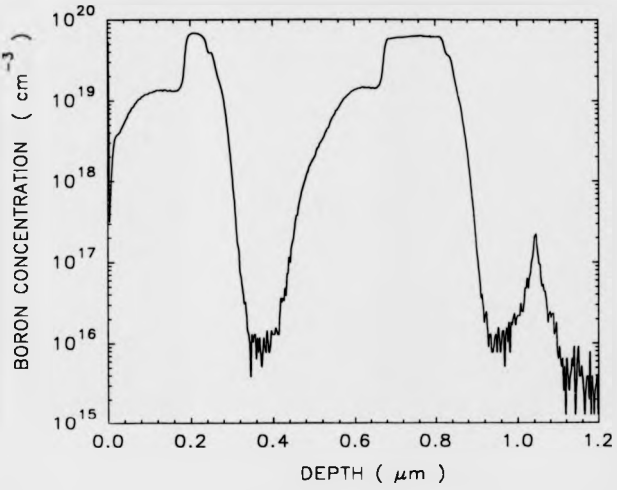

Fig.3.7a Boron SIMS depth profile of a modulation doped structure grown at 700°C and at a rate of 0.10 nms^{-1} (structure D).

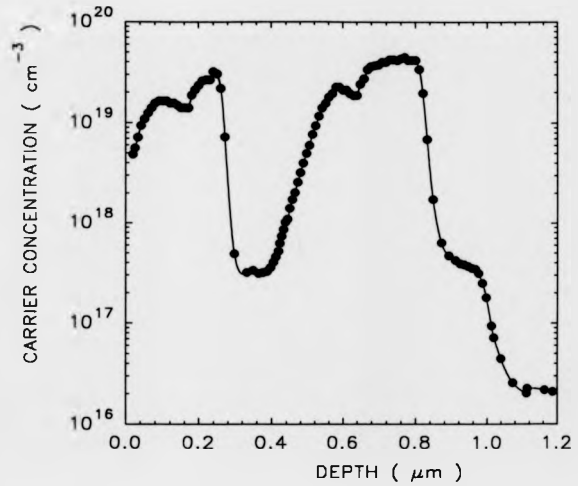

Fig. 3.7b E-CV depth profile of structure D. The spikes in the SIMS are not seen in the carrier concentration profile.

level corresponding to the maximum amount of dopant which can be incorporated at that temperature. However, does the level in the shoulders correspond to the *equilibrium* solid solubility of boron? At temperatures above 700°C, the levels in the shoulders appear to correlate with published solid solubility limits of boron in Si, obtained by bulk annealing of highly doped layers [Vick and Whittle 1969, Schwettman 1974]. However, MBE growth is strictly a non-equilibrium process, since growth takes place under conditions of high supersaturation [Kasper 1982]. It has been suggested that the high quality of epitaxial layers implies that at higher temperatures "local equilibrium" is formed at the growing surface in terms of the time scale of most experiments [Herman and Sitter 1989].

Fig. 3.8 shows a graph of shoulder level in structures B C and D versus growth rate, for layers grown at 700°C. This graph indicates that there is a discernible dependence of shoulder level on growth rate at this temperature. This weak dependence of shoulder level on growth rate in this intermediate temperature regime (see section 3.3.3c), suggests that the surface incorporation processes occurring at higher temperatures may be in equilibrium, therefore additional structures were grown to investigate this.

3.5.2 SOLUBILITY LIMITS IN BULK DOPED LAYERS

The wealth of *bulk* solubility data in the literature is obtained by annealing highly-doped layers until equilibrium between precipitates and surrounding dopant is achieved. (The term bulk, in this context, is used to refer to uniformly boron doped layers.) These are often doped by ion implantation or by diffusing boron onto the surface of a wafer. Once it is established that continued annealing does not produce any change in carrier concentration, the measured value is assumed to be at the solid solubility at that temperature [Armigliato *et al* 1977]. Other workers have used SRP depth profiles to determine solubility limits by measuring shoulder levels in the diffusion tail formed after annealing ion implanted layers [Landi *et al* 1988 and Solmi *et al* 1990]. The shoulders are formed by boron diffusion out of the

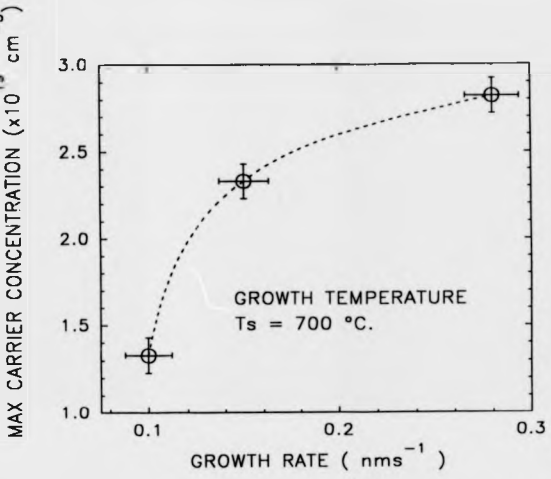

Fig. 3.8 Plot of peak concentration in the shoulders of structures B, C and D grown at 700°C, against growth rate. The discernible dependence of shoulder level on growth rate, at this temperature, is not observed at temperatures above 750°C.

saturation doped region, at a level limited by the solubility limit at the anneal temperature.

In such studies precipitation occurs after solid solubility limits have been exceeded, causing dopant deactivation [Armigliato *et al* 1977, and Solmi *et al* 1990]. Dopant atoms diffuse towards precipitation centres that may either grow at the expense of surrounding dopant or act as sources of boron, depending on the temperature. Once equilibrium between the inactive precipitates and the surrounding dopant has been reached, the measured carrier concentration is at the solid solubility limit at that temperature. The time taken for equilibrium to be reached in bulk-doped material depends, initially, on the time for nucleation of precipitates [Landi *et al* 1988] and then on boron diffusion rates [Ham 1958]. The nucleation time has been shown to decrease with increasing degrees of dopant saturation and increasing material damage (due to implantation for example). Hence the time necessary to establish equilibrium at lower temperatures varies and can be as long as 40-200 hours at 750°C, for example, leading to discrepancies in published data and a lack of information on solid solubility limits at temperatures below 900°C.

Solid solubility limits during MBE can be determined by making electrical measurements of maximum carrier concentrations on uniformly doped layers. These were grown with boron concentrations well above previously published solid solubility data, and at temperatures ranging from 450 to 800°C. Carrier concentrations in these samples (see Table 3.1) were determined from Hall measurements using a scattering factor $r=0.7$ appropriate for boron at these high doping levels [Sasaki *et al* 1988]. All samples showed bulk-like mobilities [Sasaki *et al* 1988].

These samples show contrasting incorporation behaviour, demonstrating dopant deactivation by combinations of precipitation and surface accumulation processes.

TABLE 3.1

Maximum carrier concentrations of uniformly doped samples grown by Si MBE at various growth rates and temperatures.

Sample I.D.	Growth rate/nms^{-1}	Growth Temp/°C	Boron conc. x10^{19}cm^{-3} ±5%	Carrier conc. x10^{19}cm^{-3} ±10%	Hole mobility cm^{2}V^{-1}s^{-1} ±10%	Epilayer Thickness nm
A	0.28	800	20	3.5	36	840
B*	0.1	760	13	2.8	46	300
C*	0.1	670	14	4.1	44	300
D*	0.1	600	13	13	38	300
E**	0.01	600	2.8	2.8	40	20
F**	0.01	450	35	36	35	20

* ** Superscripts denote same boron flux rate.

At temperatures of 670°C and above (see samples A-C), a comparison of SIMS and carrier concentrations indicates that considerable dopant deactivation has occurred with maximum carrier concentrations lower than boron chemical concentrations and in the $10^{19}cm^{-3}$ range. This difference in concentrations is due to boron in excess of the solubility limit going into the formation of inactive precipitates. A comparison of SIMS and e-CV depth profiles of sample C confirms this behaviour (see Fig. 3.9).

From an equilibrium thermodynamics argument solubilities should fall with decreasing temperature [Armigliato *et al* 1977]. However at 600°C and below (D-F in Table 4.1), SIMS and Hall concentrations were in good agreement with carrier concentrations up to $3.6x10^{20}cm^{-3}$. This indicates complete activation of dopant in this low temperature range, consistent with the present author's earlier observations of low temperature incorporation behaviour [Parry *et al* 1991 B].

At very low growth rates and at 600°C (see sample E grown at $0.01nms^{-1}$), dopant concentrations were much lower than intended, owing to a reduction in boron incorporation efficiency rather than precipitation. Samples E and F were grown at 600 and 450°C respectively. These layers were exposed to the same boron flux and grown at the same rate, yet they show markedly different carrier concentrations. Unlike samples grown at 670°C and above, both show complete activation of dopant. The reduced boron carrier concentration observed at 600°C cannot be attributed to dopant deactivation, therefore the reduction must be due to a decrease in boron incorporation efficiency at the lower growth rate. Measurements on modulation doped structures (discussed in the previous section) suggest that the reduction in maximum obtainable carrier concentration, at this temperature and growth rate, is due to strong surface accumulation of boron. Surface accumulation shows a growth rate dependence (see Chapter 4), and the increased growth rate is responsible for the increase in maximum achievable carrier concentration in sample D (also grown at 600°C but at $0.1\ nms^{-1}$).

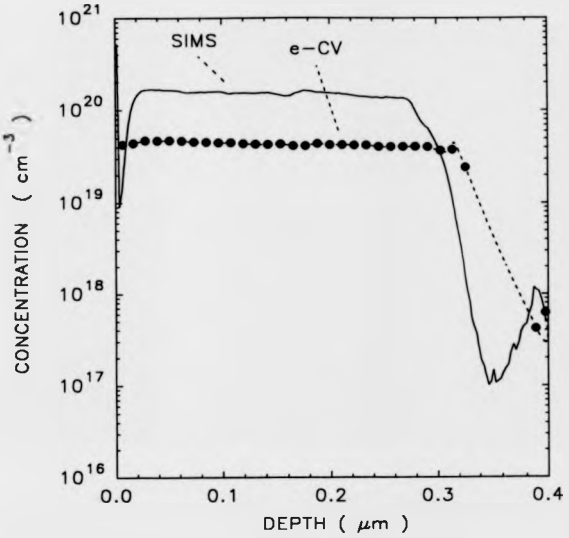

Fig. 3.9 SIMS and E-CV depth profiles of sample C, a uniformly boron doped layer grown at 670°C (see Table 4.1). The difference between chemical and carrier concentrations indicates that boron deactivation has occurred.

3.5.3 SUMMARY OF MBE SOLUBILITY DATA

Fig. 3.10 summarizes the present data of measured boron solubility limit. The data points are taken from the levels in the shoulders in structure B and from the Hall concentrations of the uniformly doped layers grown at lower rates and different boron fluxes (see Table 4.1). Also included for comparison are the bulk data of Vick and Whittle (1969), and Schwettman (1974). Good agreement with Schwettman is obtained, and the present results are within 20% of those of Vick and Whittle, consistent with their use of Irwin's resistivity versus carrier concentration curve to establish carrier concentrations from resistivity data. The solid solubilities determined from shoulder levels show an exponential temperature dependence, with an activation energy of 0.8 ± 0.1 eV which compares favourably with the value 0.75 eV obtained from electrical measurements of annealed bulk-doped layers [Armigliato *et al* 1977]. This, and the good agreement of solid solubility, determined from the shoulders in structure B, with that determined from the Hall measurements of uniformly doped layers, provides qualitative evidence of the assumption that the levels in the shoulders do define *equilibrium* solid solubilities. In fact the shoulders define solid solubility limits more precisely than the carrier concentrations in the narrow spikes in Fig. 3.2b. Carrier concentrations in the immediate region of the precipitates are actually higher than the solid solubility. This displacement of the equilibrium condition towards higher solid solubility values is due to a free-energy term induced by the curved surface of the precipitates [Armigliato *et al* 1977].

In the case of non-equilibrium incorporation ($< 700°C$), the maximum carrier concentrations do not represent solid solubilities but define the maximum electrically active levels achievable under the growth conditions specified. Hence they are only expected to have general applicability to the case of MBE growth. It is expected that, by reducing further the Si growth rate at low temperature, the measured maximum carrier concentrations will reach the equilibrium values.

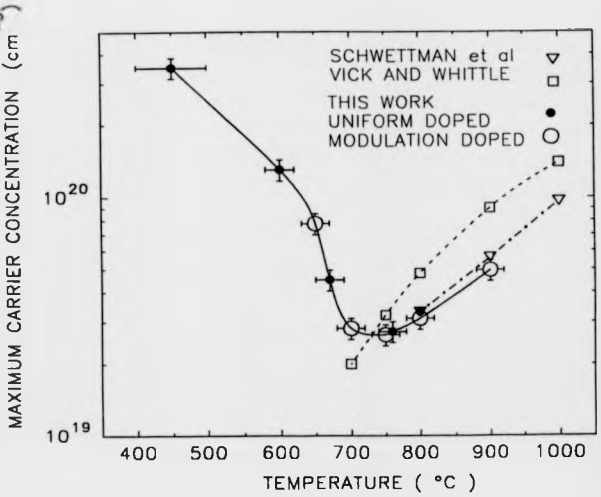

Fig. 3.10 Solid solubility of boron in Si as a function of temperature, as determined from the shoulders of modulation doped structures, and from uniformly doped layers grown at different rates and boron fluxes. At 450°C higher levels may be possible. Previously published bulk data are given for comparison [Vick and Whittle 1969, and Schwettman 1974].

3.6 DISCUSSION OF BORON INCORPORATION DURING HEAVY DOPING

As well as determining solubility limits from SIMS depth profiles it is also possible to infer processes occurring at the growing surface during Si MBE by comparing observed incorporation phenomena, in this case surface accumulation and surface clustering, with predictions from published models for dopant incorporation. The lateral distribution of the precipitates and the formation of a self-limiting boron phase cannot be explained by models of surface segregation, which invoke back-diffusion of dopant from underlying layers [Barnett and Greene 1985, Greene *et al* 1985, Jorke 1985, Jorke *et al* 1988 and Jorke and Kibbel 1990]. Such models propose that surface enrichment takes place by diffusion of previously incorporated dopant back to the surface of the growing layer, or the exchange of subsurface dopant atoms and deposited Si atoms (see Chapter 4). The observed distribution of the precipitates requires a net lateral displacement or clustering of dopant atoms. This cannot be explained by exchange of boron and Si atoms, or back diffusion of dopant. Jorke and Kibbel suggest a mechanism for surface clustering without lateral diffusion at the surface [Jorke and Kibbel 1990]. They point out that the exchange of a Si atom and a subsurface boron atom causes a *net* lateral translation of $\pm a_o/2\sqrt{2}$ of the boron atom across the Si(100) surface. However the observed spacings of the precipitates are too large for them to be produced by this mechanism (see Fig. 3.3b), suggesting stronger surface diffusion of dopant.

A comparison of samples E and F in Table 3.1 shows further deviation from this proposed method of clustering. Surface enrichment is very much evident in sample E (see Table), since it shows a reduction in boron incorporation efficiency so that the total boron concentration is less than sample F. However, a consequence of the exchange process is that any strong surface enrichment would, directly, produce precipitates. Although sample E shows a strong reduction in incorporation efficiency, it is completely activated.

Dopant accumulation as proposed by Andrieu *et al* (1989) involves the lateral motion of dopant atoms at the surface as a precondition for surface accumulation. In this model the lateral migration of dopant is a pre-requisite for describing incorporation behaviour. Despite these differences in the surface accumulation mechanism, this theory results in identical rate-dependent kinetic equations to those obtained by Barnett and Greene. Previously observed accumulation behaviour can be well accounted for by both. This is particularly so for profile smearing and its dependence on temperature and growth rate. The present work provides the first experimental evidence to favour one model rather than the other.

3.7 CONCLUSIONS

The formation of a boron surface-accumulated phase has been observed, during heavy doping at temperatures above 650°C. Surface-accumulated boron phases, formed during deposition, are limited to a coverage of 0.25ML over a wide range of temperatures and growth rates. Any attempt to exceed this amount of surface coverage, leads to the formation of precipitates. A mechanism for boron precipitation during Si MBE has been suggested, involving simultaneous surface accumulation, and lateral diffusion of boron atoms.

The subsequent incorporation behaviour of the boron surface phase means that measurements of maximum carrier concentrations can be made by observations of peak doping levels in the shoulders of suitable modulation doped structures, as well as by measuring carrier concentrations in uniformly doped layers. Using this method, equilibrium solubility limits of boron in Si have been determined in the temperature range 900 to 700°C. For temperatures above 700°C measured solubility limits show an exponential temperature dependence, with an activation energy of 0.8 ± 0.1 eV, in good agreement with previously published data obtained by annealing of bulk-doped Si.

At intermediate substrate temperatures maximum carrier concentrations, as determined from the shoulders in modulation doped structures, were found to be growth rate dependent, decreasing with decreasing growth rate.

For growth at or below temperatures of 600°C, boron levels were completely activated, with bulk-like mobilities. The maximum carrier concentration achieved was $3.6 \times 10^{20} cm^{-3}$ at 450°C, and any reductions in maximum carrier concentrations were due to surface accumulation rather than precipitation. The upper limit to maximum carrier concentrations at low temperature has yet to be determined.

The present observations of rapid boron precipitation and the formation of a self-limiting surface phase during heavy doping are qualitatively consistent with models of MBE growth considering processes occurring at the *immediate* surface. However the difference between surface phases formed under dynamic and static conditions cannot readily be explained using previously reported models for dopant incorporation, and further *in-situ* study into their formation is likely to be necessary.

CHAPTER 4

THE INFLUENCE OF A SURFACE PHASE ON BORON ACCUMULATION IN SILICON

4.1 INTRODUCTION

In Chapter 3 the formation of a surface accumulated phase of boron was observed at doping levels of $1x10^{20}cm^{-3}$ and at temperatures above 650°C. Of interest in this Chapter is how the presence of the surface phase influences boron incorporation and profile smearing at different temperatures and growth rates. It will be shown that boron *does* show profile smearing, which is dependent on temperature and growth rate, previously associated only with other dopants [Kubiak and Parry 1991]. In the absence of any surface phase, the degree of profile smearing is so small that it can only be determined by high resolution SIMS measurements. For the case of boron incorporation at higher doping levels ($>10^{19}cm^{-3}$), the effects are much more severe. The results presented here suggest that, after a boron surface phase has formed, stable clusters of boron exist on the surface that impede boron incorporation. This behaviour is discussed in the context of previously published models for dopant incorporation. These models are introduced, beforehand, by a review of previous attempts to characterise boron profile smearing (section 4.5). The data obtained in the present study are presented in section 4.6 and evaluated thereafter.

4.2 THE SURFACE ACCUMULATION PHENOMENON

In general terms *surface accumulation* describes the phenomenon of surface enrichment by a dopant during Si MBE, often observed during coevaporation doping. Surface enrichment was observed during initial work using Auger and XPS studies for Sb [Bean 1978] Ga and Al [Becker and Bean 1977] though the

mechanism causing it was not clear. Accumulated dopant smears profiles by acting as a reservoir of dopant after the source has been terminated. Terminating the dopant flux (by closing a shutter) will not produce a sharp interface because dopant incorporation will still take place from the surface accumulated layer. This accumulated layer continues to act as a secondary source of dopant, as growth continues, until it is depleted over a thickness that is a characteristic of the dopant and growth conditions (see Section 4.4). This effect can smear profiles more severely than solid state diffusion effects. For example, at 600°C solid state diffusion of Ga and Sb is negligible during the growth of MBE layers, yet profile smearing by surface accumulation can be $\approx 100\ \mu m$ for Sb [Jorke 1985] and $\approx 1\ \mu m$ for Ga [Allen *et al* 1982]. It was established at the onset that, for a given dopant, surface accumulation and associated profile smearing show a temperature and growth rate dependence [Iyer *et al* 1981, Tabe and Kajiyama 1983]. Later, different incorporation models were suggested to account for this. The progress towards a better understanding of dopant incorporation kinetics is presented here.

4.3 MODELS FOR SURFACE ACCUMULATION

Coevaporation doping during Si MBE relies on 'spontaneous' incorporation of dopants, at a surface site, during epitaxial growth. However for most dopants this process does not always occur for significant fractions of impinging flux. After the deposition of consecutive monolayers, any dopant that has not incorporated will collect (*accumulate*) at the surface. Most shallow dopants in Si MBE tend to accumulate at the surface to some extent and show associated profile smearing. This not only restricts the choice of dopants, but prevents the production of *atomically* sharp doping profiles. It was not until very recently, when an improved understanding of accumulation and particularly its temperature dependence was achieved, that MBE fulfilled its initial promise of the ultimate in sharp doping [Mattey *et al* 1990]. Many authors have used phenomenological approaches to characterise the observed surface enrichment and profile smearing dependencies on

temperature and growth rate, and to establish the optimum conditions for the production of sharp doping profiles. These are discussed here, though not in detail, and the reader is referred to the review articles given in the text.

4.3.1 SURFACE ACCUMULATION AND DOPANT STRAIN

Pindoria *et al* (1990 A) discussed accumulation in qualitative terms noting that dopants in matrices such as GaAs and Si show a propensity to surface accumulate that can be related empirically to the ratios of their covalent radii and that of the matrix. This is seen in Fig. 4.1, which shows the radii of dopants against reported accumulation behaviour of dopants in Si and Ge (the radii are normalised to that of the matrix). The approach in their work was to assume a relationship between size and accumulation behaviour must reflect the *strain* produced by the incorporation of an atom that is different in size from that of the host matrix. The larger the strain, the more likely a given dopant surface accumulates, in agreement with observed behaviour for most dopants, though the authors did not establish a direct relationship between strain and accumulation behaviour. A quantitative account of surface accumulation during epitaxial growth of covalent semiconductors could not be obtained because little is known about surface energetics in the presence of reconstruction. However, the strain model hypothesis does suggest a physical basis for the accumulation process.

4.3.2 SURFACE ACCUMULATION BY SEGREGATION

The segregation model, developed by Barnett and Greene (1985), was the first attempt to explicitly account for surface enrichment, using a combination of classical segregation and kinetic theory (see Chapter 1). Surface enrichment was expressed in terms of dopant segregation, by invoking enhanced diffusion of dopant from some distance below the surface. Phenomenological equations were established by determining the net incorporated flux as a balance of competing

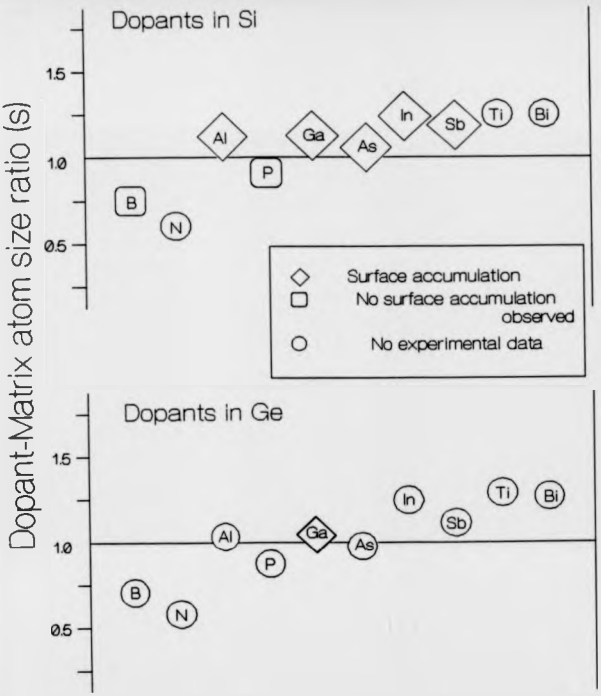

Fig 4.1 Schematic representation of dopant/matrix atomic radii and the observed accumulation behaviour for different dopants in Si and Ge matrices (after Pindoria *et al* 1990).

processes of arrival, desorption, and segregation (see Fig. 4.2). These can be used to calculate depth profiles for dopants in Si MBE using thermodynamic data and by fitting unknown parameters such as diffusion coefficients. The diffusion coefficients are assumed to show both a temperature and depth dependence, with dopant fluxes contributing from ≈ 1 nm below the surface. This distance was used to achieve best agreement with obtained experimental data. Good agreement with observed temperature and growth rate dependence on profile smearing is achieved using these parameters. However the solutions are empirical and only valid for a given dopant under pre-established incorporation conditions.

4.3.3 ACCUMULATION BY DOPANT-SI EXCHANGE PROCESSES

It was proposed by Jorke (1985) that a dopant atom immediately below the surface could 'swap' position with a surface Si atom (see Fig. 4.3), and that this process would contribute to a net surface enrichment of dopant. The process is considered to be driven by the difference in energies between atoms in the bulk and at surfaces, similar to a surface segregation mechanism except that, unlike the Barnett and Greene hypothesis, only atoms immediately below the surface contribute to surface enrichment. After the growth of the next monolayer, the exchange process is strongly hindered and dopants are effectively considered to be 'buried'. The exchange process will occur if the surface site is energetically favourable compared to the subsurface site and if dopant atoms have enough energy to overcome an energy barrier associated with the breaking of atomic bonds (see Fig. 4.4). This means that the process will be thermally activated and hence the rate at which it occurs will show a temperature dependence. The number of atoms that can make the exchange shows a growth rate dependence because the exchange is frozen after the deposition of the next monolayer of Si. Jorke derived expressions for the degree of surface enrichment using rate equations for the exchange processes during successive layers to obtain r_d, the segregation coefficient, defined as the ratio of the surface density to bulk concentration.

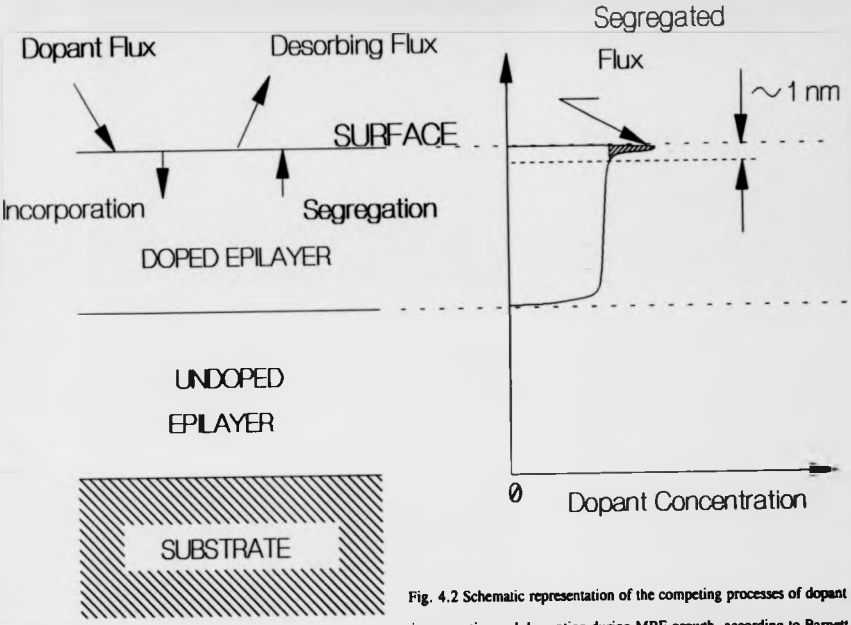

Fig. 4.2 Schematic representation of the competing processes of dopant segregation, incorporation and desorption during MBE growth, according to Barnett and Greene (1985).

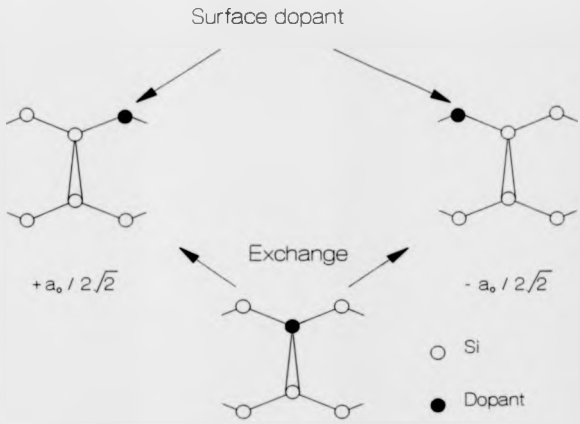

Fig. 4.3 Schematic representation of the exchange process between a subsurface dopant atom and a surface Si atom, postulated by Jorke (1985) as a mechanism for Sb surface enrichment during Si MBE.

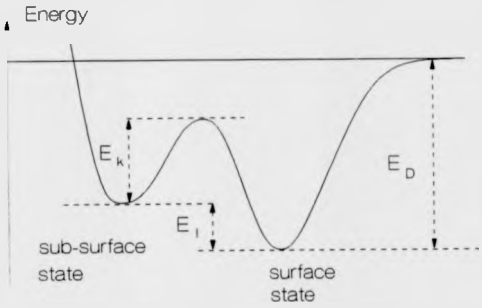

Fig. 4.4 Potential energy diagram used by Jorke (1985) to describe the exchange process between surface and subsurface states. E_a represents the energy change associated with the exchange process, E_k the energy barrier associated with it. E_D represents the desorption energy.

The solutions provided by Jorke reduced at higher temperatures to expressions similar to those for equilibrium segregation coefficients, given as:

$$r_d = \frac{a_o}{4}\exp\left(\frac{-E_s}{kT}\right) \qquad (4.1)$$

where E_s is the energy change associated with the exchange process, $a_o/4$ is the thickness of a monolayer (0.136 nm).

At low temperatures the expression for r_d was different, owing to the influence of the energy barrier E_k. In this temperature regime the segregation coefficient r_d is expressed as

$$r_d = \frac{a_0}{4}\exp\left\{\frac{\nu a_0}{4R}\exp\left(\frac{-E_k}{kT}\right)\right\} \qquad (4.2)$$

where ν - frequency factor (s^{-1})

E_k - energy barrier to dopant accumulation

R - growth rate (nms^{-1})

$a_o/4$ - thickness of a monolayer (0.136 nm)

At higher temperatures surface enrichment will increase with decreasing temperature in agreement with observed Sb data [Jorke 1985]. However, at low temperatures the exchange process becomes kinetically limited, owing to the presence of the activation barrier associated with it. This is seen as a sharp reduction in r_d. Hence below some critical temperature, surface enrichment will become strongly hindered despite the fact that it becomes increasingly thermodynamically favourable. The kinetic limitation is less severe as the growth rate R is reduced, because surface atoms have more time to make the exchange, so that the transition between the two regimes will occur at lower temperatures.

This model is more satisfactory than that of Barnett and Greene in that it involves no equilibrium thermodynamic assumptions and was developed using

kinetic theory. Therefore it is applicable over a wide variation of temperatures and growth rates. The quantitative solutions were produced by fitting observed Sb accumulation behaviour in the temperature range 700 to 450°C [Jorke 1985]. The transition rates for the exchange processes were modelled using a "successful attempt" frequency factor (ν in equation (4.2)) that was assumed to be independent of temperature. The model was therefore still an empirical one, but the work was very influential in that it predicted and verified the existence of a temperature regime for the production of atomically sharp interfaces during coevaporation doping in Si MBE, and was exploited subsequently in the production of abrupt Sb doping superlattices, a dopant previously thought to be unusable as a conventional coevaporated source [Jorke and Kibbel 1989].

4.3.4 SURFACE ACCUMULATION BY DOPANT STEP-CLIMBING

Andrieu *et al* (1989) discussed the incorporation behaviour of different dopants in GaAs and Si, proposing that dopants can 'segregate' by climbing over Si steps. This occurs instead of incorporation at a kink site (shown schematically in Fig. 4.5), leading to surface enrichment by the dopant. Andrieu *et al* set up rate-dependent kinetic equations for dopant incorporation in successive layers by considering a balance between competing processes of dopant step-climbing and incorporation. Regular solutions were produced, without assuming equilibrium thermodynamics, though these were similar in form to those obtained by Barnett and Greene [1985].

One favourable aspect of the step-climbing model is that the activation energies associated with dopant step-climbing (and hence the propensity to surface accumulate) increases with atomic radius, in agreement with Pindoria *et al* (1990 A). Hence the dopant strain effect is explicitly accounted for, rather than implied, in expressions derived for dopant segregation. The model is not as flexible as that of Jorke in that it does not account for the presence of any energy barrier

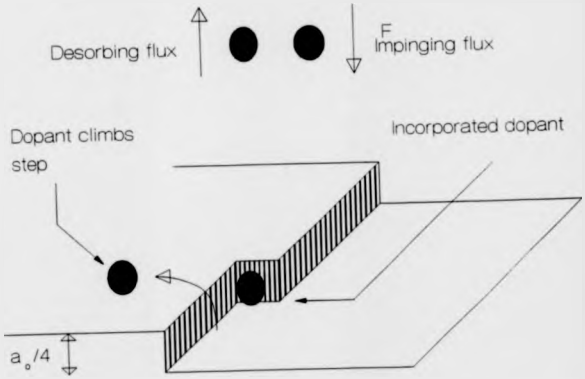

Fig. 4.5 Schematic representation of the step-climbing process as proposed by Andrieu *et al* 1989. Dopant atoms can avoid incorporation, by climbing the Si steps, thus contributing to a surface enrichment of dopant compared to the bulk.

likely to be associated with breaking of atomic bonds during the step-climbing process. Hence the solutions are only valid at temperatures corresponding to equilibrium incorporation conditions and cannot be applied to the low temperature kinetically-limited accumulation regime.

However, there exists a physical similarity between the step-climbing process and the dopant-Si exchange process that will be discussed further.

4.4 METHODS FOR QUANTIFYING DOPANT ACCUMULATION

It is important to quantify profile smearing produced by accumulation, at any given temperature and growth rate, both to characterise the incorporation behaviour and to establish favourable regimes for the production of sharp doping profiles. A number of methods are possible. Most *in-situ* studies such as Auger and XPS, used in the assessment of dopant accumulation, determine the surface enrichment of dopants directly. For such work the segregation ratio r_d is used. However most *in-situ* methods tend to have poor detection limits and limited depth resolution, and are therefore not ideal for the quantitative determination of boron accumulation from elemental sources. This is especially so for boron at low growth temperatures. Most require some form of growth interrupt and, as has already been shown in Chapter 3, surface accumulation under dynamic and static conditions are different, making this a dubious procedure. In the production of devices growth interrupts are undesirable, due to incorporation of impurities from the residual gas (such as carbon and oxygen) into the active part of the device, so that boron incorporation studies during continuous growth are more relevant.

For this work the most suitable parameter, from the point of view of characterisation of the accumulated phase during growth, is the degree of profile smearing in depth profiles as the accumulated phase depletes. This was obtained using high resolution SIMS (see Appendix I). The SIMS nomenclature is used throughout the present work, ie trailing edge slopes refer to the upslope in the

boron profile (formed by *opening* the cell shutter), and leading edge slopes refer to the downslope.

Slopes in SIMS boron depth profiles tend to be linear on a logarithmic (concentration) vs depth plot. The exponential dependence of concentration versus depth in decay slopes is a characteristic of 'first-order' incorporation and has been observed for all dopants investigated in Si MBE on Si(100) substrates (eg Sb [Allen *et al* 1982], In [Knall *et al* 1984], Ga [Nakagawa *et al* 1988] and boron [Tatsumi *et al* 1988 B]. It appears from the present work that this is also the case for boron, with the SIMS dopant profiles showing linear behaviour over a wide range of temperatures, growth rates, and doping levels. The SIMS leading edge slope is characterised by the exponential decay constant Δ (nm) that is defined as the growth distance for the boron concentration, n, to fall from an initial value n_o to n_o/e. The boron concentration in the SIMS leading edge slope can be expressed as

$$\text{boron concentration} \quad n = n_o \exp(-x/\Delta) \qquad (4.3)$$

It is usually more reliable to determine the degree of profile smearing in the leading edge slopes, since these are least affected by SIMS induced broadening (see Appendix I), allowing determination of Δ with good accuracy for $\Delta \gtrsim 1.3$nm for the case of boron [Dowsett *et al* 1992]. However the boron trailing edge slopes are also of interest [Mishima *et al* 1990] and qualitative discussions of these are included in this Chapter.

Δ was measured by first fitting the inverse slopes (using a linear regression), to give a value in nm/decade, and then converting this into an exponential decay length, by multiplying by $\log_{10}e$. For boron coevaporation at the temperatures used in the present work the Δ parameter and the surface enrichment parameter r_d (see section 4.3.3) are equivalent. It should be noted that, in general, the two will be equivalent whenever dopant is not desorbing in significant quantities from any surface-enriched layer. Evidence from the areas of boron doped regions grown at

temperatures between 900 and 450°C (see Fig. 3.1a) suggests that boron desorption is not significant during the temperatures commonly used for MBE.

4.5 BORON ACCUMULATION IN Si MBE (PREVIOUS WORK)

During the period of this study, there developed a strong world-wide interest in coevaporation p-type doping, especially using elemental boron. This was because early work suggested that elemental boron did not show significant profile smearing or the temperature dependent incorporation properties inherent to other dopants [Kubiak *et al* 1985A, Kubiak *et al* 1985B and see Chapter 1]. However the high crucible temperatures necessary to evaporate the element dissuaded many workers from its use, most preferring to use compound boron species (see Chapter 1). A summary of these boron incorporation studies is presented here.

4.5.1 PROFILE SMEARING USING COMPOUND BORON SOURCES

Previous work using *compound* sources demonstrated boron profile smearing, as seen from Auger, XPS, and SIMS studies [de Frésart *et al* 1988, Tatsumi *et al* 1988 B, Jackman *et al* 1988 and 1989]. De Frésart *et al* observed a temperature dependence of boron profile smearing over a wide range of temperatures, but their results were closely correlated with oxygen incorporation from the use of a compound (B_2O_3) source that was also temperature dependent. Above 700°C boron profile smearing was determined to decrease with increasing temperature, in agreement with equilibrium segregation theory, with an activation energy of ≈ -0.33eV. Below this temperature boron profile smearing was sharply reduced but the doped material became polycrystalline and it was not clear whether the transition was associated with the corresponding reduction in material quality. This phenomenon was also observed by Jackman *et al* (1988 and 1989) who observed a sharp reduction in HBO_2 profile smearing at temperatures below 700°C, for which oxygen incorporation was $\approx 10^{20}$cm^{-3}. Jackman *et al* could not obtain any

quantitative data on the temperature dependence of profile smearing, since the boron doped layers were grown too close together to resolve the leading edge slopes.

Tatsumi *et al* used XPS to determine the degree of boron surface enrichment at 750 and 800°C using a HBO_2 source. Growth at these elevated temperatures avoided oxygen incorporation, but meant that much of the observed profile smearing was caused by solid state diffusion.

4.5.2 PROFILE SMEARING USING ELEMENTAL SOURCES

Before the work of Jorke and Kibbel (1990) and Parry *et al* (1991 A 1991 B) elemental boron was thought to be a well-behaved dopant, not displaying any profile smearing (see Chapter 1). To some extent this was true on a nanometre scale and only revealed by high resolution SIMS measurements once the fabrication of *atomically* abrupt doping profiles was needed (see section 1.5.1). However, the present author also discerned that elemental boron could produce relatively *severe* profile smearing at higher doping levels ($> 10^{19}cm^{-3}$) [Parry *et al* 1991 A and 1991 B]. These levels are often associated with the growth of narrow boron doped delta layers with sheet densities $\approx 10^{14}cm^{-2}$ [Mattey *et al* 1990]. Hence a knowledge of profile smearing at higher doping levels, and its temperature and growth rate dependence, is of considerable interest.

4.6 INFLUENCE OF A SURFACE PHASE ON BORON PROFILE SMEARING

4.6.1 PROFILE SMEARING IN THE LEADING AND TRAILING EDGE

In Chapter 3 evidence for the formation of a surface phase of boron was found from SIMS measurements of the leading edge of highly doped layers (see Fig. 3.2a). This was formed under dynamic growth conditions, and was

self-limiting to a coverage equivalent to 0.25 ML. The effect of the surface phase on boron incorporation was determined by measuring the accumulation parameter Δ, at several growth temperatures, for layers doped at $5x10^{18}$ cm^{-3} and $1.4x10^{20}$ cm^{-3} (see Figs. 3.1a and 3.2a respectively). These were grown at temperatures between 900 and 450°C, and at a growth rate of 0.28 nms^{-1}. The Δ values obtained are plotted in Fig. 4.6. The solid line represents the data obtained from for the highly doped structure and the broken line for the lower doped structure. The vertical and horizontal error bars reflect the error in the SIMS profile and substrate temperature respectively.

A difference in Δ for the two doping levels is observed at temperatures above 600°C. The degree of profile smearing is significantly less in the low doped structures, although the accumulation broadening behaviour is qualitatively similar. At temperatures below 600°C the doping level dependence on Δ is not observed. This is seen as a merging of the two curves into a common line (discussed later). But what mechanism is responsible for the apparent dependence of Δ on temperature?

For the case of the trailing edges, there appears to be little discernible dependence of profile smearing on doping level. This is seen in Fig. 4.7 which shows a plot of Δ against growth temperature for the SIMS trailing edge. Although a quantitative determination from the trailing edge slopes is unreliable (see Appendix I), it appears that Δ values, at the start of co-evaporation doping are similar, at levels up to $1x10^{20}cm^{-3}$. In Chapter 3 it was suggested that a surface accumulated boron surface phase only forms after *continued* heavy doping. This suggests that the existence of a surface phase of boron is responsible for the apparent increase in surface accumulation behaviour, in the SIMS leading edge, at higher doping levels. There is no influence of the surface phase on dopant incorporation at the onset of heavy doping, however, because it has not had time to form, so that a doping level dependence of Δ is not observed in Fig. 4.7. Hence, Δ does not show a doping level dependence, as such, but is influenced by the presence

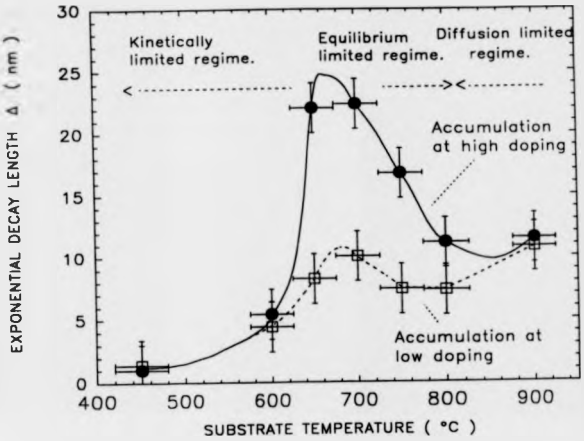

Fig. 4.6 Plot of leading edge profile broadening parameter Δ (nm) versus temperature for a highly doped (≈ $1x10^{20}cm^{-3}$) boron layers (solid line). The broken line is obtained from a similar structure grown at lower doping levels (≈ $5x10^{18}cm^{-3}$).

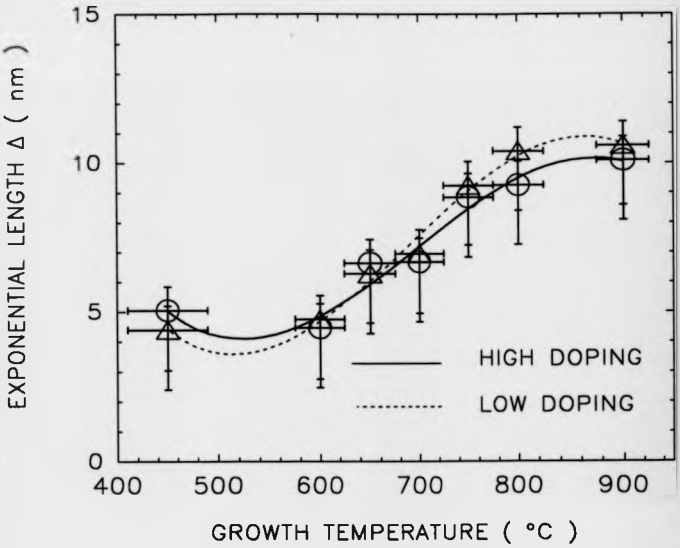

4.7 Plot of *trailing* edge profile broadening parameter Δ (nm) versus temperature for a highly doped boron layers (solid line), grown at temperatures between 900 and 450°C. The broken line represents layers grown at lower doping levels ($\approx 5x10^{18}cm^{-3}$).

of a surface phase, reflected as a difference in the leading edge but not in the trailing edge slopes of highly doped structures.

The Δ values in the SIMS leading edge (see Fig. 4.6) show a number of 'classic' features associated with accumulated dopants. Firstly a rapid transition in the temperature dependence of Δ is observed at ≈ 670°C. This is characteristic of a transition from equilibrium to kinetically limited boron accumulation.

To determine whether the transition was associated with impurity incorporation at lower temperatures, the layers grown at levels of $1x10^{20}cm^{-3}$ and $\approx 5x10^{18}cm^{-3}$ were profiled for oxygen and carbon using SIMS using a Cs^+ primary ion beam (see Fig. 4.8a and Fig. 4.8b). Oxygen incorporation in both layers is below the SIMS detection limit of $5x10^{17}cm^{-3}$, except at temperatures of 450°C for which an oxygen level of $3x10^{18}cm^{-3}$ is observed. This is due to uptake from the residual gas at low temperature, which is desorbed at temperatures above this. However at 900°C there are significant increases in oxygen and carbon levels in the highly doped structure. This is consistent with 'cracking' and subsequent incorporation of CO_x species at the Si surface occurring at the highest temperatures, though further experiments are necessary to investigate this.

Although oxygen incorporation at these levels is of some concern, its level is at least two orders of magnitude less than that associated with compound sources, and is not present at a level high enough to be detrimental to crystalline quality. Indeed an XTEM micrograph (see Fig. 3.3) confirmed that the defect level in the higher doped structure was $< 10^5\ cm^{-2}$, the detection limit of the technique. Carbon incorporation is observed only at the highest doping level throughout the temperature range. This suggests that it is derived from the source, which uses a graphite crucible.

The relatively low levels of impurity incorporation and the crystalline quality of the boron doped layers suggest that the results presented in Fig. 4.6 reflect a genuine transition in the temperature dependence of boron profile smearing and not one which is associated any drastic change in material quality.

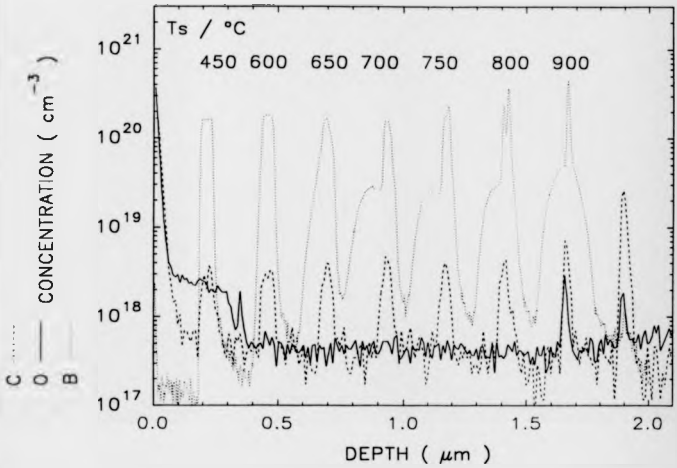

Fig. 4.8a SIMS C and O depth profiles of highly doped boron layers, grown at temperatures from 900 to 450°C using an elemental source.

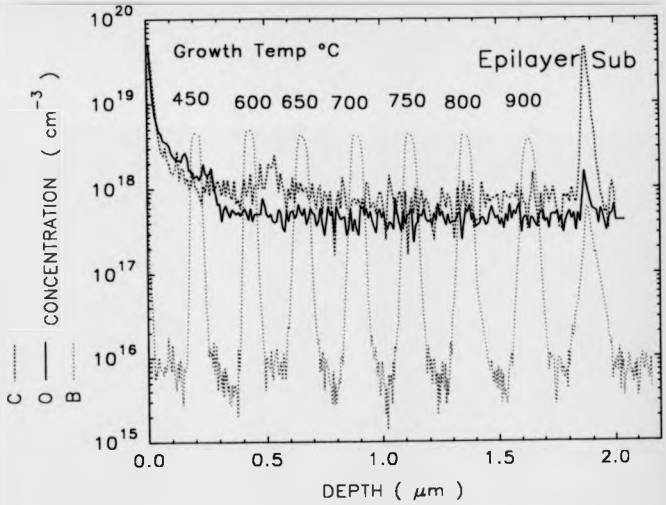

Fig. 4.8b SIMS C and O depth profiles of low doped boron layers, grown at temperatures from 900 to 450°C using an elemental source.

Two distinct temperature regimes are observed in temperature dependence of boron profile smearing. In the high temperature regime (>700°C), Δ increases with decreasing temperature at a level which is higher in the presence of a surface phase. In the low temperature regime (<650°C), Δ decreases sharply with decreasing temperature, owing to a reduction in the influence of the surface phase as its formation becomes increasingly kinetically limited. The two different temperature regimes are discussed separately.

4.6.2 HIGH TEMPERATURE REGIME (T > 650°C)

At temperatures of 700°C, and above, the profile smearing follows the classic equilibrium form showing an accumulation dependence on substrate temperature, increasing with decreasing temperature, according to equation (4.1). The error in the data points in this temperature regime do not allow precise determination of E_a. Also solid state diffusion is apparent in highly doped boron layers at temperatures of and above 800°C. However E_a is certainly negative (so that Δ increases with decreasing temperature) and at a value of -0.4 ± 0.1 eV. This result compares with that achieved by de Frésart *et al* who determined a value of -0.33 eV in the same temperature regime. Tatsumi and co-workers determined a value of -0.0075 eV, from measurements at 700 and 850°C, an unrealistically low value and probably owing to solid state diffusion effects at high temperatures (see equivalent temperatures in Fig. 4.6). It is intriguing to note that profile smearing by surface accumulation of dopant at 700°C is significantly worse than that due to solid state diffusion at 900°C. Diffusion effects are much more significant in the leading edges of the lower doped structure (see Fig. 4.6) precluding any accurate determination of E_a, though it certainly lower than that associated with heavy doping.

There exists some debate in the literature over the sign of E_a. For instance Jorke and coauthors have published E_a (as defined by equation 4.1) for Sb as -1.2 eV and $+1.2$ eV in consecutive papers [Jorke 1985, Jorke and Kibbel 1989].

Andrieu *et al* (1989) argue that E_a should *never* be negative, owing to the nature of the accumulation process. In fact the form of their accumulation equation was different to that commonly used in the literature, and they used an *incorporation* expression which is proportional to the inverse of Δ. It is obvious that in the present work, E_a must be negative to account for the observation of decreased profile smearing at temperatures above 700°C.

4.6.3 LOW TEMPERATURE INCORPORATION REGIME (T < 650°C)

For temperatures below 650°C the degree of profile smearing reduces sharply (see Fig. 4.6) as the rate-dependent processes causing surface accumulation become kinetically limited. Hence although boron surface enrichment is thermodynamically favourable in this temperature regime (see equation 4.1), there exists a kinetic barrier so that most atoms do not have enough energy to do so. This makes this temperature regime ideal for the growth of abrupt highly doped structures.

It is difficult to characterise Δ at the lowest temperatures, since accumulation broadening becomes comparable to SIMS mixing effects (ie for $\Delta \lesssim$ 1.3nm). For such slopes the profile abruptness may be steeper than that indicated. An attempt at 'fitting' Δ in equation (4.2) for the highly doped layers, at temperatures below 650°C yielded $E_k \approx + 0.4 \pm 0.1$eV and $\nu \approx 10^{3} s^{-1}$ Previous studies have used frequency factors $\nu \approx 10^{13} s^{-1}$ to characterise dopant incorporation at high temperatures [Allen *et al* 1982, Barnett and Greene 1985 and Andrieu *et al* 1989], though the lower value of ν obtained here is consistent with other low temperature (<600°C) phenomena [Jorke *et al* 1989]. However the paucity of data points in this temperature regime precludes any precise evaluation of E_k or ν. For this reason further boron doped layers were grown in the low temperature regime, discussed in the next section.

The merging of the high and low doped curves seen in Fig. 4.6 is probably not associated with any reduction in the influence of the surface phase at low temperature, but reflects a kinetic limiting of its formation.

4.7 BORON ACCUMULATION VERSUS GROWTH RATE

To determine the dependence of boron accumulation in Si on growth rate, further structures were grown at a rate of 0.1 nms^{-1} at temperatures varying from 650 to 450°C. The SIMS profiles of these structures are shown in Chapter 5. These structures were doped at a level $\approx 10^{19}cm^{-3}$, ie below the boron solubility limit (see Chapter 3). This was confirmed by e-CV measurements that indicated complete activation of dopant throughout the temperature range. The results of Δ versus temperature at 0.1 nms^{-1} are presented in Fig. 4.9. At this growth rate, the temperature for the transition in accumulation behaviour occurs at a temperature of $\approx$600°C, lower than that at a growth rate of 0.28 nms^{-1} ($\approx$650°C). This indicates that the temperature for the onset of kinetically limited accumulation is reduced by decreasing the growth rate. This is presumably because the equilibrium regime is extended to lower temperatures at the lower growth rate, because the surface has more time to reach equilibrium. E_x and ν were fitted using equation (4.2) and determined as 0.48 ± 0.05 eV and 1500 ± 300 Hz respectively, ie within the error of the values obtained for the high doped structure, grown at a growth rate of 0.28 nms^{-1}.

This extension of the equilibrium limited regime to lower temperatures, by decreasing the growth rate, also gives an increased maximum of Δ. This is seen in Figs. 4.6 and 4.9 for which Δ reaches a maximum of 24 and 32 nm, at growth rates of 0.28 and 0.1 nms^{-1} respectively. However the Δ versus temperature curve at 0.1 nms^{-1} is more similar to the 0.28 nms^{-1} curve corresponding to Δ values during the influence of a surface phase. This is despite the fact that the layers grown at 0.1 nms^{-1} were only doped at $10^{19}cm^{-3}$, which raises the question as to

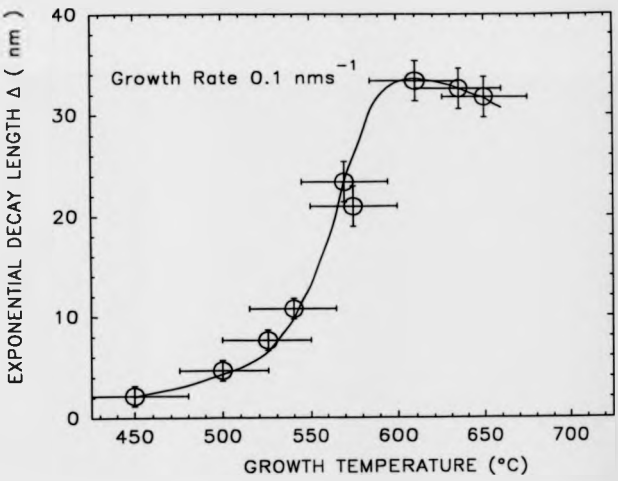

Fig. 4.9 Plot of decay constant Δ versus temperature for boron layers grown at 0.1 nms^{-1}, doped at a level of 1x10^{19}cm^{-3}.

whether the influence of a boron surface phase is seen at 'intermediate' doping levels.

The surface phase in the highly doped structure *saturates* at a coverage equivalent to 0.25 ML, but by the time the leading edge has been reached most of the surface phase has incorporated at the solubility limit (see Chapter 3). The difference in accumulation behaviour in high and low doped layers, grown at 0.28 nms^{-1}, suggests that the effects of the surface phase are still 'felt' even though most of it has depleted. It seems likely that the if the surface phase is partly formed in local 'clusters', these will modify dopant incorporation behaviour. The resemblance in layers doped at $\approx 1x10^{19}cm^{-3}$ to the accumulation behaviour observed in the presence of a surface phase suggests that a surface phase is *forming*, at 0.1 nms^{-1}, at a level sufficient to affect dopant incorporation. Hence it may not necessary to dope at $\approx 1x10^{20}cm^{-3}$ to observe the increased accumulation behaviour associated with surface phases.

4.8 RESULTS SUMMARY

The present work confirms a temperature and growth rate dependence of profile broadening for boron in Si, as well as a strong influence of the presence of a surface accumulated phase on boron incorporation behaviour. Boron accumulation is generally less severe than that associated with other dopants, and at 450 °C profile broadening is probably less than the resolution of the SIMS technique. The obtained data were found to be in good agreement with equations (4.1) and (4.2), in the high and low temperature regimes respectively, yielding $E_a = -0.4 \pm 0.1 eV$, $E_a = 0.48 \pm 0.05$ eV and $\nu = 1500 \pm 300$ Hz.

The dependence of temperature, growth rate, and doping level on boron accumulation in Si is summarised in Fig. 4.10. This shows the degree of profile smearing at *high* and *low* doping levels, at a growth rate of 0.28 nms^{-1} (solid and dashed line respectively), and for *moderate* doping levels ($\approx 10^{19}cm^{-3}$) at a growth rate of 0.1 nms^{-1} (dotted line). The present data can be used as a device grower's

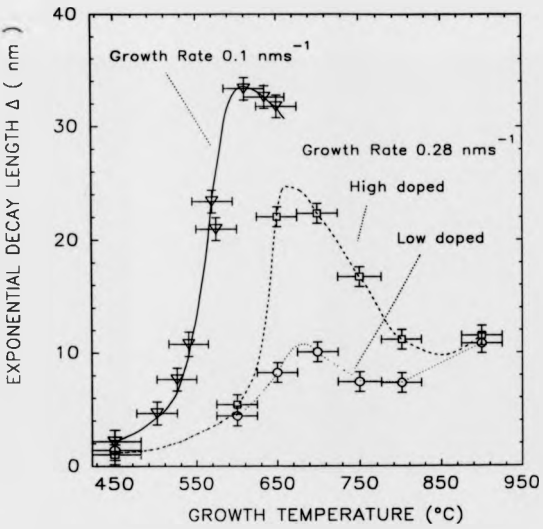

Fig. 4.10 Summary of the dependence of Δ on temperature, doping level, and growth rate seen in Figs. 4.6 (solid line), 4.6 (dashed line), and 4.7(dotted line).

chart for the production of sharp, well-defined doping profiles such as those that are necessary for modulation doped requiring a nominally undoped spacer layer between the doping and the quantum well (see section 1.5.1).

The influence of a boron surface phase on boron incorporation is now discussed in the context of models for dopant accumulation given earlier in this Chapter.

4.9 DISCUSSION

The temperature dependence of boron accumulation behaviour shows a distinct transition from equilibrium to kinetically limited incorporation processes, previously predicted and verified for Sb doping in Si [Jorke 1985]. It appears likely that equilibrium-like incorporation is achieved during boron doping, as suggested for Sb by Barnett and Greene (1985), Jorke (1985) and Andrieu *et al* (1989), but only at temperatures above $\approx 600°C$. In the low temperature regime, however, the influence of a kinetic barrier produces a strong reduction in boron profile smearing that is consistent with Jorke's analysis of dopant incorporation. However these models do not account explicitly for the observed influence of a surface phase on accumulation behaviour, though it will be shown that models considering processes occurring at the *immediate* surface provide a better qualitative explanation than those invoking segregation form below the surface.

The existence of dopant phases on Si(100) surfaces have previously been shown to increase Sb and Ga desorption rates [Iyer *et al* 1981 and Allen *et al* 1982] and Ga profile smearing [Schäffler and Jorke 1990].

Lifshits *et al* (1989) studied the behaviour of Ag impurities on Si(111) surfaces. It was shown that if impurities formed surface clusters, their mobilities were reduced. This was thought to be caused by interactions within the surface clusters causing them to bind together more strongly.

Boron does not desorb in measurable quantities at temperatures up to 900°C (see Chapter 3), therefore the desorption and accumulation phenomena cannot be

directly related. However the increased binding in surface clusters can explain the observed increase in boron profile smearing using models accounting for processes occurring at the immediate surface. For the case of the Barnett and Greene model of surface enrichment by surface segregation, the increased accumulation cannot be accounted for. The authors acknowledge this in a discussion of Sb incorporation at high doping levels using an arbitrary coverage factor to 'fit' previously observed depth profiles [Barnett and Greene 1985]. However, for the case of the step-climbing model proposed by Andrieu *et al*, the increased accumulation behaviour may be explained by considerations of the strain in a surface step when incorporating significant amounts of dopant which are tightly bound in localised clusters. Because the model considers *in-surface* processes, such as migration of dopant and interactions of dopants with steps, as a pre-requisite for profile smearing behaviour, it is therefore more suited to providing a physical account of the present results. The Jorke 'exchange' model yields analytical solutions for the temperature and growth rate dependence of accumulation which show good agreement with present data, both in the quantitative determinations of Δ, and the qualitative description of the transition from equilibrium to kinetically limiting of surface enrichment.

The step-climbing and surface-subsurface exchange models are very similar in that they both consider processes occurring in consecutive surface layers, and it seems likely that a more complete model of surface accumulation will be a hybrid of the two.

4.10 CONCLUSIONS

Boron doping shows accumulation behaviour previously only associated with the use of compound sources. A temperature regime has been established for the production of high doped structures featuring atomically abrupt doping profiles. Boron incorporation has been shown to be influenced by the presence of a surface

phase manifested by an increase in profile smearing in the SIMS leading edges of layers.

A mechanism for this behaviour has been suggested involving interactions between Si steps and boron surface clusters that are more tightly bound than 'free' ad-adatoms. These present results are more consistent with models considering processes occurring at the immediate surface, rather than those presuming segregation of dopant.

CHAPTER 5

B AND Ge ACCUMULATION DURING $Si_{1-x}Ge_x$ MBE

5.1 INTRODUCTION

Devices exploiting the capability to tailor band offsets at $Si/Si_{1-x}Ge_x$ heterojunctions, by varying the Ge fraction, require good control of the doping and Ge interfaces involved. Such devices include the $Si_{1-x}Ge_x$ base heterojunction bipolar transistor (HJBT) [Schreiber *et al* 1989, Tatsumi 1990A, Iyer *et al* 1990]. The narrow highly doped boron spikes, necessary for the efficacy of the HJBT, impose stringent demands on profile abruptness, since, for optimum performance of the HJBT, all the dopant should be confined within the base region [Prinz *et al* 1991]. Boron accumulation is a potential source of 'out diffusion' (see Chapter 4), yet surprisingly little qualitative data has been published on boron and Ge incorporation, and their temperature dependence, during coevaporation doping. SIMS depth profiles of boron doped $Si_{1-x}Ge_x$ base HJBT's have been presented in the literature [Kibbel *et al* 1990, and Tatsumi 1990A], but the only previously reported quantitative study of boron accumulation in $Si_{1-x}Ge_x$, was carried out by Jorke and Kibbel (1990) who determined the degree of profile smearing in boron delta layers in $Si_{0.8}Ge_{0.2}$, showing a reduction in boron profile smearing in the alloy. No analysis of the incorporation behaviour was given.

Uncertainty in the incorporation properties of boron in $Si_{1-x}Ge_x$ has meant that extra $Si_{1-x}Ge_x$ "spacer" layers have been grown in the base of HJBT's, moving the p-type doping spike away from the heterointerface, unsatisfactory from the point of view of device performance [Kibbel *et al* 1990, and Tatsumi 1990A]. Hence, so that quantitative studies of boron profile smearing during $Si_{1-x}Ge_x$ MBE are of considerable interest.

Other than the influence of boron accumulation on device performance, the study of boron incorporation in $Si_{1-x}Ge_x$, discussed in this Chapter, yields useful information on dopant incorporation in the general case. To the author's best knowledge previous studies of dopant segregation during Si MBE have investigated its temperature and growth rate dependence [see for example Barnett *et al* 1985, Jorke 1985 and Andrieu *et al* 1989]. By altering the lattice parameter, using coevaporation of Ge, the present study has been able to evaluate how a change of *matrix* affects boron incorporation.

Previous empirical work suggests that the effective increase in lattice parameter over that of Si, produced by coevaporation of Ge, should make boron more likely to surface accumulate [Pindoria *et al* 1990A]. However, as well as the influence of matrix size on accumulation, another important consideration deriving from observations of III-V incorporation behaviour is the effect of the availability of surface Ge sites on boron incorporation behaviour during $Si_{1-x}Ge_x$ MBE. Coevaporation of Ge, which is larger in size than Si, introduces compressive stress at the surface, whereas for boron incorporation tensile surface stress is introduced. X-ray studies of *bulk* doped $Si_{1-x}Ge_x$ have shown some evidence for strain compensation during coevaporation of Ge and boron [Tatsumi 1990A]. It may be possible that local strain compensation may also occur at the surface, if boron incorporates at a Ge site. This process would lead to a *decrease* in boron accumulation and a reduction in boron profile smearing. The question then arises, will coevaporation of Ge, during boron doping, result in increased accumulation behaviour owing to the change in matrix size, or will it reduce boron accumulation by offering favourable incorporation sites at the immediate surface?

With respect to Ge incorporation many groups have observed Ge "segregation", determined by SIMS and XPS [Gravesteijn *et al* 1989, Zalm *et al* 1989, Nakagawa and Miyao 1991]. Observation of significant Ge profile smearing is inconsistent with the model of Pindoria *et al* (1990A) for surface accumulation, which suggests that the similarity in size between Si and Ge atoms should mean that

Ge will not accumulate. Results of Ge incorporation during coevaporation of Ge, presented in this Chapter, appear to suggest that boron doped Ge layers apparently do not show a profile smearing dependence on temperature and growth rate. These results are compared with those previously published in the literature.

5.2 BORON INCORPORATION IN $Si_{1-x}Ge_x$

5.2.1 BORON INCORPORATION IN $Si_{0.8}Ge_{0.2}$

For the first part of the present study, boron accumulation in $Si_{1-x}Ge_x$ was investigated by comparing accumulation in a Si and $Si_{0.8}Ge_{0.2}$ multilayer structure. This was grown at temperatures of 650, 600 and 450°C and at a rate of 0.1 nms^{-1}. The structure features 50 nm thick boron doped layers, grown in Si and $Si_{0.8}Ge_{0.2}$ regions of total thickness 275 nm and 240 nm respectively. The boron flux was increased by 20% in the $Si_{0.8}Ge_{0.2}$ region to compensate for the increase in growth rate. Fig. 5.1a shows a SIMS depth profile of this structure. (Except when stated otherwise, SIMS depth profiles were obtained using a 4.5 keV O^+_2 primary beam, at an angle of 43° to the normal.) The temperature for each layer is indicated in Fig. 5.1a. Growth was interrupted for 10 minutes during each substrate temperature change (see figure) and a 75 nm Si cap was grown before the starting the next $Si_{0.8}Ge_{0.2}$ layer. Finally a 100 nm Si cap was grown. The individual thicknesses of the Si and $Si_{0.8}Ge_{0.2}$ layers were determined to be within 5% of that intended under the profiling conditions used, precluding any significant change in erosion rate in Si and $Si_{0.8}Ge_{0.2}$. An e-CV depth profile of this structure, obtained using a dilute 0.1M NH_4F electrolyte etch, is shown in Fig. 5.1b. This shows reasonable agreement with the SIMS, although the boron doped layers are broadened owing to depletion effects in such high/low doping structures [Casel *et al* 1990].

Comparison of boron SIMS profiles in Si and $Si_{0.8}Ge_{0.2}$, grown at the same temperature, reveals two features. Firstly, under the growth conditions used in this

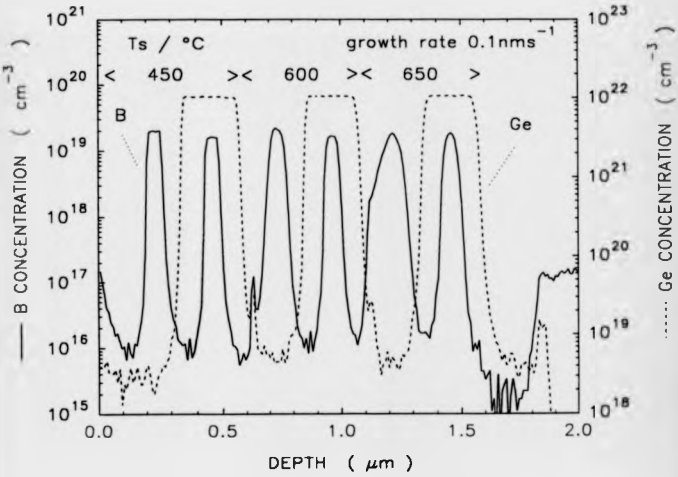

Fig. 5.1a Boron and Ge SIMS depth profiles of a modulation doped structure grown in $Si/Si_{0.8}Ge_{0.2}$ at a rate of 0.1 nms^{-1}, and at the growth temperatures indicated. Significant improvements in boron profile abruptness are observed in the alloy.

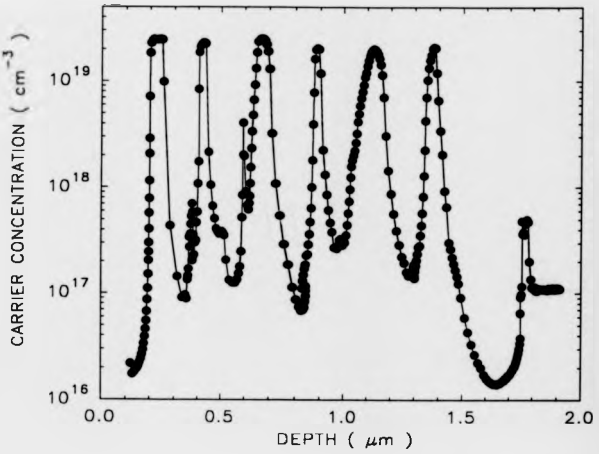

Fig. 5.1b E-CV depth profile of the boron doped structure in Fig. 5.1a.

structure, dopant profiles are significantly more abrupt in the $Si_{0.8}Ge_{0.2}$ alloy than in the Si suggesting reduced boron accumulation there. This is seen most clearly at 650°C. Secondly the areal densities of the boron spikes are lower in $Si_{0.8}Ge_{0.2}$ than in Si, over the complete temperature range, by about 60%. This is a SIMS effect caused by a reduction in boron yield in the alloy (see Appendix I).

It should be pointed out that the total thickness of this structure exceeds the critical thickness (h_c) obtainable for this Ge fraction. The stress produced at the $Si_{0.8}Ge_{0.2}$ interface by exceeding h_c caused the layer to 'relax' [Iyer *et al* 1990]. This was confirmed by defect etch measurements that showed a misfit dislocation density of $\approx 10^8$ cm^{-2}.

5.2.2 BORON INCORPORATION IN $Si_{0.9}Ge_{0.1}$

The reduced boron accumulation in the $Si_{0.8}Ge_{0.2}$ layers led the author to suspect that boron accumulation was generally less in $Si_{1-x}Ge_x$, though further structures were grown to investigate this.

Fig 5.2a and 5.2b show SIMS and e-CV depth profiles respectively of a boron doped $Si/Si_{0.9}Ge_{0.1}$ structure grown at a rate of 0.1 nms^{-1} and 0.05 nms^{-1}, at temperatures of 500 and 525°C (see figure). These structures features 30 nm boron spikes grown in Si and $Si_{0.9}Ge_{0.1}$ regions each 100 nm thick. The Ge fraction of 10% was used to allow the growth of thick spacer layers without the structure relaxing. This was verified by defect etch reveal measurements showing dislocations at a level of 10^4 - 10^5 cm^{-2}, but not showing misfit dislocations associated with relaxed $Si/Si_{1-x}Ge_x$ structures [Bean 1988]. For this structure, however, the degree of boron accumulation in the $Si_{0.9}Ge_{0.1}$ alloy is visibly *greater* than in the Si, a reversal of the behaviour observed at Ge fractions of 20% (see Fig. 5.1a), and this was qualitatively confirmed by the e-CV measurements in Fig. 5.2b.

Another structure was grown similar to that shown in Fig. 5.2a except that growth temperatures of 550 and 575°C were used. The SIMS depth profile of this structure is presented in Fig. 5.3. Again for this Ge fraction and under the growth

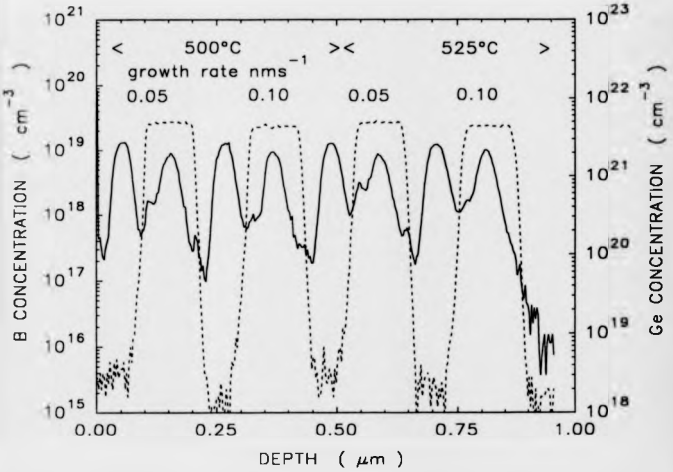

Fig. 5.2a Boron and Ge SIMS depth profiles of a modulation doped structure grown in $Si/Si_{0.9}Ge_{0.1}$ at rates and temperatures indicated.

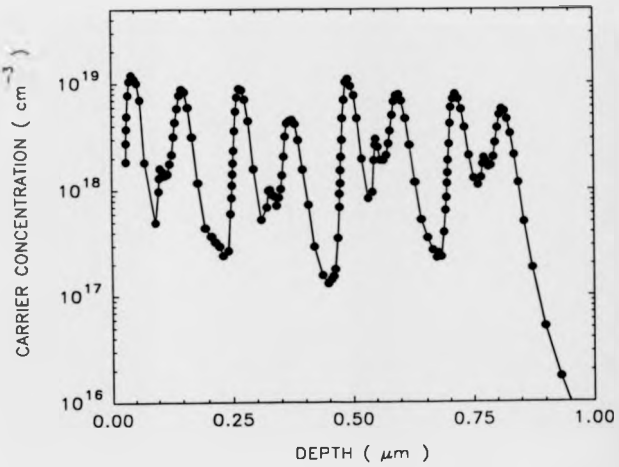

Fig. 5.2b E-CV depth profile of the boron doped structure in Fig. 5.2a.

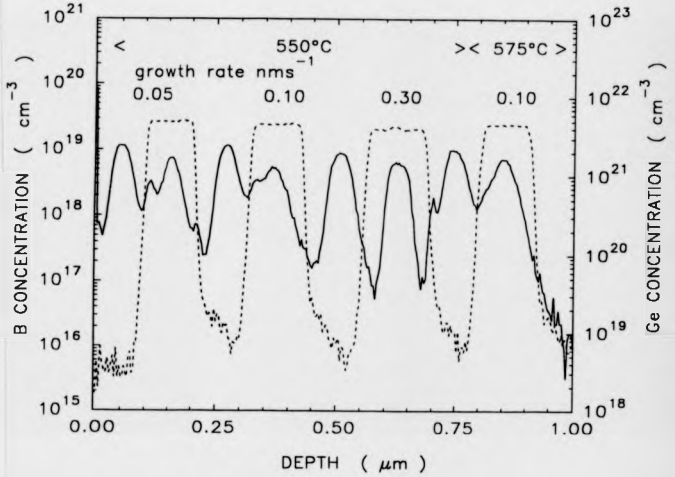

Fig. 5.3 Boron and Ge SIMS depth profiles of a modulation doped structure grown in $Si/Si_{0.9}Ge_{0.1}$ at rates and temperatures indicated.

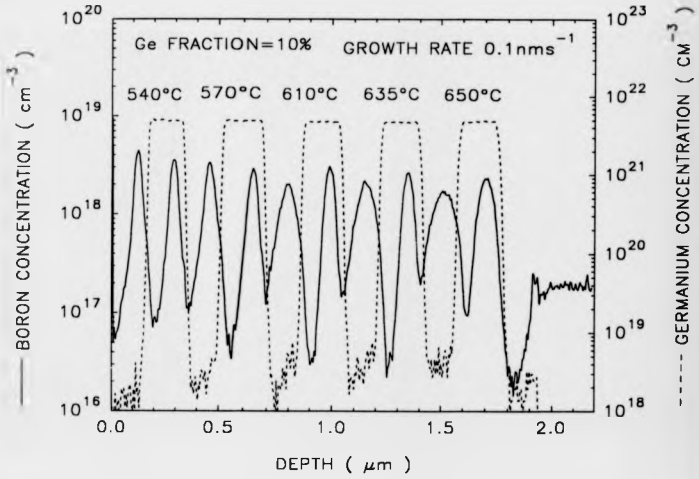

Fig. 5.4 Boron and Ge SIMS depth profiles of a modulation doped structure grown in $Si/Si_{0.9}Ge_{0.1}$. This structure features thicker layers so that the boron doped regions are resolved more clearly.

conditions specified, boron profiles in the $Si_{0.9}Ge_{0.1}$ alloy were more smeared than those in Si. In fact for the $Si_{0.9}Ge_{0.1}$ layers grown at 550 and 575°C, the degree of accumulation is so severe that determination of the leading edge slope abruptness becomes difficult because the boron profile has 'smeared' into the next boron doped layer. Leading edge slopes were also difficult to determine from severely smeared profiles owing to the presence of boron spikes observed at the points where the temperature and growth rate were changed. These are due to incorporation of previous surface-accumulated boron, after growth is recommenced at the new temperature and growth rate.

These structures, however, were 'first attempts', and to determine leading edge slopes more precisely another structure was grown with thicker spacer layers at temperatures between 540 and 650°C and at a growth rate of 0.1 nms^{-1}. Boron doped layers in this structure were 40 nm thick and grown in Si and $Si_{0.9}Ge_{0.1}$ layers each 180 nm thick. The SIMS depth profile of this structure is shown in Fig. 5.4. The difference in boron accumulation in Si and $Si_{0.9}Ge_{0.1}$ is shown more clearly in this thicker structure, since the interfaces of the boron doped layers are observed over a greater dynamic range of concentrations.

The leading edge slopes of the boron doped structures grown at 0.1 nms^{-1}, at Ge fractions of 10%, and at temperatures between 500 and 650°C were determined in nm/decade and converted to the profile broadening parameter Δ (nm) (see Chapter 4). This data is summarised in Fig. 5.5. Also included for comparison is the Δ parameter for boron in Si at a growth rate of 0.1 nms^{-1}. In this plot the complex relationship between Δ and growth temperature is seen more clearly as a reduction in accumulation behaviour in $Si_{0.9}Ge_{0.1}$ over that in Si, at temperatures above 550°C. The data points in $Si_{0.9}Ge_{0.1}$ at 550 and 575°C are probably spurious, owing to the large error in the determination of the leading edge slopes in layers situated too close to each other. Also these layers were doped at $\approx 10^{19} cm^{-3}$ (see Fig. 5.3), and the possibility of increased accumulation behaviour in the presence of a boron surface phase should also be considered (see Chapter 4).

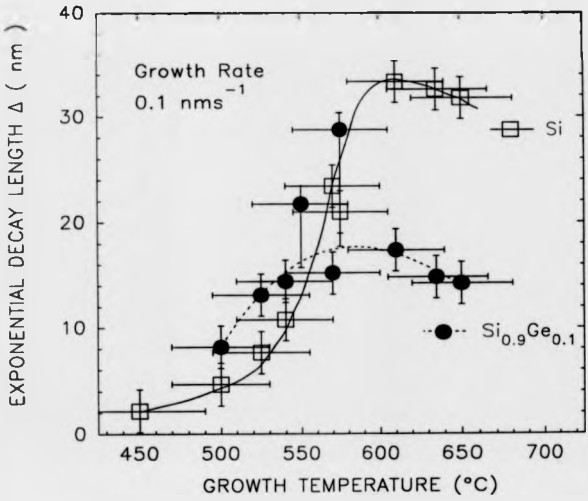

Fig. 5.5 Plot of the profile broadening parameter Δ, in the leading edge slopes, against temperature for boron in Si and $Si_{0.9}Ge_{0.1}$.

Otherwise the data reflects an apparent reduction in profile smearing in $Si_{0.9}Ge_{0.1}$ for boron doped layers grown at temperatures above 550°C.

Below this temperature Δ is significantly greater in the alloy than Si grown at the same temperature, though the difference is close to the error of the experiment.

5.2.3 BORON INCORPORATION IN $Si_{1-x}Ge_x$ ($0 < X < 25\%$)

The difference in accumulation behaviour in $Si_{1-x}Ge_x$ for Ge fractions of 10 and 20% was investigated further by growing boron doped layers at constant growth temperatures and rates, but with different Ge fractions. As well as yielding information about boron incorporation in $Si_{1-x}Ge_x$ such data is also important for the growth of HJBT's with a boron doped $Si_{1-x}Ge_x$ base that is 'graded' for Ge levels between 20 and 10% [Iyer *et al* 1990]. Fig. 5.6 shows a SIMS depth profile of the first attempt at investigating boron incorporation as a function of Ge fraction. This was grown at a temperature of 550°C and at a growth rate of 0.1 nms^{-1}. Boron doped layers were grown in $Si_{1-x}Ge_x$ regions with Ge fractions between 1 and 20%. The boron doped Si regions were used to identify any loss in depth resolution during the SIMS measurement. A Ge dependence of boron accumulation is observed, increasing to a maximum at Ge fractions of ≈7%, and significantly worse than in the Si. For Ge fractions of 20% the degree of profile smearing is significantly improved in the alloy. The leading edge slopes are not well defined in this structure, since the Si and $Si_{1-x}Ge_x$ spacer layers are not thick enough to allow boron levels to decrease sufficiently to measure them accurately. However this in itself is qualitative evidence of stronger boron accumulation at these Ge fractions than in layers for which the leading edges are more clearly defined.

Another structure was grown featuring thicker spacer layers and grown at a constant temperature of 510°C. The SIMS depth profile of this structure is shown in Fig. 5.7. The growth rate used was also 0.1 nms^{-1} and Ge fractions were varied

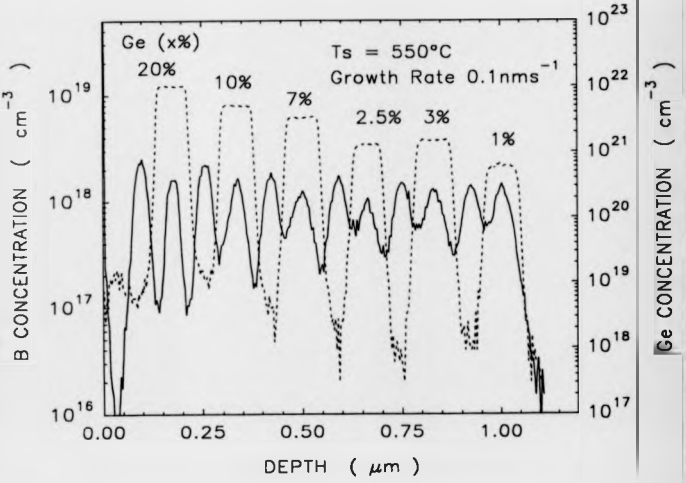

Fig. 5.6 Boron and Ge SIMS depth profiles for a boron doped $Si_{1-x}Ge_x$ structure ($0 < x < 20\%$), grown at a temperature of 550°C. The boron doped Si spacer layers are used to determine the degree of crater roughening during the SIMS profile.

between 25 and 1% (see figure). The profile smearing behaviour is broadly similar though at a much reduced level at this temperature.

The accumulation parameter Δ was determined from the leading edge slopes of the boron doped $Si_{1-x}Ge_x$ layers grown at 550 and 510°C. These are summarised in Fig. 5.8. Larger error bars in the structure grown at 550°C are due to the difficulties in determining the leading edge slopes. The very different behaviour observed over a narrow temperature range (≈40°C) reflects the abrupt changes in incorporation processes near transitions from equilibrium to kinetically limited regimes.

5.3 BORON INCORPORATION IN $Si_{1-x}Ge_x$ DISCUSSION

Boron incorporation in $Si_{1-x}Ge_x$ shows a temperature and growth rate dependence that is different from that observed in pure Si, as well as demonstrating a dependence on Ge fraction, at a given temperature and growth rate. The Δ versus temperature plot at Ge fractions of 10% at a growth rate of 0.1 nms^{-1} (see Fig. 5.5) reveals that at temperatures above 550°C boron profile smearing is significantly less in the alloy than in the Si, for boron layers otherwise grown under identical conditions. At temperatures below this, boron accumulation is discernibly *greater* in the alloy, though the difference is close to the error of the experiment.

The higher temperature results are consistent with the *site occupancy* models for MBE doping [Pindoria *et al* 1990A and see Chapter 4]. For the case of boron in $Si_{1-x}Ge_x$, the emphasis at higher temperatures appears to a tendency for boron to favour Ge site-occupancy providing surface stress relief, thus showing the decrease in profile smearing in the alloy. This can occur in the high temperature regime because boron atoms have sufficient energy to migrate across the surface to a Ge site.

In the low temperature regime (<550°C), however, the surface migration of boron will become kinetically hindered, so that atoms will become increasingly unable to migrate to Ge sites. In this temperature regime the unfavourable change in

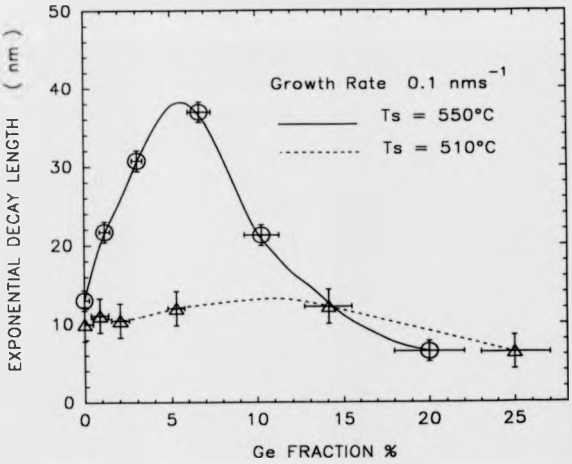

Fig. 5.8 Plot of profile broadening parameter Δ in the leading edge slopes, for boron in $Si_{1-x}Ge_x$ layers grown at temperatures of 510 and 550°C.

matrix, induced by coevaporation of Ge, becomes more significant reflected by the increase in boron profile smearing observed at temperatures below 550°C seen in Fig. 5.5.

Further evidence for both surface site occupation and change of matrix size influence on boron incorporation behaviour in $Si_{1-x}Ge_x$ comes from the boron accumulation versus Ge fraction plot in Fig. 5.8. Increasing the Ge fraction from zero increases the amount of surface stress producing the increase in boron accumulation behaviour with increasing Ge fraction seen at 550°C. This occurs up to levels of about 10%, though the scarcity of data points about the maximum precludes its precise determination. Further increases in the Ge fraction however, multiply the number of Ge incorporation sites. This decreases the distance boron atoms have to diffuse to reach Ge sites, causing the reduction in accumulation behaviour observed at Ge fractions >20%. For the second structure in Fig. 5.8 grown at 510°C, boron accumulation is more strongly kinetically limited, though a Ge dependence of accumulation behaviour is discernible. At the lower temperature, the decrease in boron accumulation in $Si_{1-x}Ge_x$ due to preferential site occupancy does not dominate until higher Ge coverages, owing to the reduced surface mobility of the boron atoms. However, the transition between the two accumulation mechanisms is not as well defined owing to the paucity of data points and further experiments are necessary.

However, the present data suggests that for a complete understanding of boron incorporation in $Si_{1-x}Ge_x$ *both* the change of matrix and the availability of favourable incorporation sites will need to be considered.

5.4 Ge INCORPORATION DURING $Si_{1-x}Ge_x$ MBE

The SIMS Ge profiles of the boron doped $Si_{0.9}Ge_{0.1}$ layers grown at 0.1 and 0.05 nms^{-1}, and between temperatures of 500 and 650°C (see Figs. 5.2a., 5.3, 5.4, 5.6 and 5.7), were used to determine Δ values at a given temperature and growth rate. These were determined from the leading edge slopes of the SIMS depth

profiles. These were found to be non-linear on a logarithmic (concentration) versus depth profile, the slope increasing with increasing Ge fraction. Hence Δ was determined over a fixed change in Ge fraction (10^{22} to 10^{21} cm^{-3}). This contributes to a larger error in the determination of Δ than is the case for boron. Δ is plotted as a function of temperature and growth rate in Fig. 5.9. The data do not show any discernible temperature dependence of Δ, over the range of temperatures and growth rates used, though it is possible that the temperature dependence is at a level too small to be detected, even in high resolution SIMS depth profiles.

Hence the present results do not confirm the temperature dependence of undoped Ge profile smearing behaviour observed during MBE reported by previous authors [Nakagawa and Miyao 1991].

A mechanism possibly responsible for reports of Ge "segregation" interpreted from SIMS studies [Gravesteijn *et al* 1989, Zalm *et al* 1989] was discovered by profiling a $Si/Si_{0.75}Ge_{0.25}$ structure using an O^+_2 primary ion beam at 4 keV, *but at normal incidence*. Fig. 5.10 shows the Ge depth profile using these conditions. (The same structure has already been presented in Fig. 5.1a, profiled at 4.5 keV at an angle of incidence of 43°.) This profile shows shoulders (see figure) in the growth direction, apparently indicating Ge accumulation. For the case of profiling at an angle of 43° to the normal (see Fig 5.1), the shoulders observed in Fig. 5.10 are not seen, and it is therefore concluded that one of the Ge profiles must be produced by some SIMS artefact. The boron profiles do not appear to show a dependency on primary ion angle.

The question arises, which is the 'real' Ge depth profile? This was investigated by SEM micrographs of SIMS craters produced after bombardment at normal incidence and 43°. These are shown in Figs. 5.11a and 5.11b. Fig. 11a shows large 'saucer-like' features etched after profiling using a normal incidence beam. Fig. 11b however does not show such features though 'pin-hole' defects are present in SIMS crater of this relaxed structure. It is suspected (although further work is necessary) that the features are etched dislocations. Both the pin-holes and

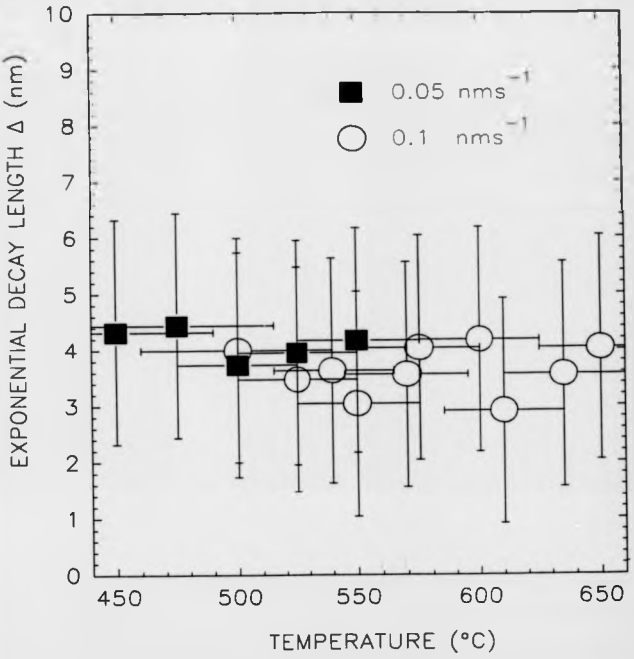

Fig. 5.9 Ge profile broadening parameter Δ determined from the SIMS leading edges of the boron doped $Si_{0.9}Ge_{0.1}$ layers grown at 0.1 and 0.05 nms^{-1} (see Figs. 5.2a, 5.3, 5.4, 5.6 and 5.7). The large error bars reflect the non-linearity in the Ge slopes.

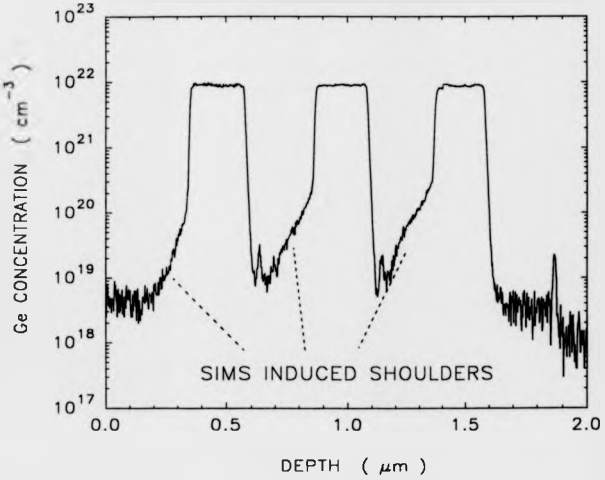

Fig. 5.10 SIMS Ge depth profile of a boron doped $Si/Si_{0.75}Ge_{0.25}$ structure, obtained using an O^+_2 primary ion beam at 4 keV, but at normal incidence. The shoulders observed in the depth profile under these conditions are not seen in the same structure profiled at an angle of 43° (see Fig. 5.1a).

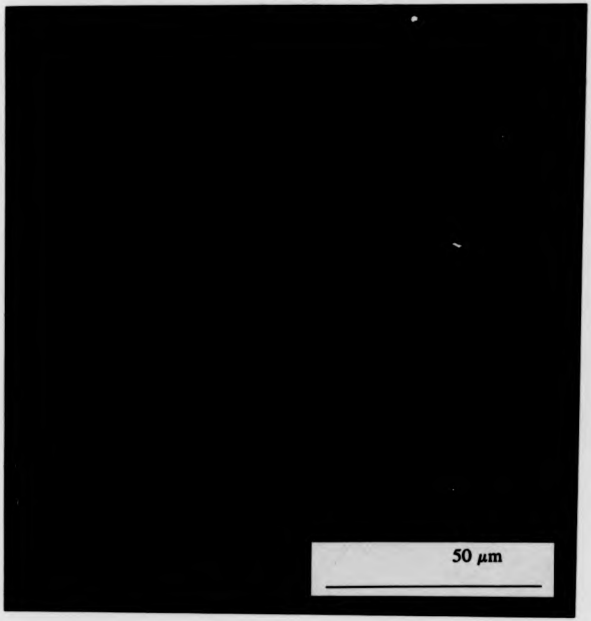

Fig. 5.11a SEM micrograph of the SIMS crater produced by 4 keV O_2^+ bombardment at normal incidence.

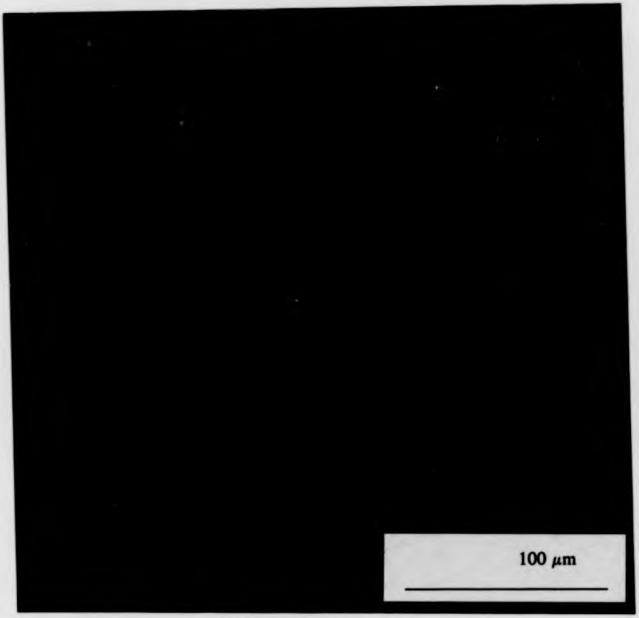

Fig. 5.11b SEM micrograph of the SIMS crater produced by 4.5 keV O_2^+ bombardment at 43° to the normal.

saucer-like defects are present at approximately the same density in the SIMS craters and close to the dislocation density measured from defect etching. It seems likely both the pin-hole and saucer-like features share a common origin, namely dislocations present in the $Si/Si_{0.8}Ge_{0.2}$ epilayer. The saucer-like defects are caused by anisotropic etching by the primary ion beam. Sputter rates are fastest at an angle of 45° to the normal [Dowsett *et al* 1991], so that the preferential etching of the dislocations is not as important as it is at normal incidence. Therefore it is supposed that the shoulders, observed at normal incidence, are induced by the SIMS measurement and that the more abrupt Ge profiles obtained at 43° are closer to the real Ge depth profile.

5.5 DISCUSSION OF Ge INCORPORATION DURING MBE

XPS results published by other authors show a Ge incorporation dependence on temperature [Nakagawa *et al* 1991]. Previous SIMS studies have showed strong Ge profile smearing, though this did not have any temperature or growth rate dependence [Zalm *et al* 1989, Gravesteijn *et al* 1989]. The apparent irreconciliation between these results and the lack of any temperature dependence of Ge profile smearing observed in the present work is discussed further.

In the aforementioned XPS investigation Ge 'segregation' was determined by the rate of incorporation of a Ge adlayer, produced by evaporating 3 ML of Ge onto clean Si(100) and Si(111) surfaces, and monitoring the Ge surface coverage, while Si growth continued, until the Ge adlayer had depleted to ≈1% of 1 ML. The rate of Ge depletion was found to be temperature dependent in the range 750 to 450°C, which the authors interpreted as Ge segregation. The high surface coverages were presumably used owing to the relative insensitivity of the XPS technique (cf 0.01% of a ML for Ge SIMS), but they may encroach on solubility limits of Ge in Si. This is a contentious point. Ge solid solubilities in Si are unknown except for a single point at the eutectic temperature [Trumbmore 1960]. Solubility limits in MBE decrease with decreasing temperature in the 'equilibrium regime' (see Chapter

3), and then show a sharp upturn owing to a reduction in the accumulation processes limiting them. Therefore it is possible that the temperature dependence of incorporation rate, established by the previous authors, is limited by the solubility of Ge in Si.

For the case of Ge accumulation, determined by SIMS studies, asymmetric smearing directed towards the surface has been observed in Ge depth profiles [Zalm *et al* 1989, Gravesteijn *et al* 1989]. Care was taken to eliminate the possibility of SIMS induced artefacts, by using different primary ion species at differing energies, though the authors did not give details of incidence angles of the primary beams. The authors observed these shoulders limited to ≈ 0.3 ML over a wide range of Ge fractions and temperatures. The authors suggested that this inferred the presence of a surface phase. Recent evidence suggests Ge surface phase can form on Si(111) surfaces [Tatsumi *et al* 1990A], though no other experimental evidence for surface phases on Si(100) has been reported to this author's knowledge. However, the authors reported that the incorporation of the surface phase does not show any temperature dependence. The shoulders seem unlikely to be caused by SIMS effects associated with defects, since the authors used plan view XTEM analysis of the samples to check for this.

Hence, these SIMS studies of Ge incorporation and the results presented in this Chapter are clearly inconsistent, though similar temperatures and growth rates were used in both studies. However there is one important difference between the $Si_{1-x}Ge_x$ studied in the present work and those for which Ge 'segregation' has been observed. The layers used in the present study feature boron doping, which may influence (favourably) Ge incorporation. This seems unlikely since the boron atoms are incorporated at levels orders of magnitude lower than those of Ge, though further investigations are necessary.

5.6 CONCLUSIONS

Boron and Ge incorporation, during $Si_{1-x}Ge_x$ MBE, have been investigated using high resolution SIMS measurements.

The first results obtained for boron incorporation in $Si_{1-x}Ge_x$ suggest that boron profile smearing shows a complex dependency on temperature, growth rate and Ge fraction. However the results are consistent with a model accounting for the influence of the change of *matrix* induced by Ge coevaporation, and the availability of *favourable incorporation sites*. The influence of these depends on the growth temperature and corresponding mobility of boron adatoms. This behaviour is also consistent with the surface migration models used in Chapters 4 and 5 to evaluate precipitation and surface clustering phenomena, as well as the influence of a boron surface-accumulated phase on dopant incorporation. At high temperatures, the availability of favourable incorporation sites dominates reflected by a significant increase in profile abruptness in the alloy. Reductions in growth temperature inhibit the surface migration of boron (and Ge) atoms so that the change of matrix becomes more important.

For the case of Ge incorporation, these results are inconsistent with previously observed determinations of Ge profile smearing. SIMS has been shown to distort profiles for highly defected $Si_{1-x}Ge_x$ layers, when profiling at normal incidence, though the structures used to determine Δ showed relatively low dislocation levels and were profiled at 43° to the normal.

However the present work differs from previous studies in that Ge layers were boron doped. Clearly further work is necessary to determine whether the apparent absence of Ge profile smearing, in the present study, is due to coevaporation of boron, or some fundamental flaw in using SIMS to determine Ge depths profiles.

CHAPTER 6

CONCLUSIONS

In this thesis boron and Ge profile smearing by surface accumulation occurring during MBE growth of Si and $Si_{1-x}Ge_x$ has been presented and discussed.

Although boron is a relatively well behaved dopant in MBE, the degree of profile smearing observed can be significant on a nanometer scale. Such smearing is however likely to be important to future generations of devices, which rely on the would be grower being able to obtain near abrupt *p*-doping profiles.

Boron accumulation in Si is shown to be temperature and growth rate dependent, and can be classified into two temperature regimes; the equilibrium (high temperature) regime and the kinetically limited (low temperature) regime. In the high temperature regime, profile smearing decreases with increasing temperature, according to equilibrium thermodynamics. However at lower temperature, the processes causing profile smearing become kinetically limited, seen as a sharp decrease in boron accumulation with a correspondingly dramatic increase in profile abruptness. The kinetically-limited accumulation regime is likely to be extremely important in the production of delta layers and other modulation doped structures. However, the temperature for the onset of kinetically limited boron accumulation shows a growth rate dependence. At a Si growth rate of 0.28 nms^{-1} the transition occurs at $\approx 650°C$ decreasing to $\approx 600°$ at a growth rate of 0.1 nms^{-1} at C. Thus the data presented in this thesis will be helpful in establishing the ideal incorporation conditions for boron in Si over a range of growth rates.

Another consequence of boron accumulation during Si MBE is that it limits the maximum carrier concentration that can be achieved at a given temperature. At higher doping levels boron accumulates, leading to the formation of *a surface phase of boron*. This accumulated phase is limited to a coverage equivalent to 0.25 ML. Any attempt to increase doping in the presence of a complete surface phase leads to the formation of inactive boron precipitates, observed in XTEM as discrete

platelets of boron, and in SIMS depths profiles as narrow 'spikes'. During coevaporation doping the accumulated phase resides on the surface at very high coverages but once the doping is terminated, and growth continues, the surface phase rapidly incorporates at a level *limited by the solubility of boron in Si*. This was used to determine solubility limits of boron in Si during MBE, for the first time, over the temperature range 900 to 650°C. Solubility limits are important in the growth of narrow highly doped boron delta layers with sheet concentrations $\approx 10^{14}cm^{-2}$. These limits were found to be in the $10^{19}cm^{-3}$ range for temperatures above 700°C, decreasing with decreasing temperature, and in good agreement with equilibrium solubility limits. As the accumulation processes become kinetically limited, at temperatures <600°C, there is an abrupt increase in solubility. The highest carrier and chemical concentration achieved was $4x10^{20}cm^{-3}$ at 450°C, and indeed higher levels may be possible allowing the production of devices with highly doped contacting layers, without the need for any *ex-situ* implantation stage. All dopant was found to be completely activated at temperatures below 600°C, though an upper limit to maximum carrier concentrations was found under certain growth conditions.

Another interesting property of boron accumulated phases is that as they incorporate they are shown, for the first time, to smear boron profiles much more severely than those doped at a lower level. The strong surface accumulation seen in the presence of a surface phase is thought to be due to the existence of stable surface clusters of boron that are less disposed to incorporation than atoms which are distributed more randomly over the growing Si surface. Initial results suggest that at lower growth rates these surface clusters can form at levels of $\approx 10^{19}cm^{-3}$. Such conditions are commonly used in the growth of modulation doped structures which rely on the production of sharp interfaces to provide mobility enhancements over bulk doped layers. However further *in-situ* monitoring techniques would be needed to confirm the range of incorporation conditions for the observation of boron surface clustering during MBE.

Also presented, for the first time, in this thesis are results of boron incorporation in $Si_{1-x}Ge_x$ ($0 < x < 25\%$). Boron incorporation in $Si_{1-x}Ge_x$ shows a temperature, growth rate and Ge fraction dependence, suggesting that it is influenced both by the change of matrix size induced by coevaporation of Ge, and the availability of favourable Ge incorporation surface sites. The change in matrix size in $Si_{1-x}Ge_x$ is due to the 4% lattice mismatch between Si and Ge. Accumulation processes depend on the relative sizes of dopant and matrix atoms. A consequence of this is that, under commensurate growth, boron accumulates more in $Si_{1-x}Ge_x$ than in Si, owing to the effective increase in matrix size, resulting in stronger profile smearing. However offset against this effect is the accommodation of surface stress by incorporation of boron at Ge surface sites. This stress compensation results in a *reduction* in boron accumulation in $Si_{1-x}Ge_x$. Evidence in this work suggests that *both* the change of matrix and strain compensation can affect boron accumulation in $Si_{1-x}Ge_x$, though the strain compensation dominates if the boron atoms have enough surface mobility to reach a Ge incorporation site. The surface mobility of boron is a function of temperature, and this is reflected in the results of the temperature dependence of boron incorporation in $Si_{1-x}Ge_x$.

The results of boron incorporation in Si and its doping level dependence, the formation of boron precipitates by surface clustering, as well as boron incorporation in $Si_{1-x}Ge_x$, are inconsistent with commonly favoured models for dopant incorporation. This is especially true for models invoking back-diffusion of dopant from the underlying layers. There exists no physical justification for this process, and discrepancies arise when considering extremes of incorporation conditions such as temperature $< 600°C$ and doping level $> 10^{19}cm^{-3}$. Instead boron incorporation in Si and $Si_{1-x}Ge_x$ has been found to be in accord with models that account explicitly for processes occurring at the *immediate* surface, such as migration and dopant step-climbing. These results suggest that surface migration models deserve more attention than they currently receive.

Much of the present work has progressed as far as it can, relying as it does mostly on analysis by SIMS methods as they stand at present. Profiles obtained in the equilibrium temperature regime can be so sharp that they can exceed the resolution of the SIMS technique. To improve our general understanding of boron incorporation in the temperature regime of most interest, it seems likely that further improvements in SIMS are necessary.

Although SIMS profiles are useful in the quantitative determination of profile smearing they can only be used to *infer* surface processes in the context of previously published models. It is not clear for instance why profile smearing, and surface phase formation are found to be different for the case of continuous coevaporation doping, and during interrupted growth. No existing model can account for this observation and to develop these models further the direct observation of boron surface clustering, boron surface migration and step-climbing processes is needed. This is best achieved by *in-situ* monitoring processes, such as LEED and STM for example.

REFERENCES

Abbinks H C, Broudy R M and McCarthy G P, "Surface processes in the growth of silicon on (111)silicon in ultra high vacuum", J. Appl. Phys. **10**, 4673 (1968).

Aizaki N and Tatsumi T, "Boron doping in silicon molecular beam epitaxial films by coevaporation of boron oxide", 17th Conf. on Solid State Devices and Materials, pp301-304, (Published by the Japanese Society of Applied Physics, Tokyo) 1985.

Aizaki and Tatsumi, "In-situ RHEED observations of selective diminution at Si(001)-2x1 superlattice spots during Si MBE" Surf. Sci., **174**, 658 (1986).

Allen F G, Iyer S S, Metzger R A "Dopant incorporation studies during Si molecular beam epitaxy." Applic. Surf. Sci., **11/12**, 517 (1982).

Andrieu S, "Boron doping of Si molecular beam epitaxy layers:A new high-temperature effusion cell", J. Vac. Sci. Tech. B6(3), 835 (1988).

Andrieu S, Arnaud d'Avitaya F, and Pfister J C, "Surface segregation mechanism during two-dimensional epitaxial growth", J. Appl. Phys. **65**(7), 2681 (1989).

Armigliato A, Nobli D, Ostoja P, Servidori M and Solmi S, in "Semiconductor silicon 1977", edited by H. Huff and E. Sirtl (Published by the Electrochemical Society, Pennington N.J. 1977) vol. 77-2, pp638-647.

ASTMS, standard F-76, "Annual book of ASTMS standards", vol 43, American Society for Testing and Materials, Philadelphia (1976A).

ASTMS, standard F-47, "Annual book of ASTMS standards", vol 43, American Society for Testing and Materials, Philadelphia (1976B).

Augustus P D, Barlow R D and Parry C P, "Delineation of boron delta layers in cross-sectional TEM samples of MBE Si" Trans. of Roy. Micro. Soc. vol 1, pp 161-164, Adam-Hilger Press 1990.

Barnett S A and Greene J E, "Si molecular beam epitaxy: A model for temperature dependent incorporation probabilities and depth distributions of dopant exhibiting strong surface segregation", Surf. Sci., **151**, 67 (1985).

Barnett S A and Rockett A, "Monte Carlo simulations of Si(001) growth and reconstruction during molecular beam epitaxy", Surf. Sci. **198**, 133 (1988).

Basaran E, (1991), *unpublished data*.

Bean J C, "Arbitrary doping profiles produced by Sb-doped Si MBE", Appl. Phys. Lett. **33**(7), 654 (1978).

Bean J C, Feldman L C, Fiory A T, Nakahara S and Robinson I K, "Ge_xSi_{1-x}/Si strained layer superlattice grown by molecular beam epitaxy", J. Vac. Sci. Technol. **A2**(2), 436 (1984).

Bean J C, "Silicon-based semiconductor heterostructures", Chapter 11 in *Silicon Molecular Beam Epitaxy*, edited by E. Kasper and J.C. Bean (CRC Press, Florida) 1988.

Becker G E and Bean J C, "Acceptor dopants in silicon molecular beam epitaxy", J. Appl. Phys. **48**(8), 3395 (1977).

Bevk J, Mannaerts J P, Ourmazd A, Feldman L C and Davidson B A, "Ge-Si layered structures: artificial crystals and complex cell ordered superlattices", Appl. Phys. Lett. *49*, 286 (1986).

Bhatia M S, Joshi A, Patel K and Chatterjee, "Observation of non-linearity in e-beam evaporation from a water-cooled crucible", J. Appl. Phys. **66**(3), 1159 (1989).

Blood P, "Capacitance-voltage profiling and the characterisation of III-V semiconductors using electrolyte barriers", Semicond. Sci. and Technol. **1**, 7 (1986).

Burton F C, Cabrera N and Frank F C, "The growth of crystals and the equilibrium structure of their surfaces", Philos. Trans. Roy. Soc. **243A**, 299 (1951).

Casel A, Jorke H, Pawlik M, Groves R and Frenzel E, "A comparison of electrical and chemical profiling of doping superlattices in silicon", J. Appl. Phys. 67(4), 1740 (1990).

Chadi D J, "Stabilities of single-layer and bilayer steps on Si(100) surfaces", Phys. Rev. Lett. 59(15), 1691 (1987).

Denhoff M W, "Boron evaporator for doping silicon thin films", J. Vac. Sci. Tech. B8(5), 1035 (1990).

Doi T and Ichikawa M, "Microscopic observations of Si MBE on Si(100) surface using microprobe RHEED", page 112 of Proc. II Int. Symp. on Si MBE, J.C. Bean Ed. (Published by the Electrochemical Soc. , Pennington, NJ) 1988.

Dominguez E and Jarais M, "A non-Fickian model of the diffusion of boron in silicon diffusion from BN sources", J. Electrochem. Soc. 133(9), 1895 (1985).

Dowsett M G, Barlow R D, Fox H S, Kubiak R A A and Collins R, "SIMS depth profiling of boron, antimony and germanium deltas in silicon and implications for profile deconvolution", *to appear in J. Vac Sci Tech 1992.*

Eberl K, Iyer S S, Delage S L, Ek B A and Cottee J M, "Boron doping in Si-MBE", *MRS Proc* 220, 121 (1991).

Farley C W, Crook G E, Kesan V P, Block T R, Stevens H A, Mattord T J, Neikirk D P and Streetman B G, "Substrate rotation and carbon generation in a molecular-beam epitaxy system", J. Vac. Sci. Technol. B5(5), 1374 (1988).

de Frésart E, Rhee S S and Wang K L, "Boron oxide interaction with silicon in silicon molecular beam epitaxy", Appl. Phys. Lett., 49(14), 847 (1986).

de Frésart E, Wang K L and Rhee S S, "Boron surface segregation in silicon molecular beam epitaxy", Appl. Phys. Lett. 53(1), 48 (1988).

Gogol C A and Cipro C, "An improved deposition process controller for MBE applications" pg 415 of Proc. I[st] Symp. on Si MBE, J C Bean Ed, (published by the Electrochemical Soc., Pennington NJ) 1985

Graper E B, "Evaporation characteristics of materials from an electron beam gun", J. Vac. Sci. Technol. A5(4), 2718 (1987).

Gravesteijn D J, Zalm P C, van der Walle G F A, Vriezema, van Gorkum A A and Ijzendoorn L J, "Ge segregation during molecular beam epitaxial growth of $Si_{1-x}Ge_x$/Si layers", Thin Solid Films 183, 191 (1989).

Greene J E, Barnett S A, Rockett A and Bajor G, "Modelling of dopant incorporation, segregation, and ion/surface interaction effects during semiconductor film growth by molecular beam epitaxy and plasma based techniques", Applic. Surf. Sci. 22/23, 520 (1985).

Ham F S, "Theory of diffusion limited precipitation", J. Phys. Chem. Sol. 6, 335 (1958).

Headrick R L, Weir B E, Levi A F G, Eaglesham D J and Feldman L C, "Si(100)-(2x1)boron reconstruction: Self-limiting monolayer doping", Appl. Phys. Lett. 57(26), 2779 (1990).

Herman M A and Sitter S, chapter 6 of "*Molecular beam epitaxy:Fundamentals and current status*", (Springer Series in materials science vol 7, published by Springer-Verlag, Berlin) 1989.

Higgs V, Davies G and Kubiak R, "The influence of metallic contamination on the lattice relaxation of Ge_xSi_{1-x} epitaxial alloys", Mat. Sci. Forum 65-66, 351 (1990).

Hill R J, "Physical Vapour Deposition" (published by Airco Temescal, Inc., California) 1976.

Honig R E,"Vapour pressure data for the solid and liquid elements" RCA Review, 567, December 1962.

Iyer S S, Metzger R A and Allen F G, "Sharp profiles with high and low doping levels in silicon grown by molecular beam epitaxy", J. Appl. Phys. **52**(9), 5608 (1981).

Iyer S S, Patton G L, Stork M C, Meyerson B S and Harame L, "Heterojunction bipolar transistors using Si-Ge alloys", Appl. Phys. Lett., **36**(10), 2043 (1989).

Iyer S S, Patton G L, Harame D L, Stork J M C, Crabbé E F and Meyerson B S, "Narrow band gap base heterojunction bipolar transistors using Si-Ge alloys", Thin Solid Films **184**, 153 (1990).

Jackman T E, Houghton D C, Denhoff M W, Kechang S, McCaffrey J, Jackman J A and Tuppen C G, "Boron redistribution in doping superlattices grown by silicon molecular beam epitaxy", Appl. Phys. Lett. **53**(10), 877 (1988).

Jackman T E, Houghton D C, Jackman J A, Denhoff M W, Kechang S, McCaffrey J and Rockett A, "Annealing studies of highly doped boron superlattices", J. Appl. Phys. **66**(5), 1984 (1989).

Jain S C and Hayes W, "Structure, properties and applications of Ge_xSi_{1-x} strained layers and superlattices", Semicond. Sci. Technol. **6**, 547 (1991).

Jorke H and Herzog H-J, "Mobility enhancement in modulation doped $Si/Si_{1-x}Ge_x$ superlattices grown by silicon molecular beam epitaxy", pages 352-359, Proc. Ist Int. Symp. on Si MBE, vol 85-7, Bean J C Ed, published by the Electrochem. Soc., Pennington NJ, (1985).

Jorke H, "Surface segregation of Sb on Si(100) during molecular beam epitaxy", Surf. Sci., **193**, 569 (1988).

Jorke H and Kibbel H, "Growth and transport properties of Si_mSb_1 superlattices", Thin Solid Films, **183**, 323 (1989).

Jorke H, Kibbel H, Shaffler F and Herzog H-J,"Low temperature kinetics of Si(100) MBE growth", Thin Solid Films **183**, 307 (1989).

Joyce B A, Neave J H, Watts B E, "The influence of substrate surface condition on the nucleation and growth of epitaxial thin films", Surf. Sci. **15**, 1 (1969).

Kaplan R, "LEED study of the stepped surface of vicinal Si(100)", Surf. Sci., **93**, 145, (1980).

Kasper E, "Growth kinetics of Si-molecular beam epitaxy", Appl. Phys. **A28**, 129 (1982).

Kelley M J, Ponec V, "Surface compositions of binary alloys", Prog. Surf. Sci. **11**, 139 (1981).

Kibbel H, Kasper E, Narozny P and Schreiber H -U, "Boron doping of heterobipolar transistors" Thin Solid Films **184**, 163 (1990).

Knall J, Sundgren J -E, and Greene J E, "Indium incorporation during the growth of (100)Si by molecular beam epitaxy", Appl. Phys. Lett. **45**(6), 689 (1984).

Kohama Y, Watanabe Y and Fukada, "Electron-beam-induced current observation of misfit dislocations at $Si_{1-x}Ge_x$/Si interfaces", Jap. J. Appl. Phys. **26**(12), L1944 (1987).

Kryistyan S, "Diffusion to the surface in the case of weak segregation of binary alloys", Surf. Sci. **224**, 476 (1989).

Kubiak R A A, Leong W Y L, Parker E H C, "P-type doping in silicon molecular beam epitaxy by coevaporation of the element", Appl. Phys. Lett. **44**(9), 878 (1985 A).

Kubiak R A A, Leong W Y and Parker E H C, "Coevaporation of boron doping of Si grown by MBE", pages 169-178 of Proc. Ist Symp. on Si MBE, J C Bean Ed, (published by the Electrochemical Soc., Pennington NJ) 1985 B.

Kubiak R A A, Leong W Y and Parker E H C, "Potential enhanced doping of Si grown by molecular beam epitaxy", J. Electrochem. Soc. **132**, 2738 (1985 C).

Kubiak R A, Patel G P, Leong W Y Houghton R and Parker E H C, "Co-evaporation phosporous doping in Si grown by molecular beam epitaxy", Appl. Phys. **A41**, 233 (1986).

Kubiak R A A, Newstead S M, Leong W Y, Houghton R F and Parker E H C, "The electrical properties of doped silicon grown by molecular beam epitaxy", Appl. Phys. **A 42**, 197 (1987).

Kubiak R A , Parker E H C and Iyer S S, Chapter 2 in *Silicon Molecular Beam Epitaxy*, edited by E. Kasper and J.C. Bean (CRC Press, Florida) 1988.

Kubiak R A and Parry C P, "An overview of doping strategies in Si:MBE", presented at the MRS Spring Meeting 1991, Annaheim, to appear in J. Cryst. Growth. *MRS Proc* **220**, 63 (1991)

Landi E, Armigliato A, Solmi S, Kogler R and Wieser E, "Electrical activation of boron-implanted silicon during rapid thermal annealing", Appl. Phys. **A47**, 359 (1988).

Leong W Y, Kubiak R A A and Parker E H C, "Dopant profiling of Si MBE material using the electrochemical CV technique", pages 140-149 of Proc. I[st] Symp. on Si MBE, J C Bean Ed, (published by the Electrochemical Soc., Pennington NJ) 1985.

Lifshits V G, Akilov V B, Churusov B L and Gavriljuk Yu L, "The role of surface phases in processes on silicon surfaces", Surf. Sci. **222**, 21 (1989).

Lin T L, Fathauer R W and Grunthaner P J, "Maximum boron doping concentrations without oxygen incorporation for silicon molecular beam epitaxy using HBO_2 and B_2O_3 as dopant sources", Thin Solid Films, **184**, 31 (1990).

Luryi S and Sze S M , Chapter 8 in *Silicon Molecular Beam Epitaxy*, edited by E. Kasper and J.C. Bean (CRC Press, Florida) 1988.

Matthews J W, Blakesee A E, and Mader S, "Use of misfit strain to remove dislocations from epitaxial thin films", Thin Solid Films *33*, 253 (1976).

Mattey N L, Hopkinson M, Houghton R F, Dowsett M G, McPhail D S, Whall T E, Parker E H C, Booker G R and Whitehurst J, "P-type delta doping in Si MBE" Thin Sol. Films **184**, 15 (1990).

McPhail D S, Dowsett M G, Fox H S, Houghton R F, Leong W Y, Parker E H C and Patel G K, "Quantifying the effects of uneven etching during the SIMS analysis of periodic doping structures grown by silicon MBE" Surf. and Inter. Analysis **11**, 80 (1988).

Maurice L, Duval P and Gorinas G, "Oil backstreaming in turbomolecular and oil diffusion pumps", J. Vac. Sci. Tech. **10**, 1941 (1979).

Miller D L and Sullivan G J, "A simple effusion source for uniform and reproducible deposition of dopant silicon in III-V molecular beam epitaxy", J. Vac. Sci. Tech. B5(5), 1377 (1987).

Mishima T, Fredriksz C W, van der Walle G F A, Gravesteijn D J, van der Heuvel R A and van Gorkum A A, "Effect of interface quality on the electrical properties of p-Si/$Si_{1-x}Ge_x$ 2DHG systems", Appl. Phys. Lett. **57**(24), 2567 (1990).

Nakagawa K, Miyao M and Shiraki A, "MBE-related surface segregation of dopant atoms in silicon", Jap. J. Appl. Phys. **27**(11), L2013 (1988).

Nakagawa K and Miyao M, "Reverse temperature dependence of Ge surface segregation during Si-molecular beam epitaxy", J. Appl. Phys. **69**(5), 3058 (1991).

Newstead S M, Kubiak R A, Parry C P, Naylor T N, Parker E H C and Whall T E, (1992), "Design and performance of a simple high temperature boron source", *in preparation*.

Ni W -X, Knall J, Hasan M -A, Hansson G V, Sundgren J -E, Barnett S A, Markert L C and Greene J E, "Kinetics of dopant incorporation using a low energy antimony ion beam during growth of Si(100) films by molecular beam epitaxy", Phys. Rev. B40, vol 15, 40, (1989).

Ota Y, "Silicon molecular beam epitaxy", Thin Solid Films **106**, 3 (1983).

Parry C P, Kubiak R A, Newstead S M, Whall T E, Parker E H C, "Boron accumulation behaviour during Si MBE", *MRS Proc* 220, 121 (1991 A).

Parry C P, Newstead S M, Barlow R D, Augustus P D, Kubiak R A A, Dowsett M G, Whall T E and Parker E H C, "Elemental boron doping behaviour in Silicon molecular beam epitaxy", Appl. Phys. Lett. 58(5), 483, (1991 B).

Parry C P, Kubiak R A, Newstead S M, Whall T E and Parker E H C P, "Temperature dependence of surface processes occurring during elemental boron doping in silicon molecular beam epitaxy", to appear in J. Appl. Phys., January 1992.

Parry C P, Kubiak R A, Newstead S M, Whall T E, Parker E H C, "An investigation of boron incorporation in SiGe MBE", 1991 *MRS Proc* 220, 103 (1991 D).

Patton G L, Iyer S S, Delage S L, Tiwari S and Stork J M C, "Silicon-germanium-base heterojunction bipolar transistors by molecular beam epitaxy", IEEE Electron Device Lett., 9(4), 165 (1988).

Pawlik M, "On the determination of abrupt doping profiles in MBE by spreading resistance", pages 184-193 of Ist Int. Symp. on Si MBE (published by the Electrochemical Soc. Pennington, NJ 1985).

Pawlik M, "Assessment of layers", Chapter 11 in *Silicon Molecular Beam Epitaxy*, edited by E. Kasper and J.C. Bean (CRC Press, Florida) 1988.

Pearsall T P, Bean J C, People R and Fiory, "Ge_xSi_{1-x} modulation doped p-channel field-effect transistors", pages 400-404 of Proc. Ist Int. Symp. on Si MBE, Bean J C Ed., (published by the Electrochemical Soc. Pennington, NJ, 1985.

People R and Bean J C, "Calculations of critical layer thicknesses versus lattice mismatch for Ge_xSi_{1-x}/Si strained layer heterostructures", Appl. Phys. Lett. 47(3), 322 (1985).

People R and Bean J C, "Band alignments of coherently strained Ge_xSi_{1-x}/Si heterostructures on <001> Ge_ySi_{1-y} substrates", Appl. Phys. Lett. **48**(8), 538 (1986).

Pindoria G, Kubiak R A, Newstead S M and Woodruff D P, "The influence of atomic size on dopant accumulation and site occupancy in molecular beam epitaxy", Surf. Sci., **234**, 17 (1990 A).

Pindoria G, Houghton R F, Hopkinson M, Whall T, Kubiak R A A and Parker E H C, "Particulate contamination in silicon grown by molecular-beam epitaxy", J. Vac. Sci. Tech. **B8**(1), 21 (1990B).

Powell A, Kubiak R A A, Parker E H C P, Bowen K and Polcarova M, "X-ray characterisation of a V90S SiGe MBE system", published in Proc. Mat. Res. Soc. pg. 161 vol 208 (1991).

Prinz E J, Garone P M, Schwartz P V, Xiao X and Sturm J C, "The effects of base dopant outdiffusion and undoped $Si_{1-x}Ge_x$ junction spacer layers in $Si/Si_{1-x}Ge_x/Si$ heterojunction bipolar transistors", IEEE Electron Device Lett. **12**(2), 42 (1991).

Ravi K V, "Imperfections and Impurities in Semiconductor Silicon", (J. Wiley & Sons Inc., New York 1981).

Roth A, "Vacuum technology", (North-Holland publishing Co., Amsterdam, 3rd Edition) 1979.

Sakamoto K, Sakamoto T, Miki K, "Observation of Si(100) vicinal surfaces on RHEED", J. Electrochem. Soc., **136**(9), 2705 (1989).

Sardela Jr M R, Ni W -X, Ekberg J O, Sundgren J -E and Hansson G V, "Surface segregation of boron during Si-MBE growth", *MRS Proc* **220**, 109 (1991).

Sasaki Y, Itoh K, Inoue E, Kishi S and Mitsuishi, "A new experimental determination of the relation between the Hall mobility and hole concentration in heavily doped p-type silicon", Solid-State Elect. **31**(1), 5 (1988).

Schäffler F and Jorke H, "Gallium doping of silicon molecular beam epitaxial layers at low temperatures and under Si^+ ion bombardment", Thin Solid Films **184**, 75, (1990).

Schimmel D G, "Defect etch for <100> Si evaluation", J. Electrochem. Soc., **126**, 479 (1979).

Screiber H -U, Bosch B G, Kasper E and Kibbel H, "Si/SiGe heterojunction bipolar transistor with base doping highly exceeding emitter doping concentration", Electronics Lett. **25**(3), 185 (1989).

Schwettman F N, "Characterisation of incomplete activation of high-dose boron implants in silicon", J. Appl. Phys. **45**(4), 1918 (1974).

Slotboom J W, Streutker G, Pruijmboom A and Gravesteijn D J, "Parasitic energy barriers in SiGe HJBT's", IEEE Electron Dev. Lett. **12**(9), 486 (1991).

Solmi S, Landi E and Baruffaldi F, "*Θιηθ γοξγεξυσαυιοξ βοσοξ διζζφτιοξ ιξ τιμγοξετικφμαυιοξ οζ τσεγιπιυαυιοξ πθεξονεξα*", J. Appl. Phys. **68**(7), 3250 (1990).

Sze S M, "Physics of semiconductor devices" 2nd Ed., (published by John Wiley and Sons, NY) 1981.

Tabe M and Kajiyawa K, "Kinetics of antimony doping in silicon molecular beam epitaxy" Jap. J. Appl. Phys. **22**(3), 423 (1983).

Tatsumi T, Hirayama H and Aizaki N, "Boron doping for Si molecular beam epitaxy using HBO_2 source", pages 430-437 of Proc. II Int. Symp. on Si MBE, J.C. Bean Ed. (Published by the Electrochemical Soc., Pennington, NJ) 1988 A.

Tatsumi T, Hirayama H and Aizaki N, "Surface segregation at boron planar doping in silicon molecular beam epitaxy", Jap. J. Appl. Phys. **27**(6), L954 (1988 B)

Tatsumi T, Hirosawa I, Niino T, Hirayama H and Mizuki K, "$\sqrt{3}x\sqrt{3}$ B structure on a (5x5) Ge_xSi_{1-x}/Si(111) surface" Appl. Phys. Lett. **57**(14), 1395 (1990 A).

Tatsumi T, "Boron doping using compound source", Thin Solid Films, **184**, 1 (1990 B).

Trumbmore F A, "Solid solubilities of impurity elements in Ge and Si", Bell Syst. Tech. J., **39**, 205 (1960).

Tuppen C G, Prior K A, Gibbings C J, Houghton D C and Jackman T E, "Oxygen incorporation in molecular beam epitaxial silicon doped using a boric oxide source", J. Appl. Phys. **64**(5), 2751 (1988).

Unvala B A, "Epitaxial growth of Silicon by vacuum evaporation", Nature, **194**, 966 (1962).

Van der Merwe J H, "The theory of strained layer growth", Proc. R. Soc. London Ser. A, 198, 125 (1955).

Van der Pauw L J, "A method of measuring the resistivity and Hall coefficient on lamellae of arbritrary shape", Phillips Tech. Rev. **20**(8), 220 (1958).

Vick G L and Whittle K M, "Solid solubility and diffusion coefficients of boron in silicon", J. Electrochem. Soc. **116**, 1142 (1969).

Voigtlander K, Rishen H, Kasper E, "Modified growth theory for high supersaturation", Appl. Phys. A**39**, 31 (1986).

Wagner G R and Janocko "Observation of two dimensional hole gas in boron doped $Si_{0.5}Ge_{0.5}$/Ge heterostructures", Appl. Phys. Lett. **54**(14), 1395 (1989).

Wilson R G and Novak S W, "Systematics of SIMS relative sensitivity factors versus electron affinity and ionization potential for a variety of matrices determined from implanted standards of more than 70 elements", J. Appl. Phys. **69**(1), 466 (1991).

Won T and Morcoç H, "High-speed performance of $Si/Si_{1-x}Ge_x$ heterojunction bipolar transistors", IEEE Electron Device Lett. **10**(1), 33 (1989).

Zalm P C, van de Walle G F A, Vriezema C J and van Gorkum A A, "Ge segregation at $Si/Si_{1-x}Ge_x$ interfaces grown by molecular beam epitaxy" Appl. Phys. Lett. **55**(24), 2520 (1989).

APPENDIX I - SIMS

A 1.1 INTRODUCTION

Much of the data obtained in the present study relies primarily on the analysis and interpretation of depth profiles obtained by SIMS. This is especially so in Chapters 4 and 5, which discuss the temperature dependence of boron and Ge profile smearing determined directly from SIMS depth profiles. It is therefore important to present a critical review of the SIMS technique, which highlights some of the problems associated with the determination of boron and Ge profiles.

A 1.2 QUANTIFICATION

A certain amount of processing is involved in the conversion of the raw data during a SIMS profile. The raw data consists of a count rate for the species of interest, against time. An explanation follows of the conversion of these to doping levels and depths.

A 1.2a DOPING LEVEL QUANTIFICATION

Only a fraction of the species of interest present in the sample will actually be collected as useful data. Some will either be implanted, or expelled. The expelled fraction will be a molecular, positive or negative species most as neutral atoms. For the instruments used in the present work (see section 2.3.2) positive ions are selected using an appropriate extraction potential. The fraction reaching the detector is often described as the 'useful' or 'ion' yield, which depends on the instrumental conditions eg primary ion species, energy and angle of incidence and collection optics.

In most cases, the ion yield can be determined by comparing the measured count rates with those obtained from known standards, usually ion implanted doses,

profiled under the same set of conditions. Using a standard, the error in the determination of the atomic concentration is less than 5%.

Standard implants for boron and Ge in $Si_{1-x}Ge_x$ were not available for the present work, and it is known that ion yields are dependent on the sample/matrix composition [Wilson and Novak 1991]. Indeed a difference in boron yields was observed in layers grown containing different Ge fractions, as part of a study of boron incorporation in $Si_{1-x}Ge_x$ ($0<x<25\%$). There is at present no adequate theory that allows accurate determination of the ion yield, for a given species, in a particular matrix [Wilson and Novak 1991]. However *comparative* boron ion yields can be determined by measuring the sheet density of boron spikes in Si against those obtained in identical spikes in $Si_{1-x}Ge_x$ for $0<x<25\%$ (shown in Fig. A.1). As can be seen in Fig. A.1, the boron yield decreases with increasing Ge fraction giving a boron yield in $Si_{0.8}Ge_{0.2}$ $\approx 60\%$ of that in Si. This plot can be used to obtain boron doping levels in $Si_{1-x}Ge_x$, within a 20% error, provided a boron in Si standard is profiled under identical conditions.

For the case of Ge in Si, Ge SIMS profiles are quantified by calibrating the Ge flux rate (see section 2.2.4) and normalising the Ge count rate to this value. This gives an absolute error in the Ge level of $\pm 30\%$ with a reproducibility of $\pm 10\%$.

However it should be noted that the *gradients*, determined from the slopes of modulation doped layers, will be unaffected by this reduction in ion yield, since these are determined by the depth necessary to observe a given *change* in concentration. Hence the boron slopes determined in Chapters 4 and 5 do not depend on the absolute value of the boron concentration.

A 1.2b DEPTH SCALE CALIBRATION

Accurate depth calibration is an important consideration in the work in Chapters 4 and 5, and the use of the SIMS technique to profile modulation doped structures, has been advantageous in this respect.

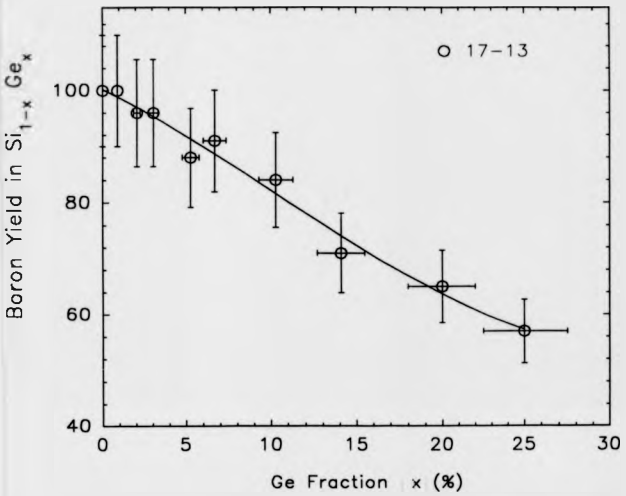

Fig. A.1 Plot of percentage boron yield against Ge fraction for profiling under otherwise identical conditions.

Depth calibration was obtained by measuring the thickness of the final crater *ex-situ*, using a surface profilometer, to an accuracy of ±5%.
For thick layers the depth X_n of the n^{th} frame is given by

$$X_n = \frac{\text{Frame no. } n \times \text{crater thickness}}{\text{total number of frames}} \qquad \text{(A 1.1)}$$

A 1.3 FACTORS AFFECTING DEPTH RESOLUTION IN SIMS PROFILES

The depth resolution of a SIMS dopant profile is affected by primary ion energy, non-uniform crater etching and the formation of a pre-equilibrium region at the start of a depth profile [Dowsett *et al* 1991]. Another effect contributing to a loss in Ge depth resolution is a dependence on the angle of incidence of the primary ion beam. Hence the depth resolution of the SIMS technique is sometimes much worse than that expected from the *ex-situ* determination of the crater depth, for reasons that will be considered here.

A 1.3.1 PRIMARY ION ENERGY DEPENDENCE ON DEPTH RESOLUTION

Ion beam mixing is the most important contribution to loss in SIMS depth resolution in abrupt profiles, such as those obtained by Si MBE, although, as will be seen in Chapters 3 4 and 5, its effect is only significant for profile abruptnesses of less than 10 nm/dec. The SIMS technique distorts profile abruptness owing to ion beam mixing effects (ion beam mixing) causing the depth profile to appear broader than the true thickness, and an apparent decrease in profile abruptness. Because the effect is due to impact events, it increases with increasing primary ion energy.

The effect has been characterised at *normal incidence* for abrupt profiles by Dowsett *et al* (1991). Fig. A.1 shows a plot of profile abruptness versus primary

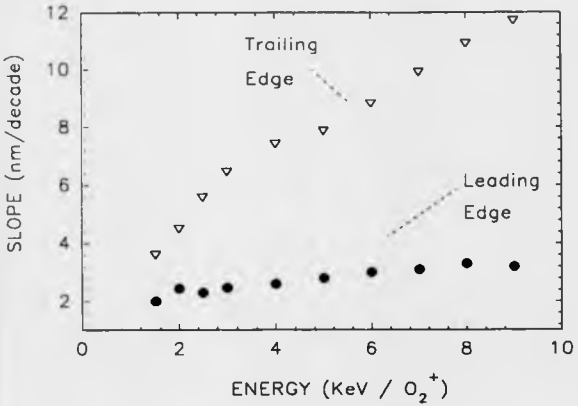

Fig. A.2 Diagram of depth resolution versus primary beam energy using an O_2^+ beam at normal incidence (after Dowsett *et al* 1991).

ion energy for for the leading and trailing edges of a narrow boron δ layer grown by Si MBE. The profile abruptness decreases with decreasing ion energy, and extrapolation to zero energy yields the true profile abruptness to a good approximation. The discontinuity at 4 keV is genuine [Dowsett *et al* 1991], thought to be associated with a transition in the influence of the change in erosion rate at the beginning of the SIMS depth profile (see section A 1.3.3). As expected, the leading edge slope is much less affected than the trailing edge varying from 3 to 2 nm/decade as the primary ion energy is extrapolated from 4 keV to zero energy. Most of the profiles in Chapter 5 were obtained using a Cameca instrument at an O_2^+ impact energy of 4.5 keV, for which primary ions impinge at 43° to the normal. The energy dependence of profile abruptness seen at normal incidence may be different at this angle. A qualitative determination of the effect of ion beam mixing, at this angle of incidence, was carried out by profiling a modulation doped structure at normal incidence and at 43° using the same primary ion energy. Measurements of the profile abruptness in the leading edge slopes suggest that ion beam mixing at 43° is *slightly* worse than at normal incidence. However, as will be seen in the discussion of Ge incorporation in Chapter 5, this barely discernible loss in depth resolution is more than compensated by the benefits associated with profiling $Si_{1-x}Ge_x$ multilayers over profiling at normal incidence.

The loss of depth resolution, by ion beam mixing, means that the sharpest profiles observed in the present work are probably more abrupt than that determined from the SIMS depth profile. However for most observations, the loss in depth resolution by ion-mixing was within the error of the depth measurement.

A 1.3.2 INSTRUMENTAL DRIFT AND CRATER UNIFORMITY

Another possible contribution to a loss in depth resolution and accuracy in the determination of the leading edge slopes is the effect of crater non-uniformity due to instrumental drift. This effect can be due to a change in the focussing and/or extraction optics used in the SIMS instrument during a depth profile.

Craters formed by the SIMS measurement are never ideally flat owing to instrumental drift and non-uniform crater etching. The effect of crater non-uniformity on depth resolution was simulated by McPhail *et al* (1988). The simulation predicted and verified that SIMS broadening, by non-uniform crater formation, is most significant in the trailing edge slopes. This is seen in a modulation doped structure grown as part of this work as a study of boron incorporation under low doping at different temperatures. Fig. A.3 shows a boron depth profile obtained by a primary ion energy of 2 keV. The depth profile measurement took more than six hours. The shoulders, discernible in the SIMS trailing edge, are due to non-uniformity of the crater bottom due to instrumental drift. Because erosion rates at an angle of 43° are much higher than at normal incidence, SIMS profiles obtained at this angle are far less likely to be affected by instrumental drift.

An examination of the crater bottom using a surface profilometer can be used to evaluate crater uniformity. A uniformity of 1% across the crater bottom is acceptable [McPhail *et al* 1988]. The monitoring of a Si matrix channel during a SIMS profile, as well as the species of interest, is also helpful in identifying instrumental drift.

A 1.3.3 EFFECTS OF NON-UNIFORM ETCHING ON DEPTH RESOLUTION

When scaling depths in thin layers, the effect of a sharp change in erosion rate at the start of a depth profile must be considered. O_2^+ ion-beam bombardment produces an SiO_x layer in the area exposed to the primary beam, at the start of a SIMS profile, denoted the altered layer [Dowsett *et al* 1991]. During this period the sample is eroded at a non-uniform rate, and sputter rates vary dramatically, until equilibrium is established. The thickness of the altered layer and therefore the effect of the pre-equilibrium region on the final depth scale varies with primary ion energy, increasing with increasing energy. For thin ($\simeq$10nm) layers the

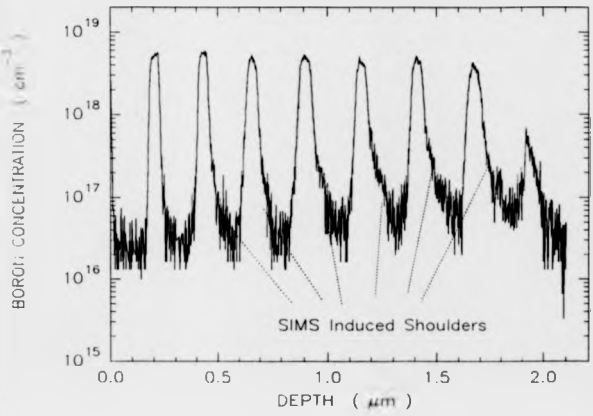

Fig. A.3 Boron depth profile obtained using a primary ion energy of 2 keV. The shoulders in the trailing edge slopes are erroneous and are caused by a non-uniform crater due to instrumental drift.

contribution to the error in the depth measurement due to a change in erosion rate becomes significant, and the depth calibration using equation (A.1) is invalid. This will be seen as an apparent shift towards the surface in the apparent depth of dopant profiles. Shallow profiles can be obtained at different energies to extrapolate the true thickness of the doping profile [Dowsett *et al* 1991]. However the effect of the pre-equilibrium region at a given energy is fixed. For thick structures (> 500 nm) it contributes by an amount that is within the error of the depth measurement and can therefore be ignored.

A 1.3.4 DEPTH CALIBRATION OF $Si_{1-x}Ge_x$ MULTILAYERS

The assumption of uniform etch rate during primary ion bombardment may not be valid for multilayer structures. If this is the case during profiling of $Si/Si_{1-x}Ge_x$ structures then the measured profile abruptnesses will contain a systematic error. This was investigated by measuring the individual thickness of $Si/Si_{1-x}Ge_x$ multilayers and comparing these with those intended according to the growth schedule. At an O_2^+ primary ion energy of 4 keV and an angle of incidence of 43°, no difference in erosion rates in Si and $Si_{1-x}Ge_x$ was observed within the 5% error of the depth measurement. This was the case for Ge fractions up to 25%.